PLASTIDIC PI TRANSPORTERS

IN *ARABIDOPSIS THALIANA*

A Dissertation

by

SONIA CRISTINA IRIGOYEN ARANDA

Submitted to the Office of Graduate Studies of
Texas A&M University
in partial fulfillment of the requirements for the degree of

DOCTOR OF PHILOSOPHY

August 2011

Major Subject: Molecular and Environmental Plant Sciences

Plastidic Pi Transporters

in A*rabidopsis thaliana*

PLASTIDIC PI TRANSPORTERS

IN *ARABIDOPSIS THALIANA*

A Dissertation

by

SONIA CRISTINA IRIGOYEN ARANDA

Submitted to the Office of Graduate Studies of
Texas A&M University
in partial fulfillment of the requirements for the degree of

DOCTOR OF PHILOSOPHY

Approved by:

Chair of Committee,	Wayne K. Versaw
Committee Members,	Thomas D. McKnight
	Kendal Hirschi
	Hongmin Qin
Intercollegiate Faculty Chair,	Dirk B. Hays

August 2011

Major Subject: Molecular and Environmental Plant Sciences

ABSTRACT

Plastidic Pi transporters in *Arabidopsis thaliana*.

(August 2011)

Sonia Cristina Irigoyen Aranda, B.S., Universidad Autonoma de Nuevo Leon, Facultad de Ciencias Biologicas; M.S., Universidad Autonoma de Nuevo Leon, Facultad de Ciencias Biologicas

Chair of Advisory Committee: Dr. Wayne Versaw

Phosphorous in its inorganic form, orthophosphate (Pi), is found in every compartment of the plant cell and serves as a substrate, product or effector for a wide range of metabolic processes. Several Pi transporters exist in plants and these help regulate Pi homeostasis within different cellular compartments. The PHT4 family of organellar Pi transporters consists of six members in the model plant *Arabidopsis thaliana*, and five of these are localized to plastids. I used gene expression analyses and reverse genetics to demonstrate functional specialization for the PHT4 family members with a focus on PHT4;1 and PHT4;2. The PHT4;1 Pi transporter is localized to chloroplast thylakoid membranes and it is expressed in a circadian manner. Plants that lack a functional copy of the *PHT4;1* gene have reduced rosette size and altered responses to photooxidative stress. The PHT4;2 transporter is localized to heterotrophic plastids in roots and other sink organs and *pht4;2* mutants exhibit decreased starch

accumulation, which is consistent with a defect in Pi export, and increased rosette size, which is caused by increased cell proliferation.

These results confirm that PHT4;1 and PHT4;2 have specialized functions and that plastidic Pi homeostasis influences broad aspects of plant metabolism, including abiotic stress response and control of lateral organ growth.

DEDICATION

To my parents, Maria Elena and Jose Luis, who have always supported me and encouraged me to follow my goals. To my sisters Luz Elena and Zaira Alejandra, thank you for bringing joy to my life. To my grandparents Jose Alberto and Teresa, who supported me for a long time.

To my best friend and husband, Kranthi Mandadi, for his love and patience

To my fellow members of the MEPS program, for all the things we have learned together

ACKNOWLEDGEMENTS

I would like to give special thanks to the individuals who, in one way or another, helped in the realization of this project. Their contributions, big or small, helped bring this work to completion.

First of all I would like to thank my advisor, Dr. Wayne Versaw, for the opportunity to join his lab and contribute to his projects. I thank him for his mentoring and support in the course of my graduate studies.

I want to also thank my committee members, Dr. McKnight, Dr. Qin and Dr. Hirschi for their insight and guidance during the duration of my project. Their insight and advice were a great help and encouragement.

Special thanks to past and present members of Dr. Versaw's lab: Patrick, Biwei, Jin, Tiffany, Pallavi. Also thanks to past and present student workers who have helped with organization and plant maintenance.

Thanks to Dr. Cornelia Spetea from the Department of Plant and Environmental Sciences, University of Gothenburg, Sweden, and her lab members, Jacob Kuruvilla and Patrik Karlsson for their collaboration on this project.

Finally, thanks to members of Dr. Thomas and McKnight labs for their help on several occasions: Jungim, Veria, Yichun, Kat, Andy, Phil, Ren, Ketan, Beth, and Kranthi.

TABLE OF CONTENTS

LIST OF FIGURES

FIGURE Page

LIST OF TABLES

CHAPTER I

INTRODUCTION

Importance of phosphate

Phosphorous is a macronutrient of crucial importance to plants. The biologically relevant form of phosphorous, orthophosphate (Pi), serves as a substrate for numerous metabolic processes; it is a structural component of nucleic acids, phospholipids and ATP; and it is also involved in regulation of numerous enzymatic reactions through protein phosphorylation. Additionally, Pi is an allosteric regulator of the partitioning of fixed carbon partitioning during photosynthesis. Although plants require a large amount of Pi throughout their lifespan, this macronutrient is one of the least available macronutrients in soil due to its tendency to form insoluble complexes and organic compounds that plants are unable to use. Plants have therefore evolved several morphological (increase of root-to-shoot ratio, formation of proteoids, mycorrhizal associations) and physiological (secretion of organic acids and phosphatases, mobilization of Pi from older leaves, etc.) adaptations to adjust to low Pi-containing soils in order to enhance Pi uptake and distribute it to all organs and tissues (Bieleski, 1973; Raghothama, 1999; Versaw and Harrison, 2002).

This dissertation follows the style of Plant Physiology.

The first barrier for Pi acquisition is the root epidermis, where specific transport proteins located in the plasma membrane are required to catalyze out Pi uptake from the soil solution. Once inside the root cells, distinct transport mechanisms are needed to regulate cellular Pi homeostasis and translocation to different organs (Bieleski, 1973; Raghothama, 1999).

Plant phosphate transporters

Several of the transporters that regulate Pi homeostasis within and between cells have been identified. These are currently categorized into five families based on sequence similarity and subcellular localization: PHT1 proteins localize to the plasma membrane, PHT2 and pPT proteins localize to the plastid inner membrane, PHT3 proteins localize to the mitochondrial inner membrane (Rausch and Bucher, 2002), and PHT4 proteins localize to either the plastid inner membrane or to the Golgi apparatus (Guo et al., 2008b).

Until recently, Pi transport in plastids has been attributed solely to members of the plastidic phosphate translocator (pPT) family (Knappe et al., 2003). This family includes the triose phosphate/phosphate translocator (TPT), which is the first transporter to be cloned from plants (Flügge et al., 1989). TPT is located in the chloroplast inner membrane and carries out export of triose phosphate (TP, glyceraldehydes 3-phosphate and dihydroxyacetone phosphate) from the chloroplast stroma in exchange for cytosolic Pi. Despite the importance of TPT for provision of carbon to the cytosol and the rest of the plant, a *tpt-1* knockout mutant has no obvious developmental defect. This suggests

the existence of mechanisms that compensate for the defects in both carbon and Pi allocation. For example, the TP export defect can be fully compensated by increased rates of starch synthesis and turnover as well as by export of glucose (Glc) and maltose (Schulz et al., 1993; Schneider et al., 2002). Other members of the pPT family include the glucose-6-phosphate/Pi transporter (GPT), which is expressed mainly in heterotrophic organs; the phosphoenolpyruvate/Pi (PEP) transporter, which localizes to both photosynthetic and non-photosynthetic organs; and the xylulose 5-phosphate/Pi translocator (XPT) (Muchhal, 1996; Kammerer et al., 1998; Flügge, 1999). Unlike TPT, these pPT translocators catalyze export of stromal Pi in exchange with the specified phosphorylated sugar.

In recent years, two additional families of plastid-localized Pi transporters, PHT2 and PHT4, have been discovered. PHT2 proteins localize to the chloroplast inner membrane, and functional analyses in yeast suggest that these proteins have low affinity for Pi and catalyze H^+/Pi symport that contribute to plastidic Pi regulation have been discovered and characterized. Among them, the PHT2 family, which comprises one family member, PHT2;1, is localized in the chloroplast inner membrane. It is a low-affinity transporter and functions as a H^+/Pi symport (Daram et al., 1999; Versaw and Harrison, 2002; Zhao et al., 2003). An Arabidopsis *pht2;1* null mutant exhibits low Pi content in leaves and reduced plant size, consistent with a defect in the import of Pi into the chloroplast and associated Pi-limited photosynthesis (Sivak and Walker, 1986; Versaw and Harrison, 2002).

PHT4 sequences are widely conserved in plants but functional analyses have thus far been limited to the six-member family in Arabidopsis. Five of these proteins, PHT4;1/4 localize plastids in either photosynthetic or heterotrophic tissues, and one, PHT4;6, localizes to the Golgi apparatus (Guo et al., 2008a). All six of these proteins mediate Pi transport that is dependent on the presence of a proton electrochemical gradient when expressed in yeast, which is suggestive of H^+/Pi symport (Guo et al., 2008a). One of these, PHT4;1, also exhibits Na^+-dependent Pi transport when expressed in *E. coli*, and this protein is targeted to the chloroplast thylakoid membrane in plants (Ruiz Pavón et al., 2008). The other plastid-localized members of this family are confirmed or predicted to reside in the plastid inner membrane (Ferro et al., 2003; Roth et al., 2004). The expression of these proteins in photosynthetic and non-photosynthetic tissues suggests functional roles in chloroplast and heterotrophic plastids. Further analysis is required to define these roles as well as the mechanism and directionality of Pi transport in the respective plastids.

The identification and characterization of these transporters has enhanced our understanding of Pi transport in plants. These transport processes, together with biochemical reactions that recycle Pi from organic forms in each cell compartment, regulate Pi homeostasis at the cellular and organismal levels (Mimura, 1999).

Plastid biology

Plastids are organelles present in all plant cells and are derived from undifferentiated proplastids found in meristematic cells. Proplastids differentiate into

specialized types of plastids during plant development and in response to environmental conditions. These specialized plastids are typically categorized based on function, e.g., photosynthesis (chloroplasts), or the types of compounds that are accumulated, e.g., starch (amyloplasts), oils (elaioplasts) and pigments (chromoplasts) (Pyke, 2009). All plastids are surrounded by an envelope, which consists of two membranes: an outer membrane permeable to small molecules and an inner membrane that constitutes the actual permeability barrier between the plastid stroma and the cytosol (Flugge and Heldt, 1991). Transport proteins within the inner envelope membrane enable controlled exchange of molecules between the plastid stroma and the cytosol (Fig. 1) to integrate plastidic metabolism with that of the rest of the cell (Flugge and Heldt, 1991; Ferro et al., 2003).

Despite the variety of plastid types, these can generally be classified as photosynthetic (chloroplasts) and non-photosynthetic or heterotrophic plastids. Chloroplasts are the best understood of all plastids due to their photosynthetic activity and their ability to fix and supply the carbon to the rest of the plant. Chloroplast structure is highly specialized for photosynthetic activity. Internal thylakoid membranes provide the surface area in which the photosynthetic machinery resides. Stacks of thylakoid membrane, or grana, are held together by electrostatic interactions between the transmembrane protein complexes (Pyke, 2009). The light reactions of photosynthesis lead to acidification of the thylakoid lumen and the resulting proton gradient across the thylakoid membrane which drives ATP synthesis. The stroma is the space between the chloroplast inner membrane and the thylakoid grana. The stroma houses a wide variety

of protein complexes and enzymes, including those responsible for carbon fixation, and is the storage site for starch granules that increase in size during the day.

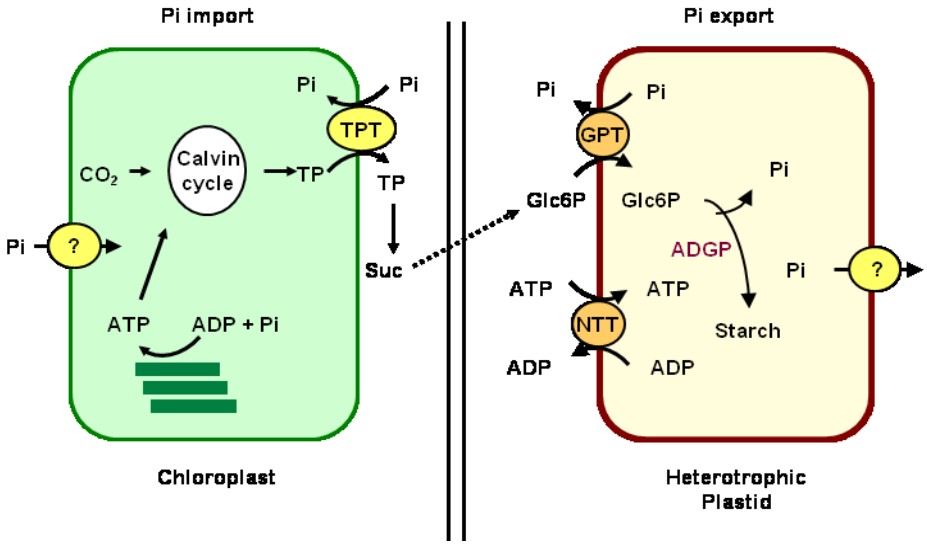

Figure 1. Pi requirements of photosynthetic and heterotrophic plastids. Chloroplasts import Pi from the cytosol in order to synthesize ATP, which then enters the Calvin cycle of carbon fixation. Chloroplasts export both sugars and ATP to be used by heterotrophic tissues. Heterotrophic plastids need to import ATP and sugars as precursors for starch synthesis via the GPT and NTT transporters, respectively. Exchange of ATP/ADP via the NTT transporter results in a net gain of one Pi in the plastid stroma, which is an allosteric inhibitor of ADP-glucose pyrophosphorylase (ADGP). Heterotrophic plastids thus need to export excessive Pi via an unidentified transporter in order to maintain starch synthesis.

Non-photosynthetic plastids such as amyloplasts are found in sink organs like roots, flowers and seeds. Amyloplasts are characterized for their ability to synthesize and

store large amounts of starch that is used as a carbon source to support respiration during the night (Pyke, 2009). Non-photosynthetic plastids cannot fix their own carbon or produce ATP by photophosphorylation. Consequently, such plastids are dependent on the import of both carbohydrates, generally Glc 6-P, and ATP from the cytosol to fuel biosynthetic reactions. These include the synthesis of starch as well as amino acids, fatty acids and purines via the oxidative pentose phosphate pathway (OPPP), hence underlining the importance of communication among different plastid types (Kammerer et al., 1998).

Despite the economic importance of non-photosynthetic plastids as storehouses of starch in grains and tubers of crop plants, our knowledge of their molecular machinery is limited (Pyke, 2009).

Pi regulation of carbon metabolism

Photosynthetic carbon assimilation takes place exclusively in the chloroplasts via the Reductive Pentose Phosphate Pathway or Calvin cycle. Inorganic CO_2 from the atmosphere is assimilated into organic compounds. Triose phosphates (TPs) are the net end products of this process, as illustrated by the following equation (Bassham et al., 1950).

$$3CO_2 + 6H_2O + Pi \rightarrow \text{Triose Phosphate} + 3H_20 + 3O_2$$

TPs further serve as substrates for synthesis of starch and sugars, cell walls, fatty acids and aminoacids (Stitt et al., 2010). In photosynthetic tissues, TP enters the sucrose synthesis pathway in the cytosol and the released Pi is shuttled back into the chloroplast

stroma in exchange for more TP. This recycling of Pi between cytosol and chloroplast maintains a Pi homeostasis on both sides of the chloroplast envelope. Not surprisingly, when cellular Pi levels are altered, a deviation from the normal carbon partitioning is observed. For example, when cytosolic Pi is insufficient, TP export is impaired and there is a simultaneous comparative increase in starch synthesis in the plastid stroma (Sheu-Hwa et al., 1975).

A more detailed description of the role of Pi in modulating carbon partitioning and photosynthesis follows. Chloroplasts at the end of the night have very low levels of starch and soluble sugar; as a result, there is a high TP-to-Pi ratio within the stroma, while in the cytosol this ratio is reversed. Excess TP in the stroma is exported to the cytosol, initiating biosynthesis of sucrose (Suc), which is then exported to sink organs. The demand for Suc in sink tissues is eventually met and the the rate of Suc export and biosynthesis decreases. As a result, less Pi is released from TP and more Pi becomes trapped in organic compounds. The depletion of the cytosolic Pi pool in turn slows TP export from the stroma and reduces stromal Pi levels. This series of events relieves the inhibition of ADGP by high Pi concentration and starch synthesis in the stroma is stimulated. Importantly, starch synthesis effectively recycles Pi from the plastidic organic phosphate pool to be used as substrate for continued ATP synthesis via photophosphorylation, thus partially uncoupling the plastid stroma from Pi supplied from the cytosol (Tegeder, 2006; Stitt et al., 2010). Finally, during the night, the starch synthesized throughout the day is degraded via a phosphorolytic route by the plastidic glucan phosphorylase. This enzyme may also provide hexose phosphates as substrates

for the plastid localized oxidative pentose phosphate pathway (OPPP) during the night (Stitt et al., 2010).

Mechanisms of organ size regulation

Organ size and shape is well defined and tightly regulated by several developmental genetic programs that vary among plant species. Variations in such predetermined size and shape are only slightly affected by environmental factors (Disch et al., 2006; Bogre et al., 2008; Lee et al., 2009).

Cell number and cell size are the primary determinants of a mature organ size. Final cell numbers in a lateral organ, such as a leaf, can be determined by three factors: (1) the rate of cell proliferation; (2) the duration of the cell proliferation and; (3) the number of initial cells in the primordial pool, i.e., cell allocation (Autran et al., 2002). Independent of the factors that determine cell number, lateral organ growth is the result of cell proliferation within a small meristematic zone, where cells are slowly pushed out from the meristems and gradually stop dividing as they continue expanding. This process is divided into two stages: (1) cell proliferation, where new cells increase in mass and divide; and (2) cell expansion, in which cells stop dividing but continue expanding, aided by water intake and loosening of the cell wall. These two stages are generally sequential but there is some overlap (Beemster et al., 2005; Bogre et al., 2008; Krizek, 2009; Massonnet et al., 2010).

Given the complexity of lateral organ size regulation, it is difficult to identify the contributing mechanisms and individual components (Bogre et al., 2008). Moreover,

multiple pathways are responsible for independently controlling cell proliferation and lateral organ size (Gonzalez et al., 2010). Nonetheless, progress has been made in recent years, largely through genetic approaches to study the control of cell proliferation in plants. Several components discovered seem to affect the duration of the cell proliferation stage in lateral organs, although the timing and/or mechanism varies among different pathways. For example, transcription factors such as AINTEGUMENTA (ANT), STRUWWELPETER (SWP), the cytochrome KLUH (KLU), the ubiquitin ligase BIG BROTHER, and the GIF family all affect cell proliferation in a dose-dependent manner. Other genes such as the putative DNA-binding protein PEAPOD, the E3 ubiquitin ligase BIG PETAL and the ubiquitine receptor DA1, negatively regulate cell proliferation in lateral organs (Mizukami and Fischer, 2000; Autran et al., 2002; Disch et al., 2006; White, 2006; Bogre et al., 2008; Li et al., 2008; Lee et al., 2009). Additional factors such as nutrient availability and plant carbon status also influence plant organ growth (Riou-Khamlichi et al., 2000; Bogre et al., 2008; Krizek, 2009). Given the influence of Pi levels in a cell on carbon partitioning, aspects of Pi homeostasis may constitute another pathway to regulate organ size. In fact, mutants that lack the functional chloroplast phosphate transporter protein PHT2;1 develop smaller rosettes than those of wild type plants, indicating that altered Pi contents in the leaves can have pleiotropic effects on leaf growth (Versaw and Harrison, 2002).

CHAPTER II

DIFFERENTIAL EXPRESSION AND PHYLOGENETIC ANALYSIS SUGGEST SPECIALIZATION OF PLASTID-LOCALIZED MEMBERS OF THE PHT4 FAMILY*

Introduction

Dynamic control of stromal Pi levels is central to the specialized metabolic functions of differentiated plastids. Notably, the concentration of Pi in the chloroplast stroma is tightly coordinated with environmental conditions to modulate both photosynthesis and the subsequent partitioning of fixed carbon (Sharkey, 1985; Walker and Sivak, 1986). Pi concentrations in amyloplasts also are held within a critical limit to prevent inhibition of starch biosynthesis (Preiss, 1982). For each plastid type, Pi concentrations are controlled through a combination of metabolic recycling in the stroma and surrounding cytosol, and the transport of Pi across the plastid limiting membrane. Recent data suggest that similar processes also link the Pi status of the chloroplast stroma and thylakoid lumen (Ruiz Pavón et al., 2008).

Plastidic Pi transport is generally attributed to members of the plastidic phosphate translocator (pPT) family (Knappe et al., 2003). These proteins are located in the inner envelope membrane and mediate strict counter-exchange of Pi for phosphorylated C3, C5 or C6 compounds. The triose phosphate/Pi translocator (TPT) was the first pPT protein to be identified, and it is expressed almost exclusively in photosynthetic tissues where it catalyzes transport of cytosolic Pi into the chloroplast in exchange for triose phosphates, the end products of photosynthesis (Flügge et al., 1989). This activity represents the major pathway for carbon allocation to the cytosol during the day as well as the primary route for Pi import into the chloroplast. Besides TPT, other members of the pPT family include the phosphoenolpyruvate/Pi translocator (PPT), glucose 6-phosphate/Pi translocator (GPT) and xylulose 5-phosphate/Pi translocator (XPT) (Fischer et al., 1997; Kammerer et al., 1998; Eicks et al., 2002). In contrast to TPT, these translocators export Pi from plastids in exchange for cytosolic metabolites that serve as precursors for biosynthetic processes within the stroma. Moreover, PPT and XPT are expressed in both photosynthetic and heterotrophic tissues, and GPT expression is restricted to heterotrophic tissues (Flügge, 2003).

Data mining of plant genome sequences coupled with plastid envelope proteomics has revealed additional classes of plastidic Pi transporters that are unrelated to members of the pPT family. PHT2;1 was identified in Arabidopsis based on its similarity with Na^+/Pi symporters from mammals and fungi (Daram et al., 1999). Functional analyses in yeast, however, suggest that PHT2 proteins catalyze H^+-dependent Pi transport (Daram et al., 1999; Versaw and Harrison, 2002; Zhao et al.,

2003). GFP translational fusions with PHT2 proteins from Arabidopsis, *Medicago truncatula*, spinach and potato are targeted to the chloroplast envelope, (Ferro et al., 2002; Versaw and Harrison, 2002; Zhao et al., 2003; Rausch et al., 2004) and localization within the inner envelope membrane is supported by subcellular proteomics and membrane fractionation/immunodetection (Ferro et al., 2002). In addition to a putative role in Pi import into the chloroplast, the presence of *PHT2;1* transcripts within the root stele suggests that the encoded protein also functions in a subset of non-photosynthetic plastids (Rausch et al., 2004).

The Arabidopsis genome also encodes six PHT4 proteins, all of which mediate Pi transport in yeast with high specificity (Guo et al., 2008a). The effects of pH and protonophores on transport activities suggest that PHT4 transporters, like PHT2 proteins, catalyze H^+-dependent Pi transport. Functional studies in *Escherichia coli* suggest that at least one of these, PHT4;1, can also mediate Na^+-dependent Pi transport (Ruiz Pavón et al., 2008). Bioinformatics and localization of PHT4-GFP protein fusions indicate that five members of this family (PHT4;1 through PHT4;5) are targeted to plastids,(Ferro et al., 2003; Roth et al., 2004; Guo et al., 2008a) and the sixth, PHT4;6, resides in the Golgi apparatus (Guo et al., 2008b). Proteomic analysis of the chloroplast envelope and envelope membrane fractionation studies confirmed that PHT4;4 is located in the chloroplast inner envelope membrane (Ferro et al., 2003; Roth et al., 2004; Ruiz Pavón et al., 2008). In contrast, PHT4;1 is located in the thylakoid membrane (Guo et al., 2008b). Despite the localization of these two proteins to chloroplast membranes, transcripts for all of the Arabidopsis *PHT4* genes have been detected in roots as well as

leaves suggesting that the encoded plastid-targeted proteins also function in non-photosynthetic plastids (Guo et al., 2008b). Previous studies have not distinguished whether these transporters are redundant or have unique specificities for different plastid types. Here we present evidence for differences in spatial expression patterns and regulation with respect to light and circadian rhythm, which suggest specialized roles for the encoded Pi transporters in different plastid types and highlight the diversity of plastids that are present in heterotrophic tissues. Moreover, comparative analyses of Arabidopsis and rice PHT4 protein sequences suggest that these transporters and their respective roles are conserved.

Results

Tissue specificity of Arabidopsis *PHT4* genes

To analyze the spatial expression patterns of the *PHT4* genes throughout plant development we used a promoter-reporter strategy in which each promoter was cloned upstream of the β-glucuronidase (GUS) reporter gene (Jefferson et al., 1987). The transcriptional fusion constructs were introduced into Arabidopsis plants, and progeny of the transgenic plants were evaluated for GUS activity using a histochemical assay. *PHT4;1* and *PHT4;4* promoters conferred nearly identical GUS expression patterns. Reporter activity was detected throughout the green tissues of seedlings (Fig. 2A, left), and in sepals of mature flowers (Fig 2B, left). In sections prepared from rosette leaves, GUS activity appeared to be present in all cell types but was not uniformly distributed in

the epidermis (Fig. 2C, right). To examine expression in epidermal cells more directly, we isolated and stained leaf epidermal peels.

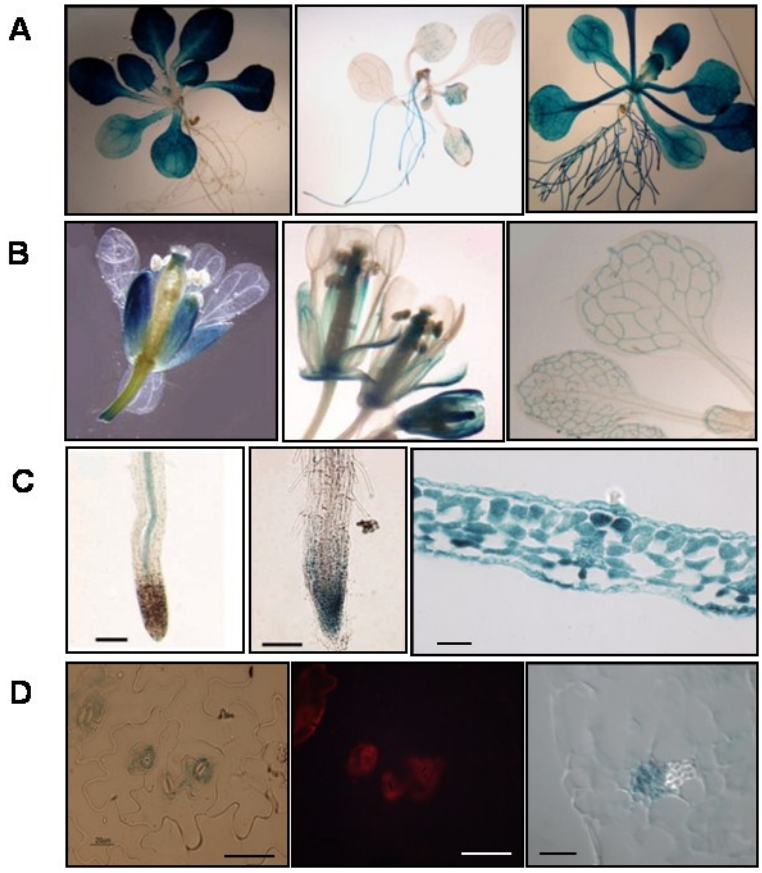

Figure 2. Localization of promoter-GUS gene fusions in transgenic *A. thaliana* plants. A, Seedlings representative of *PHT4;1-GUS* and *PHT4;4-GUS* (left); *PHT4;2-GUS* seedling (center); and *PHT4;6-GUS* seedling (right). B, flower representative of *PHT4;1-GUS*, *PHT4;4-GUS* and *PHT4;5-GUS* (left); *PHT4;4-GUS* flower (center); leaf and cotyledon of *PHT4;3-GUS* and *PHT4;5-GUS*, showing vascular-specific GUS activity (right). C, *PHT4;1-GUS* root (left); *PHT4;3-GUS* root (center); transverse leaf section representative of *PHT4;1-GUS* and *PHT4;4-GUS* plants (right). D, Leaf epidermal peel representative of *PHT4;1-GUS* and *PHT4;4-GUS* plants (left); chlorophyll auto-fluorescence of same epidermal peel (center); transverse leaf section representative of *PHT4;3-GUS* and *PHT4;5-GUS* plants showing GUS activity in phloem (right).

GUS expression was detected only in guard and subsidiary cells (Fig. 2D, left). In all cases, GUS activity co-localized with chlorophyll autofluorescence (red signal, Fig. 2D, center), indicating that *PHT4;1* and *PHT4;4* were expressed predominantly in chloroplasts of photosynthetic cells. GUS activity was, however, also detected at low levels in the root stele of seedlings containing the *PHT4;1* promoter-GUS fusion (Fig. 2C, left). Despite previous detection of *PHT4;4* transcripts in roots by RT-PCR, (Guo et al., 2008a), no GUS activity was detected in roots of plants that carried the *PHT4;4* promoter-GUS fusion. GUS expression driven by the *PHT4;2* promoter was detected throughout the root (Fig. 2A, center), but was not detected in either leaf or floral tissues.

Plants harboring the *PHT4;3* and *PHT4;5* promoter-GUS fusions also exhibited similar expression patterns, but these patterns clearly differed from those directed by the *PHT4;1* and *PHT4;4* promoters. In leaves and cotyledons, GUS expression driven by the *PHT4;3* and *PHT4;5* promoters was restricted to the veins (Fig. 2B, right). Differential interference contrast (DIC) imaging of transverse leaf sections revealed that expression in these organs was limited to the phloem portion of the vascular bundle (Fig. 2D, right). Although tissue specificity for the *PHT4;3* and *PHT4;5* promoters appeared identical in leaves, expression differed in roots and flowers. In roots, weak GUS activity was detected at the root tip in plants carrying the *PHT4;3* promoter-GUS construct (Fig. 2C, center), whereas no activity was detected in roots harboring the *PHT4;5* reporter construct. In flowers, the *PHT4;3* promoter generated no detectable staining, but the *PHT4;5* promoter directed GUS expression that was restricted to sepals, essentially the same pattern seen with the *PHT4;1* and *PHT4;4* promoters (Fig. 2B, left). PHT4;6 is the

only member of the PHT4 family that is targeted to the Golgi apparatus rather than plastids (Guo et al., 2008a). We examined the tissue specificity of this promoter to determine whether *PHT4;6* might serve as a marker for potential heterogeneity of Golgi functions in different plant tissues. No such specificity was observed. GUS activity was detected in every part of transgenic seedlings (Fig. 2A, right), as well as sepals, stamens and carpels of mature flowers (Fig. 2B, center).

Light and circadian control of *PHT4* gene expression

TPT and *PHT2;1* are expressed primarily in photosynthetic tissues, and their expression is induced by light (Schulz et al., 1993; Versaw and Harrison, 2002; Rausch et al., 2004). To determine whether light also influences expression of *PHT4* genes, we used quantitative RT-PCR to monitor transcript levels in rosette leaves of 3-wk-old plants that had been held in the dark for 3 d and at defined time points after re-exposure to light (Fig. 3). *PHT2;1* served as a positive control for light-induced expression (Versaw and Harrison, 2002; Rausch et al., 2004). As expected, *PHT2;1* transcript levels increased rapidly after exposure to light. *PHT4;1* and *PHT4;4* transcript levels also increased during the 7 hr light treatment, 20-fold and 10-fold, respectively, although transcripts for both genes accumulated only after a 3 hr lag. In contrast, the light treatment had no obvious effect on expression of *PHT4;3*, *PHT4;5* or *PHT4;6*. Transcript levels for *PHT4;2* were extremely low, i.e., maximum levels were less than 2% of the lowest value obtained for the other genes (data not shown). This low expression was consistent with promoter-GUS results indicating that *PHT4;2* is

expressed almost exclusively in roots (Fig. 2A). Consequently, we evaluated *PHT4;2* transcript levels in roots harvested from the same plants. As shown in Fig. 4, *PHT4;2* transcript levels decreased nearly 80% during the light treatment, and like *PHT4;1* and *PHT4;4*, the change in transcript abundance occurred only after a 3 hr lag.

Although *PHT2;1* expression is not under circadian control, (Sharkey, 1985; Knappe et al., 2003) it was possible that the changes in *PHT4;1*, *PHT4;4* and *PHT4;2* transcript levels during the light treatment (Fig. 3) reflect rhythmic expression rather than a response to light. To distinguish between these possibilities, transcript levels in rosette leaves of 3-wk-old plants maintained with a 14 hr light: 10 hr dark cycle (LD) were compared to those in plants that had been transferred to constant light (LL). Plants were harvested at time points corresponding to the midpoint and end of the subjective light and dark phases of two consecutive diurnal cycles. As shown in Fig. 4, *PHT4;1* and *PHT4;4* both exhibited a diurnal expression pattern under LD conditions, but this rhythmic pattern persisted in LL only for *PHT4;1*. Thus, *PHT4;1* exhibits a circadian expression pattern with peak expression during the light phase of the diurnal cycle.

Consistent with this circadian pattern, two copies of the CIRCADIAN CLOCK ASSOCIATED 1-binding site (CBS: AAAAATCT), which is important for morning specific circadian expression, (Wang et al., 1997; Michael and McClung, 2002) are located in the *PHT4;1* promoter. One CBS is located -17 bp relative to the translation start, and the other is located -281 bp and is on the complementary strand. No CBS motifs were found in the promoters of the other *PHT4* genes.

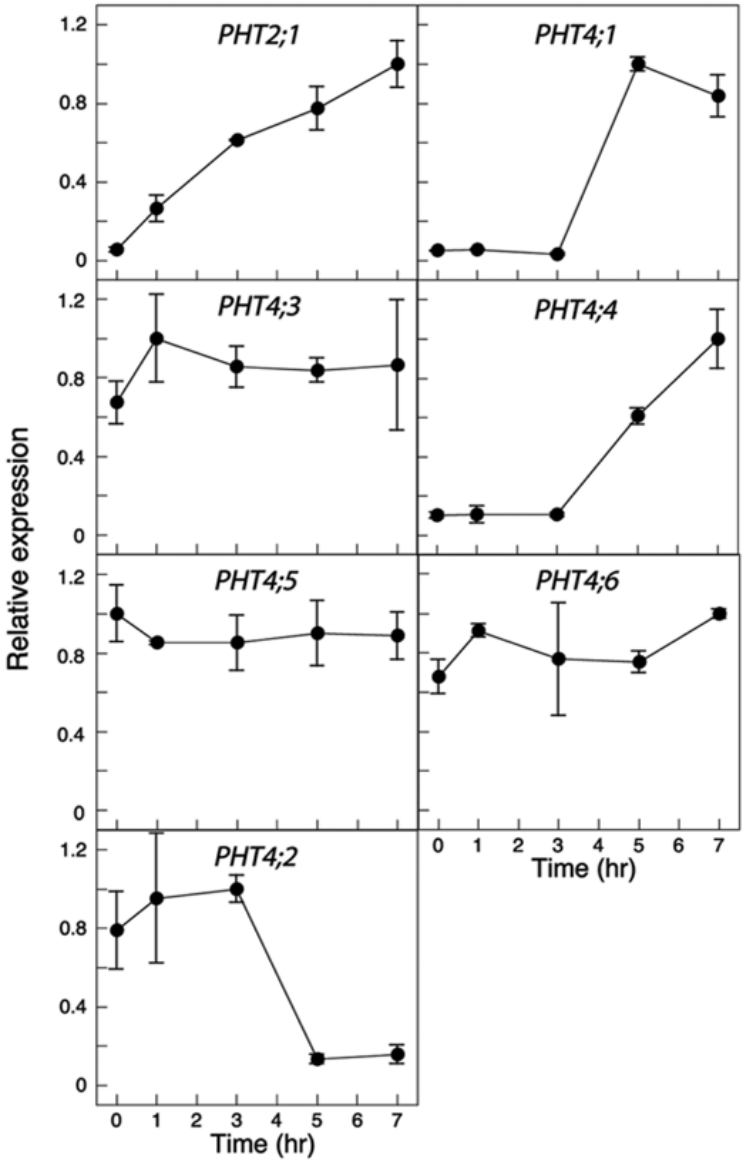

Figure 3. Effect of light on expression of *PHT4* genes. Mature plants were held in the dark for 3 d before re-exposure to light. Expression levels were determined at the indicated time points by quantitative RT-PCR and normalized to *EIF-4A2*. The values plotted are averages of two biological replicates, and error bars indicate the replicate values. For analysis of *PHT4;2*, RNA was isolated from root tissues. For all other genes, RNA was isolated from rosette leaves. *PHT2;1* serves as a positive control for light induction.

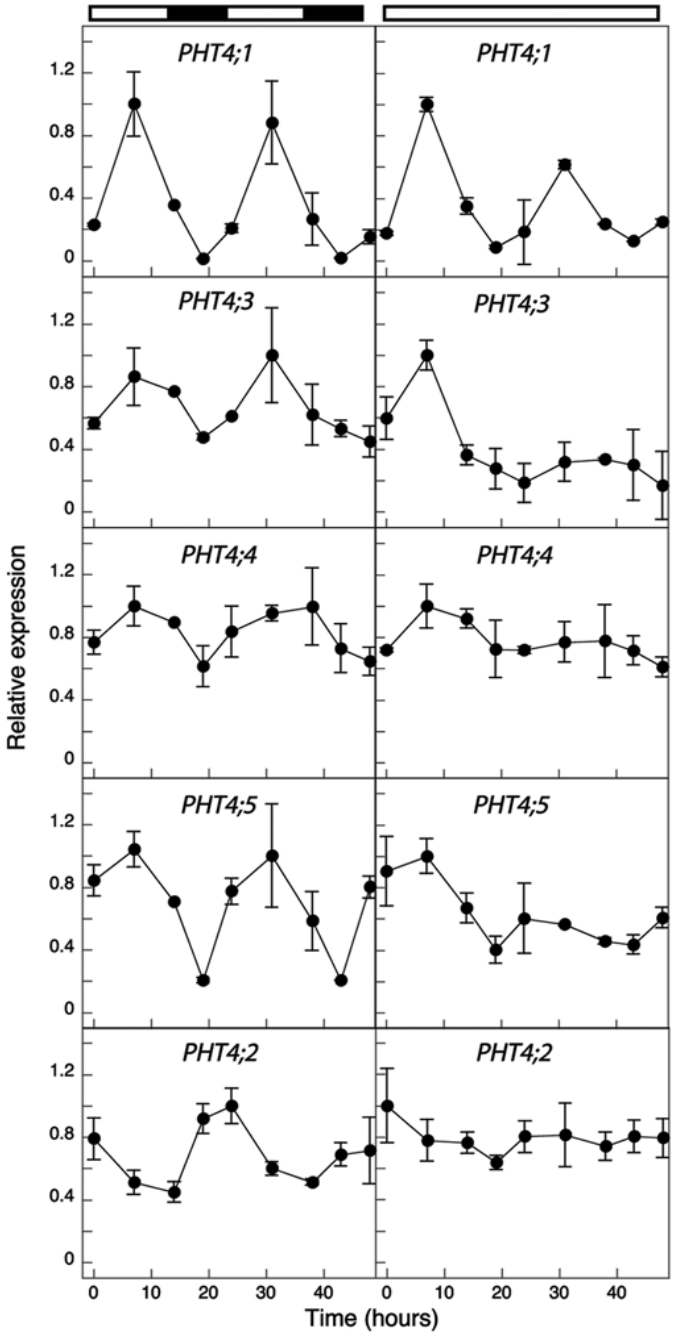

Figure 4. Expression of *PHT4* genes under light/dark and constant light conditions. Expression levels were measured at the indicated times by qRT-PCR and normalized to *EIF-4A2*. The values plotted are averages of two biological replicates, and error bars indicate the replicate values. The light and dark bars at the top of the figure indicate the respective light conditions. For analysis of *PHT4;2*, RNA was isolated from root. For all other genes, RNA was isolated from rosette leaves.

In contrast to the circadian expression of *PHT4;1*, expression of *PHT4;4* appears to be induced by light, both after a long dark period (Fig. 3) and in standard LD conditions (Fig. 4). *PHT4;3* and *PHT4;5* transcript levels, which were unaffected by light exposure treatment after a long dark treatment (Fig. 3), varied with the light/dark cycle in LD but not under LL conditions (Fig. 4). Transcripts for all three of these genes were more abundant in the light than dark.

To determine whether *PHT4;2* expression also exhibited a diurnal pattern, we compared transcript levels in roots of plants grown under LD and LL conditions. As shown in Fig. 4, transcript levels appeared rhythmic in LD with a 2.5-fold difference between the light and dark. However, the phase of this rhythm was opposite to those of the other genes. That is, *PHT4;2* transcripts were more abundant in the dark than light. This expression pattern did not persist in LL suggesting that the pattern in LD is related to exposure of the plant tissues to light rather than circadian control.

Conservation of the PHT4 family in Arabidopsis and rice

Searches of the GenBank sequence database revealed putative PHT4 homologs in multiple plant species, including rice, tomato, maize, grape and barley, suggesting that these transporters are widely conserved. However, it is difficult to determine orthology because this gene family may have undergone differential expansion in each species. The availability of the complete genome sequences for Arabidopsis and rice allowed us to address this issue for two distantly related plant species. We identified seven protein sequences through searches of the TIGR rice genome database (http://rice.tigr.org/)

(Yuan et al., 2005) that shared 70–80% similarity to Arabidopsis PHT4 proteins. Iterative searches with the rice sequences revealed no additional homologs, indicating that these seven proteins comprise the rice PHT4 family.

To estimate the phylogenetic relationship between the Arabidopsis and rice proteins, the sequences were aligned with ClustalX and M-Coffee, (Moretti et al., 2007) and neighbor joining was used to generate an unrooted phylogram (Fig. 5). The topology of this phylogram is supported by 100% bootstrap values. Furthermore, maximum parsimony analysis with the same alignments yielded trees with identical topologies (not shown). Six groups of proteins are inferred from the phylogram, each consisting of a single Arabidopsis protein and, in all but one group, a single orthologous rice protein. The exception was the group containing PHT4;6, which includes two paralogous rice sequences. The presence of both Arabidopsis and rice proteins in each group indicates that divergence of the PHT4 family occurred prior to the divergence of monocots and dicots. Like the Arabidopsis PHT4 proteins, all of the rice orthologs have poorly conserved, N-terminal sequences that share features with organellar targeting sequences. Predictions of the subcellular localization of these proteins using TargetP, (Emanuelsson et al., 2007) as well as consensus predictions derived from multiple other programs (ARAMEMNON database, http:aramemnon.botanik.uni-koeln.de/), suggest that each rice protein is targeted to the same organelle as its corresponding Arabidopsis ortholog.

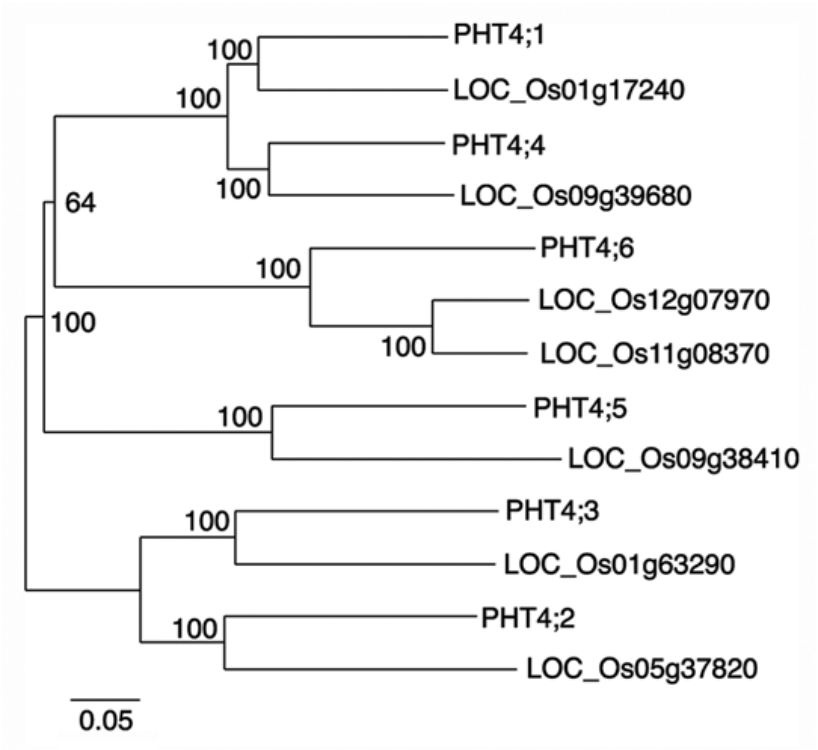

Figure 5. Neighbor joining tree of *A. thaliana* and rice PHT4 Pi transporter proteins. Rice sequences are indicated by TIGR locus assignments. The numbers at the nodes of the trees are bootstrap values (1,000 replicates). Scale bar indicates substitutions per site.

Discussion

Phylogenetic analysis suggests that members of the PHT4 Pi transporter family diverged prior to the monocot-dicot split that is estimated to have occurred 140–150 Myr ago (Chaw et al., 2004). Surprisingly, all six of the ancestral members have been preserved in Arabidopsis and rice, and only one ortholog appears to have undergone duplication. This level of conservation was unexpected given that multiple, large-scale

duplication and deletion events have occurred since the divergence of monocots and dicots (Simillion et al., 2002; Paterson et al., 2004). Indeed, a similar analysis of PHT1 Pi transporters revealed orphan homologs in both Arabidopsis and rice, as well as differential expansion of ancestral orthologs (Paszkowski et al., 2002). The simplest explanation for the conservation of individual PHT4 orthologs is that each has unique physiological roles. The overlapping but distinct expression patterns for the Arabidopsis genes support this hypothesis.

The *PHT4;1* promoter was active predominantly in photosynthetic tissues, and in the leaf epidermis, activity was restricted to cells that contain chlorophyll. This tissue and cell specificity is consistent with the recent finding that the protein is targeted to the chloroplast thylakoid membrane (Ruiz Pavón et al., 2008). This location positions PHT4;1 for a role in recycling Pi from the thylakoid lumen to the stroma. Pi is generated in the thylakoid lumen through hydrolysis of nucleotides, including the PsbO-mediated hydrolysis of GTP, which regulates dephosphorylation and turnover of the photosystem II reaction center D1 protein (Lundin et al., 2007a; Lundin et al., 2007b). Coordination of PHT4;1 activity with D1 protein turnover is an intriguing possibility given that the prerequisite events, expression of *PHT4;1* and phosphorylation of the D1 protein, are both controlled by a circadian rhythm with peak activities in the light (Booij-James et al., 2002). Circadian regulation is critical for many aspects of photosynthesis and plant growth, (Dodd et al., 2005) but to our knowledge, this is the first example of circadian control of a plant Pi transporter gene.

The stimulatory effect of low pH on Pi transport catalyzed by PHT4;1 in heterologous systems would favor export of Pi from the acidic lumen (Ruiz Pavón et al., 2008; Guo et al., 2008a). However, at this time we cannot rule out the possibility that PHT4;1 transports stromal Pi into the lumen. It has been suggested that if such an activity sequesters stromal Pi below the Km of the thylakoid ATP synthase, the resulting decrease in proton conductivity could serve as a means of down regulating photosynthetic light capture (Ruiz Pavón et al., 2008; Takizawa et al., 2008).

The *PHT4;1* promoter also exhibited weak activity in the root stele (Fig. 3B), which corroborates previous results indicating that endogenous transcripts are present in roots at low levels (Guo et al., 2008a). The physiological significance of this expression is unclear because root plastids have limited internal membranes, (Usami et al., 2004) and the metabolic contributions of plastids within the root stele have not been defined. We hypothesize that the internal membranes of these plastids represent a metabolically active compartment and that PHT4;1 is involved in its Pi homeostasis.

Chloroplasts rely on the import of Pi from the cytosol to support the synthesis of ATP through photophosphorylation and to control the subsequent partitioning of fixed carbon. Pi import is mediated mainly by TPT with strict counter-exchange of stromal triose phosphates (Fliege et al., 1978). Surprisingly, plants with reduced levels of TPT have no substantial growth phenotype or reduction in photosynthetic capacity when grown under ambient conditions (Riesmeier et al., 1993; Barnes et al., 1994; Heineke et al., 1994; Häusler et al., 1998; Schneider et al., 2002; Walters et al., 2004). Such plants do, however, exhibit increased rates of starch turnover and export of neutral sugars to

compensate for the defect in carbon allocation, which suggests that redundant or compensatory mechanisms also exist for the coupled defect in Pi import. PHT4;4 and PHT2;1 are candidates for this activity. Like TPT, both of these Pi transporters are located in the chloroplast inner envelope membrane (Ferro et al., 2002; Roth et al., 2004). Also, transcript levels for the genes increased when plants were exposed to light, although the delay in *PHT4;4* transcript accumulation may reflect regulation by photosynthates rather than a direct response to light. It is formally possible that PHT4;4 and PHT2;1 also maintain stromal Pi concentrations through export. That is, these transporters may serve as two-way valves with transport direction dependent on the Pi electrochemical gradient and proton-motive force. Experimental evaluation of this hypothesis is needed, although such flexibility would enable the fine control of stromal Pi levels, necessary to sustain high rates of transitory starch synthesis.

Unlike chloroplasts, non-photosynthetic plastids cannot synthesize ATP or precursor metabolites for anabolic processes such as the synthesis of starch, fatty acids and amino acids (Neuhaus and Emes, 2000). The import and subsequent assimilation of these compounds can lead to an imbalance in stromal Pi, which must be countered by a Pi export activity that is not directly coupled to the transport of phosphorylated carbon compounds, i.e., unidirectional Pi transport (Neuhaus and Maass, 1996). Several of the PHT4 transporters, as well as PHT2;1, may contribute to this role in different heterotrophic tissues. In roots, GUS activity driven by the *PHT4;2* promoter was observed throughout the entire organ, whereas expression under the control of the *PHT4;3* and *PHT2;1* promoters was restricted to the root cap and stele, respectively.

These expression patterns suggest that PHT4;2 functions in all root plastids and that Pi transport catalyzed by PHT4;3 and PHT2;1 may be needed to supplement that of PHT4;2 in distinct plastid types, including amyloplasts in root cap columella cells. Although PHT4;4 and PHT4;5 transcripts have been detected in roots by RT-PCR (Guo et al., 2008a) and the corresponding promoter-GUS lines described here exhibited strong activity in green tissues, no GUS activity was detected in roots. This suggests that *PHT4;4* and *PHT4;5* are expressed in root tissues at levels below the limit of detection by histochemical staining, and therefore, may have limited roles in root plastids.

Non-photosynthetic plastids occur in the sieve elements and companion cells that comprise phloem (Behnke, 1973; Behnke, 1991). Promoter-GUS fusions used in this study revealed that *PHT4;3* and *PHT4;5* were expressed in the phloem tissue of leaves and cotyledons, but not roots. Expression of both *PHT4;3* and *PHT4;5* in leaves was diurnal with transcripts more abundant in the light. Transcript abundance was not induced by light after a 3 d dark treatment suggesting that the diurnal pattern may be related to instability of the transcripts in the dark. Little has been reported on the metabolic functions of phloem plastids, although they may be the primary sites of tryptophan biosynthesis, (Lu and McKnight, 1999), and at least some of these plastids accumulate starch (Behnke, 1991). Given that amino acid and starch synthesis are ATP-consuming and Pi-liberating processes, we hypothesize that PHT4;3 and PHT4;5 contribute to Pi export from phloem plastids.

In summary, the results of this study have revealed differences in the spatial expression patterns and regulation of the plastid-localized members of the Arabidopsis PHT4 Pi transporter family. These differences provide some insight into the potential roles of these proteins in chloroplasts and in an unexpectedly wide range of non-photosynthetic plastids in root and phloem tissues. The remarkable similarity of the PHT4 family structure between Arabidopsis and rice suggests that the roles for the individual family members have been conserved since the divergence of monocots and dicots.

Methods

Plant growth conditions

Arabidopsis thaliana (L.) Heynh. (Col-0) plants were grown in chambers at 21˚C with 70% relative humidity and, unless specified otherwise, a 14 h light (150 μmol m-2 s-1): 10 h dark photoperiod. Plants were grown in soil for general propagation. For gene expression studies, plants were grown hydroponically or on agar-solidified, half-strength MS medium (Murashige and Skoog, 1962) as described previously (Guo et al., 2008a)

Construction and analysis of *PHT4* promoter-GUS fusions

Promoters for each *PHT4* gene were amplified from Arabidopsis genomic DNA using Pfx high-fidelity polymerase (Invitrogen, Carlsbad, CA) then cloned in the binary vector pBI101.1 upstream of the β-glucuronidase (GUS) gene to generate transcriptional fusions. Promoter sequences correspond to the region immediately upstream of the respective ATG start codons: 1000 bp for *PHT4;1*, *PHT4;2*, *PHT4;3* and *PHT4;4*, 623 bp for *PHT4;5*, and 1682 bp for *PHT4;6*. The *PHT4;5* promoter extends to the stop codon of the neighboring gene (At5g20390). Promoter-GUS constructs were introduced into *Agrobacterium tumefaciens* strain GV3101, and the resulting strains were used to transform Arabidopsis via the floral dip procedure (Clough and Bent, 1998). Transgenic seedlings were selected on half-strength MS medium containing 25μg ml^{-1} kanamycin.

At least 12 independent lines for each construct were examined for GUS activity by histochemical detection (Jefferson et al., 1987; Vitha et al., 1995). Briefly, seedlings were vacuum infiltrated with assay buffer (50 mM sodium phosphate pH 7.0, 0.1% (v/v) Triton X-100, 0.5 mM potassium ferrocyanide, 0.5 mM potassium ferricyanide, 10 mM EDTA) containing 0.05% (w/v) 5-bromo-4-chloro-3-indolyl glucuronide (X-gluc) then incubated in the dark at 37˚C overnight. Green tissues were de-stained with 70% ethanol prior to observation. To prepare sections, tissues were briefly fixed in 4% formaldehyde prior to staining. After staining, tissues were fixed in assay buffer containing 4% formaldehyde and 0.5% glutaraldehyde then dehydrated in an ethanol series and

embedded in Steedman's wax (polyethylene glycol 400 distearate/ 1-hexadecanol, [9:1, w/w]) (Steedman, 1957). Embedded tissue was cut into 10 μm sections using a rotary microtome.

Quantitative RT-PCR analysis

Total RNA was isolated from rosette leaves or roots of 3-wk-old plants with TRI reagent (Sigma- Aldrich, St. Louis, MO), and traces of DNA were removed with TURBO DNA-free (Ambion, Austin, TX). Two biological replicates consisting of tissues pooled from two plants were used for each analysis. One microgram of RNA was used to make cDNA with SuperScript first-strand cDNA synthesis kit (Invitrogen, Carlsbad, CA). PCR was performed with Power SYBR Green Master Mix (Applied Biosystems, Foster City, CA) using the ABI Prism 7500 sequence detection system (Applied Biosystems). Expression levels were normalized to *EIF-4A2* (At1g54270) and fold changes were calculated using the ΔΔCT method. Primers used for quantitative PCR were described previously (Guo et al., 2008a).

CHAPTER III

THE SINK-SPECIFIC PLASTIDIC PHOSPHATE TRANSPORTER PHT4;2 INFLUENCES CARBON PARTITIONING AND CELL PROLIFERATION IN *ARABIDOPSIS THALIANA*

Introduction

Unlike chloroplasts, nonphotosynthetic plastids cannot synthesize the ATP needed to fuel anabolic processes within these organelles, which include biosynthesis of starch, fatty acids and amino acids (Neuhaus and Emes, 2000). Metabolism in such plastids, therefore, is dependent on the import of ATP from the cytosol. Nucleotide transporters (NTTs), located in the plastid inner envelope fulfill this energy requirement by catalyzing the stoichiometric exchange of cytosolic ATP for stromal ADP (Reiser et al., 2004; Reinhold et al., 2007). A consequence of the unbalanced phosphate moieties associated with this exchange is that inorganic phosphate (Pi) would accumulate to deleterious levels within the stroma if not countered by Pi export. Despite the fundamental importance of Pi homeostasis to plastid functions and, in turn, to plant growth and development, the identity of the transporter(s) responsible for this activity has been elusive.

In addition to ATP/ADP exchange, NTTs can accept Pi as a third substrate to transport Pi-Pi homo-exchange or to co-transport Pi plus ADP in exchange for ATP (Trentmann et al., 2008). Although the latter activity would preclude the necessity for a distinct Pi transporter, studies with cauliflower bud amyloplasts revealed Pi export

activity in the absence of potential counter-exchange substrates, i.e., unidirectional transport, indicating that transporters other than NTTs contribute to net Pi export (Neuhaus and Maass, 1996).

Plastid-localized Pi transport systems identified to date include members of the plastidic Pi translocator (pPT), PHT2 and PHT4 families. pPTs catalyze exchange of Pi with phosphorylated compounds, and therefore would not support net Pi export (Flügge, 1999; Eicks et al., 2002). In contrast, members of the PHT2 and PHT4 families mediate H^+- and/or Na^+-dependent Pi transport (Daram et al., 1999; Versaw and Harrison, 2002; Zhao et al., 2003; Ruiz Pavón et al., 2008; Guo et al., 2008a). The role of these transporters in nonphotosynthetic plastids is unclear. Gene expression studies suggest that all of these transporters are present in limited types of heterotrophic tissues, but most are expressed predominantly in autotrophic tissues (Rausch et al., 2004; Guo et al., 2008a). *PHT4;2* is the sole exception to this expression pattern as its transcripts are nearly restricted to roots (Guo et al., 2008a).

In this study, we used *A. thaliana* mutants that lack a functional copy of the *PHT4;2* gene to gain insight into the roles of the encoded transporter in plastid and whole plant physiology. We confirmed that PHT4;2 contributes to Pi transport in isolated root plastids, and found that starch accumulation is reduced in both roots and leaves of the mutant plants. We also discovered a surprising conditional growth phenotype in which rosette leaves of *pht4;2* mutants were larger than those of wild type when plants were grown with a short (8 h) photoperiod, and increased cell proliferation accounted for the greater leaf area and biomass.

Mature leaf size is an intrinsic trait that is a function of both the size and number of cells in the organ. The mechanisms that control final leaf size are poorly understood. In some cases, a reduction in cell number through mutation or transgenes is offset by a compensatory increase in cell size (Hemerly et al., 1995; De Veylder et al., 2001; Horiguchi et al., 2006). In contrast, a number of modifiers of leaf size have been identified that primarily affect cell number, but these represent diverse functional classes, including transcriptional regulation, auxin signaling, protein synthesis and DNA replication (for review, see (Gonzalez et al., 2009; Krizek, 2009). A recent comparative analysis of a subset of these modifiers confirmed that multiple independent pathways contribute to the control of cell proliferation in leaves (Gonzalez et al., 2010). Because none of the previously described modifiers of leaf size appear to be involved in plastid functions, and because *PHT4;2* expression during vegetative growth is restricted to roots, the effect of *pht4;2* mutations on cell proliferation suggests novel signaling between roots and developing leaves that also contributes to the regulation of leaf size.

Results

***PHT4;2* is expressed in carbon-sink tissues**

We reported previously that *PHT4;2* expression was restricted to roots and exhibited a diurnal but not circadian pattern in which transcript abundance was greater in the dark than the light (Guo et al., 2008a).

Expression data in the Genevestigator microarray database (Hruz et al., 2008) support these patterns and suggest that *PHT4;2* is also expressed in floral tissues. To investigate spatial expression in greater detail, a *PHT4;2* promoter-GUS transcriptional fusion construct was introduced into Arabidopsis and GUS activity was assessed in progeny of the transgenic plants. To maximize expression, plants were grown with a short (8 h) photoperiod.

As expected, GUS activity was readily detected in roots but not in leaves (Fig. 1A). GUS activity was also detected in sepals, stamens and carpels, as well as silique valves and septum (Fig. 6A), but not in the mature seeds. Quantitative RT-PCR analysis of *PHT4;2* transcripts in wild-type plants corroborated these findings and indicated that expression was greatest in roots, followed by intermediate levels in flowers and siliques, and barely detectable levels in rosette and cauline leaves (Fig. 6B). These results extend our previous studies to suggest that in addition to roots, *PHT4;2* is broadly expressed in carbon import-dependent sink organs.

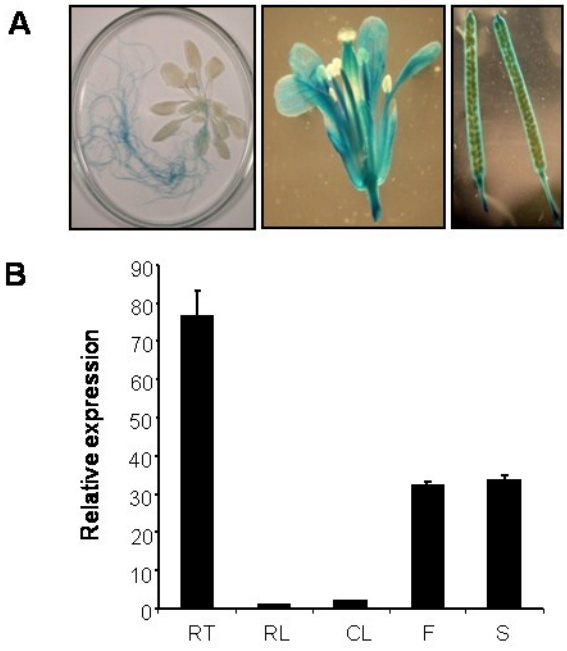

Figure 6. Localization of *PHT4;2*-GUS expression in transgenic *A. thaliana* plants. A, Representative 5-wk-old plant (left), flower (center) and mature siliques (right). B, Quantitative RT-PCR analysis of *PHT4;2* expression in different organs (RT, root; RL, rosette leaf; CL, cauline leaf; F, flower; S, silique). *PHT4;2* expression levels were normalized to *EIF-4A2*. Values shown are mean ± SE for three independent analyses.

Identification of *pht4;2* T-DNA insertion mutants

To obtain insight into the role of PHT4;2 in plastid function and overall plant metabolism, we required mutants that lacked a functional *PHT4;2* allele. We obtained two independent T-DNA insertion lines from the SALK collection (Alonso et al., 2003), SALK_019289 (*pht4;2-1*) and SALK_070992 (*pht4;2-2*). Insertions were confirmed by PCR and sequencing of amplicons that spanned the insertion junctions. The *pht4;2-1* line

has a tandem T-DNA insertion 2170 bp downstream of the translation start site, and a 7 bp deletion at the insertion site. The *pht4;2-2* line has a single T-DNA inserted within the first intron, 738 bp downstream of the translation start site, and also has a deletion of 4 bp at the insertion site. The structures of the mutant loci are represented in Fig. 7A.

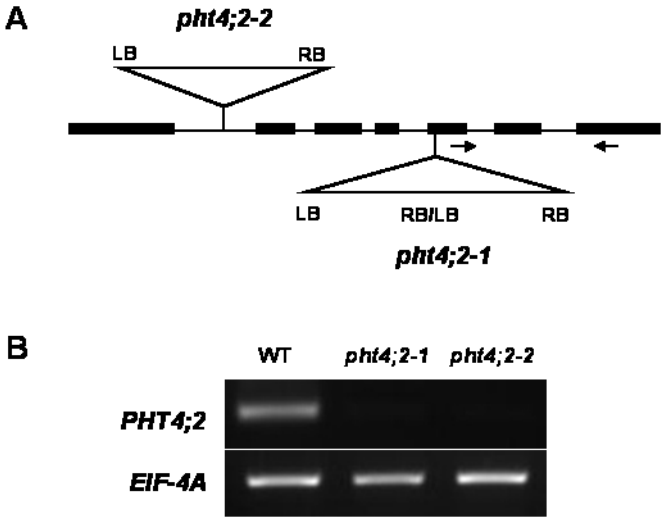

Figure 7. Molecular characterization of *pht4;2* T-DNA insertion mutants. A, Scheme indicating the positions of T-DNA insertions in *pht4;2-1* and *pht4;2-2* lines. Insertions were confirmed by PCR and DNA sequence. Arrows represent primers used for RT-PCR. B, RT-PCR analysis of total RNA isolated from roots of wild-type and *pht4;2* plants.

Homozygous mutant lines were identified by PCR then screened by DNA gel blot for the presence of additional insertions (Figures 8 and 9). At least one backcross to

wild type was required to segregate ectopic insertions from the genetic backgrounds. Only homozygous mutants that lacked ectopic insertions were used in subsequent studies. RT-PCR analysis of root RNA using primers that anneal downstream of the insertion sites revealed no *PHT4;2* transcripts in the homozygous mutants suggesting that both mutant alleles are null (Fig. 7B).

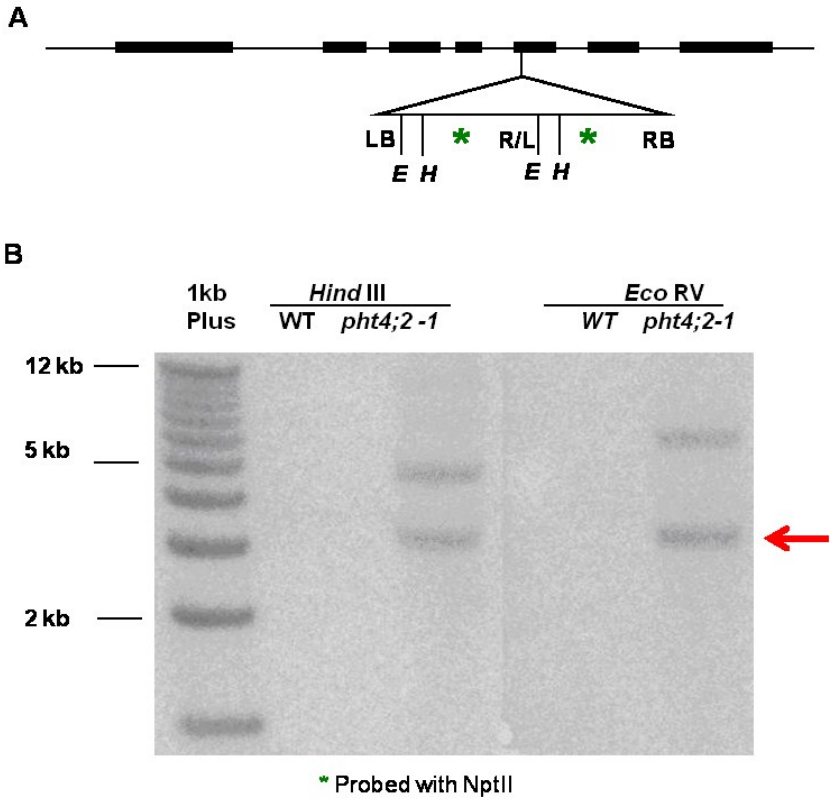

Figure 8. Molecular characterization of *pht4;2-1* T-DNA insertion mutants. A, diagram indicating the position of restriction enzymes used relative to the T-DNA insertion. B, Southern hybridization results indicate fragment corresponding to internal T-DNA (red arrow) and fragment resulting from T-DNA and genomic DNA. Green asterisk represents nptII probe.

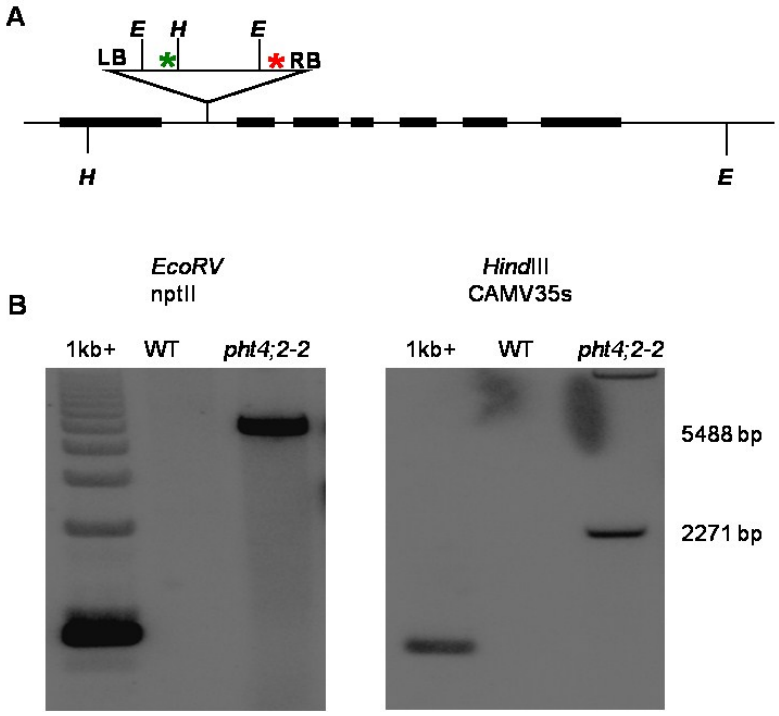

Figure 9. Molecular characterization of *pht4;2-2* T-DNA insertion mutants. A, diagram indicating the position of restriction enzymes and probes used relative to the T-DNA insertion. B, Southern hybridization results indicate the presence of a single insertion event at this position. Green asterisk represents nptII probe, red asterisk represents *CaMV35S* probe.

Localization of PHT4;2 to root plastids

To confirm localization of the endogenous PHT4;2 protein to root plastids, intact plastids were isolated from roots of hydroponically-grown wild-type Arabidopsis, and the proteins were subjected to immunoblot analysis. As shown in Fig. 10A, a single 45 kDa band reacted with the antibody. The signal intensity varied in proportion to the amount of total protein loaded in the well, and no reaction was detected when the

corresponding pre-immune serum was used, indicating that the antibody is highly specific. No reacting proteins were detected in leaf chloroplasts (data not shown), in accord with transcript localization results (Fig. 6).

Immunoblot analysis was also carried out with plastids isolated from roots of *pht4;2* mutants. Equal amounts of total plastid protein (15 μg protein per lane) from wild type and each mutant were evaluated. The 45 kDa band was detected in the wild-type preparation but in neither of the mutants (Fig. 10B), which further verified that the mutations are null.

We noted that the molecular mass of PHT4;2 estimated from its mobility in SDS-PAGE was lower than that expected from its composition. *PHT4;2* encodes a 512 aa protein (UniProt Q7XJR2) that is predicted by TargetP (Emanuelsson et al., 2007) to include an N-terminal 44 aa transit peptide. The theoretical molecular mass of the processed protein is 50.5 kDa. Two other members of the PHT4 family, PHT4;1 and PHT4;4, also exhibit anomalous migration in SDS-PAGE (Roth et al., 2004; Ruiz Pavón et al., 2008). The significance of these gel migration patterns is unclear and may be related to detergent-binding features typical of membrane proteins (Rath et al., 2009).

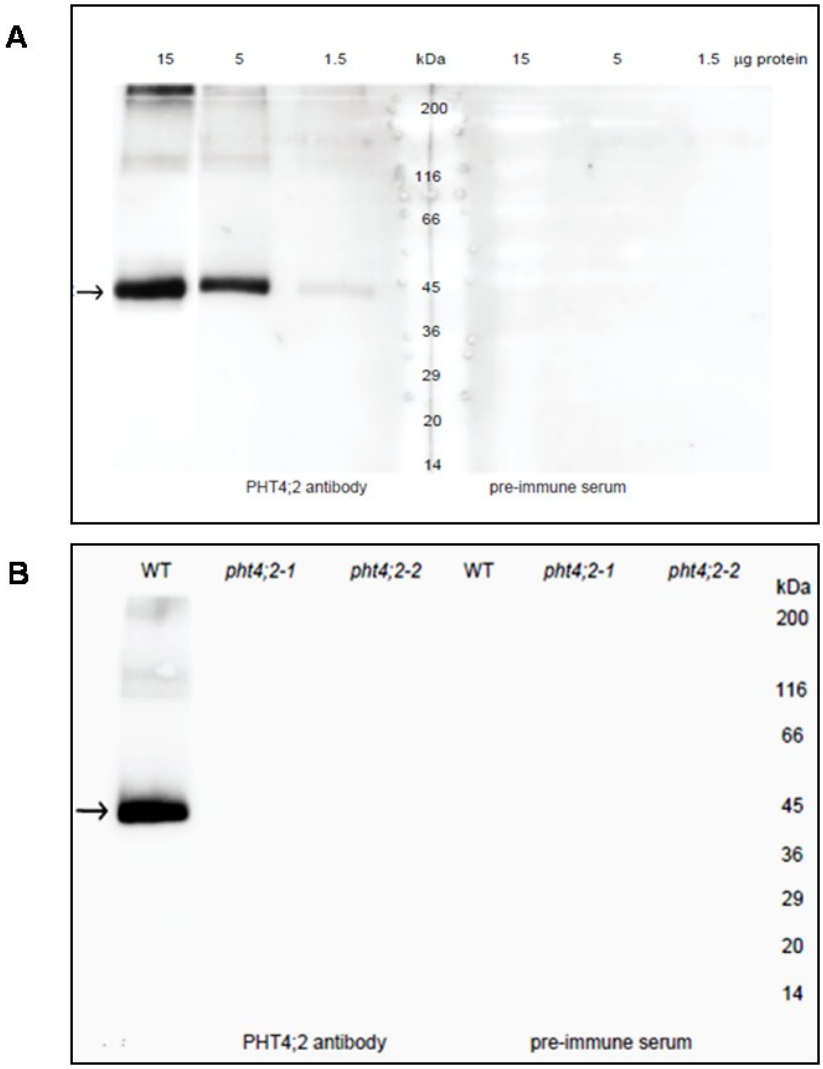

Figure 10. Localization of PHT4;2 to root plastids. A, Immunoblot of proteins isolated from wild-type root plastids using a peptide-specific antibody and pre-immune serum. B, Western blot of wild-type and pht4;2 root plastid proteins (15 mg protein/lane) with antibody and pre-immune serum. Molecular mass markers are indicated, and the position of PHT4;2 is marked with an arrow. (Figure by Cornelia Spetea and Jacob Kuruvilla).

Pi transport in isolated root plastids

Previous studies indicated that PHT4;2, as well as the other five members of the Arabidopsis PHT4 family, mediate Pi transport that is dependent on the presence of a H^+ electrochemical gradient when expressed in yeast (Guo et al., 2008a). Interestingly, one of these same proteins, PHT4;1, was found to catalyze Na^+-dependent Pi transport when expressed in *E. coli* (Ruiz Pavón et al., 2008). Thus, different heterologous systems, perhaps due to differences in membrane lipid composition and cell physiology, impart or reveal unique qualities of the Pi transport process. Here we have taken advantage of the availability of knockout lines to study PHT4;2 in its native context of root plastids.

Plastids isolated from roots of hydroponically-grown wild-type and *pht4;2* plants were equivalent with respect to intactness (70-75%), specific activity of the plastid marker nitrite reductase (NiR) and contamination by other organelles (Table I). Microbial contamination of plastid fractions, which was assessed by growth on LB agar medium, was also similar with 200-250 colony forming units/mg protein, which corresponds to a low number of microbial cells (6 to 8) in samples used for Pi transport measurements. Pi uptake by root plastids was linear for 60 s regardless of genotype, but the rate of transport measured with wild-type plastids was twice that of plastids isolated from *pht4;2* mutants (Fig. 11). Because the purity and enrichment of root plastids were equivalent, we attribute the reduced transport rates with mutant plastids solely to the absence of PHT4;2.

Table I. Distribution of organelle marker enzyme activities in isolated root plastids.
Yields are defined as the percentage of activity in the crude extract, and specific activities as units/mg protein. Mean values ± SE of three independent determinations.

	Wild type		*pht4;2-1*		*pht4;2-2*	
	Yield (%)	Specific activity	Yield (%)	Specific activity	Yield (%)	Specific activity
NiR (plastid)	6.91 ± 0.52	2.55 ± 0.87	7.73 ± 1.01	2.41 ± 0.97	7.46 ± 0.36	2.13 ± 0.01
NADH-MDH (mitochondrion, cytosol, peroxisome)	0.33 ± 0.21	0.23 ± 0.07	0.39 ± 0.32	0.49 ± 0.10	0.44 ± 0.05	0.23 ± 0.16
α-Mannosidase (vacuole)	0.56 ± 0.03	0.18 ± 0.04	0.86 ± 0.61	0.19 ± 0.14	0.55 ± 0.07	0.14 ± 0.01

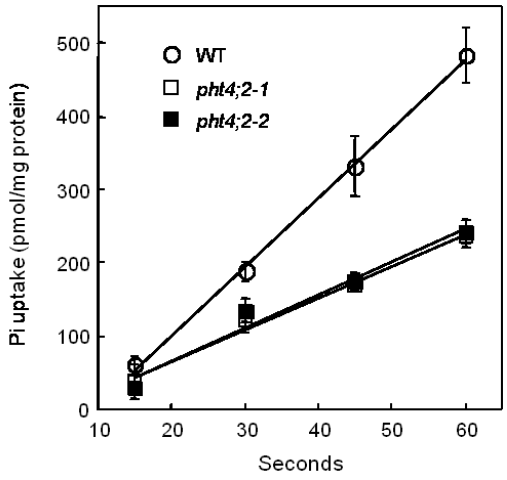

Figure 11. Rate of Pi uptake by isolated root plastids. Assays were conducted at pH 6.5 with 5 mM NaCl and 0.05 mM Pi. Plotted values are means ± SE for three independent experiments.

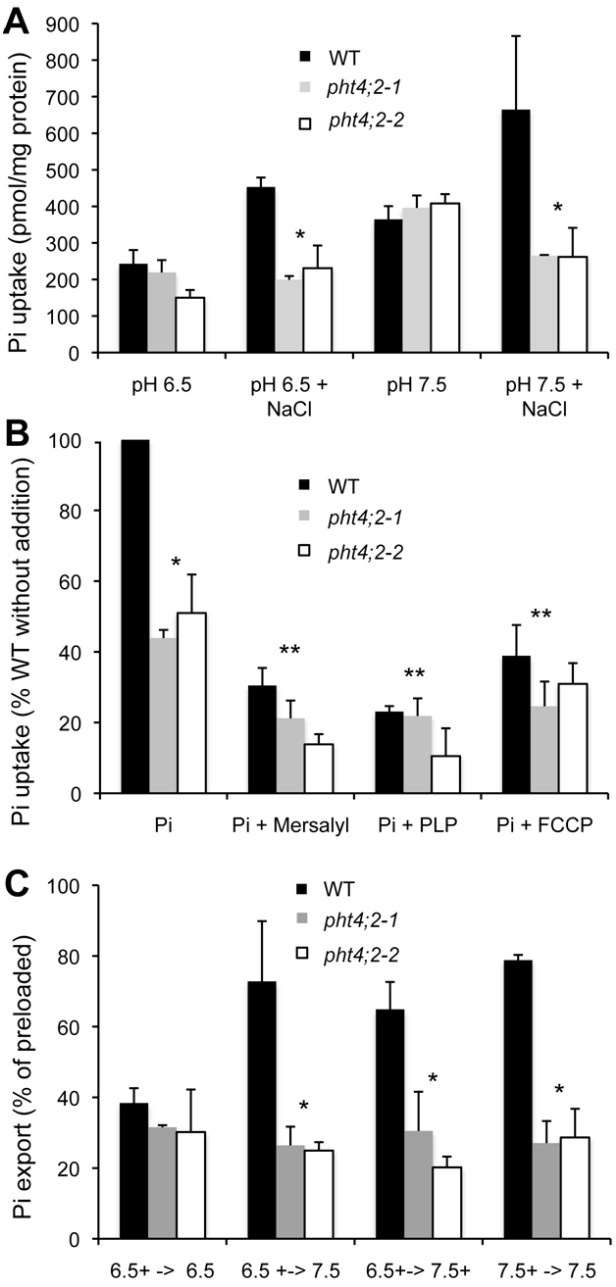

Figure 12. Characterization of Pi transport in isolated root plastids. A, Effect of pH and NaCl on Pi uptake in wild-type and *pht4;2* plastids. B, Effect of inhibitors on Pi uptake. Values are relative to untreated wild-type plastids. All assays were conducted at pH 6.5 and in the presence of 5 mM NaCl. C, Pi export from preloaded plastids. Values expressed as the percentage of preloaded Pi. Preloading and export buffer conditions indicated on the x-axis are separated by an arrow, and + indicates the presence of 5 mM NaCl. The data shown represent the mean ± SD for three independent experiments. * Significantly different from wild type ($P<0.05$, Student's t test). (Figure by Cornelia Spetea and Jacob Kuruvilla).

Pi uptake by root plastids isolated from wild-type plants was 2- to 3-fold greater than those isolated from *pht4;2* mutants when 5 mM NaCl was included in the assay, but not when this salt was omitted (Fig. 12A) or when all sources of Na^+ were substituted with K^+ (data not shown). Pi transport activities for all plastids were greater at pH 7.5 than at pH 6.5, but the differences between mutant and wild-type activities were consistently greatest at pH 6.5 in the presence of NaCl. These results suggest that PHT4;2 catalyzes Na^+-dependent Pi transport in root plastids.

To better understand the mechanism of the observed Pi uptake activity we investigated the effects of select pharmacological agents. Transport assays were conducted in the presence of NaCl and at pH 6.5, and Pi uptake was expressed as a percentage of the amount of Pi accumulated in untreated wild-type plastids. All three of the compounds we tested, mersalyl, pyridoxal 5'-phosphate (PLP) and carbonyl cyanide *p*-(trifluoromethoxy)-phenyl-hydrazone (FCCP), had a pronounced inhibitory effect on Pi transport in wild-type plastids and a lower but clearly measurable effect in mutant plastids (Fig. 12B). These results suggested that PHT4;2 is the predominant but not sole source of Pi transport activity under these assay conditions. Addition of mersalyl, a thiol-reactive agent (Amores et al., 1994), reduced wild-type transport to 35%, indicating the importance of sulfhydryl groups for PHT4;2 activity. Similarly, treatment with PLP, a lysine-reactive agent known to inhibit pPTs (Gross et al., 1990; Flügge, 1992), reduced wild-type activity to 17%. Addition of the protonophore FCCP reduced transport in wild-type plastids to 40%, indicating that the concentration and/or membrane potential

components of the H^+ electrochemical gradient also affect PHT4;2 activity. Dissipation of membrane potential by FCCP would also diminish the magnitude of a Na^+ electrochemical gradient.

The Pi uptake assays described above verified that root plastids could be preloaded with Pi to levels sufficient to assess its export. Plastids were preloaded in the presence of 5 mM NaCl at pH 6.5 or 7.5 then washed and resuspended in buffer with or without NaCl. After incubation, the amounts of Pi exported and retained in the plastid were both measured, and export was calculated as a percentage of total Pi to account for differences in preloading. As shown in Fig. 12C, Pi export was significantly reduced in root plastids isolated from *pht4;2* mutants under most of the conditions tested, confirming that PHT4;2 contributes to this activity in wild-type plastids. Export activities for wild-type plastids measured at pH 7.5 were equivalent when pH, NaCl or both were varied after preloading (Fig. 12C), suggesting an apparent lack of specificity for either H^+ or Na^+. In contrast, similarly low export activities were detected in mutant and wild-type plastids when the composition of the preloading and export solutions were identical (data not shown).

PHT4;2 affects starch accumulation

Pi is an allosteric inhibitor of ADP-glucose pyrophosphorylase (ADGP), which catalyzes the first committed step in starch biosynthesis within plastids (Preiss, 1982; Ballicora et al., 2004). Therefore, we reasoned that starch accumulation in roots could

serve as an *in vivo* indicator for defects in plastidic Pi homeostasis associated with the absence of PHT4;2.

To test this hypothesis, we measured starch contents of roots that were harvested from hydroponically-grown, 6-wk-old wild-type and *pht4;2* plants at multiple times throughout the day. As reported previously for hydroponically-grown Arabidopsis (Malinova et al., 2011), starch was distributed throughout the entire root rather than restricted to the root tip (data not shown). Starch levels in wild-type roots doubled during the first half of the photoperiod then returned to near-starting levels by the end of the photoperiod (Fig. 13). In contrast, starch remained at low levels throughout the day in *pht4;2* roots. This reduced capacity for starch accumulation is consistent with Pi inhibition of starch synthesis due to a defect in Pi export.

Starch contents of leaves were also lower in the mutants than wild type at all time points measured (Fig. 13). Because *PHT4;2* transcripts and protein in wild-type plants were restricted to roots during vegetative growth, the diminished accumulation of starch in mutant leaves presumably reflects a secondary consequence of metabolic changes in the roots.

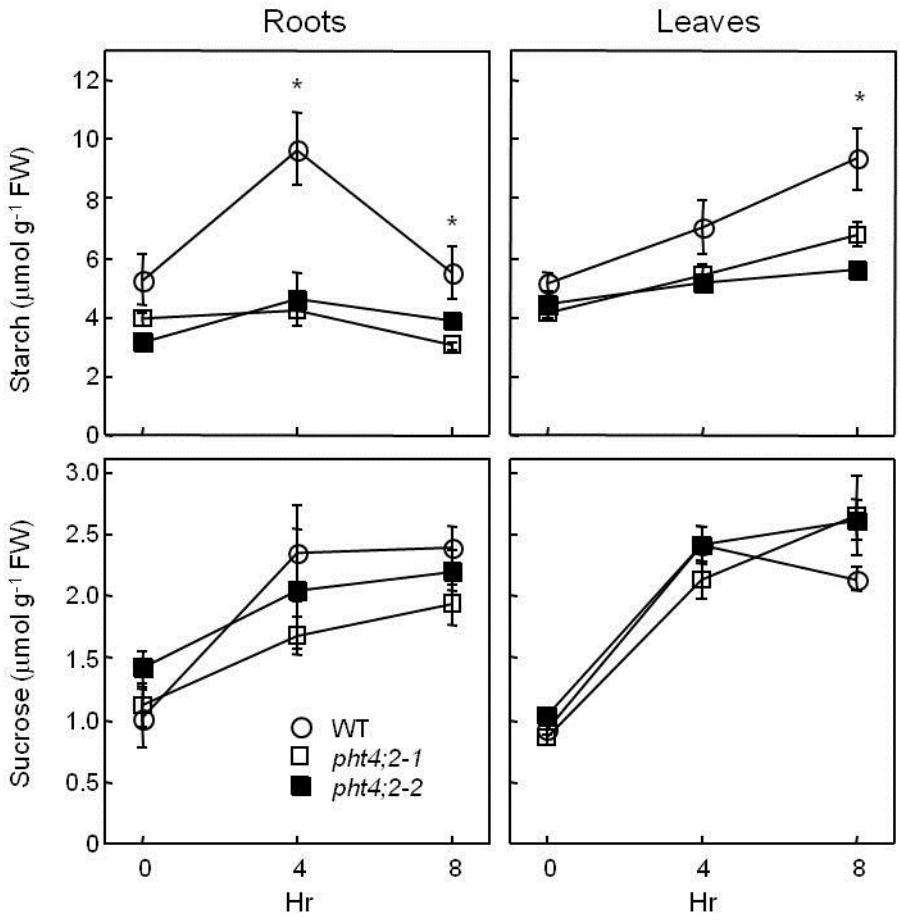

Figure 13. Starch and sucrose contents in *pht4;2* plants. Roots and rosette leaves of 6-wk-old wild-type and *pht4;2-1* plants were collected at the onset, midpoint and end of an 8 hr photoperiod. Wild type, filled circles; *pht4;2-1*, open circles.

Consistent with this idea, we detected root- and leaf-specific changes in the expression of a number of genes that are either directly or indirectly involved in starch synthesis (Fig. 14). Specifically, transcript levels for *GPT1* and *GPT2*, which encode Glc6P/Pi translocators (GPTs), and *NTT1* and *NTT2*, which encode ATP/ADP nucleotide translocators (NTTs), were induced in roots but not in leaves of *pht4;2* plants (Fig. 14A). The proposed functions of GPT and NTT are to provide nonphotosynthetic plastids with the carbon and energy, respectively, needed for starch synthesis and the oxidative pentose phosphate pathway, although mutant analyses indicate that these proteins also have roles in photosynthetic tissues (Niewiadomski et al., 2005; Reinhold et al., 2007). In addition, expression of the AGPase small subunit gene, *APS1*, was induced only in roots of *pht4;2* plants, whereas AGPase large subunit genes, *APL1* and *APL3*, were induced only in leaves (Fig. 14B). Because transcript levels for these genes were inversely correlated with starch levels, the altered expression patterns may reflect compensatory responses to the effects of *pht4;2* mutations. Similarly, the cytosolic fructose-1,6-bisphosphatase gene (*cFBP*), which encodes a key enzyme in sucrose biosynthesis (Stitt et al., 2010), was induced only in *pht4;2* leaves (Fig. 14B). But we detected no significant changes in the accumulation of Suc in leaves or roots of *pht4;2* plants (Fig. 13).

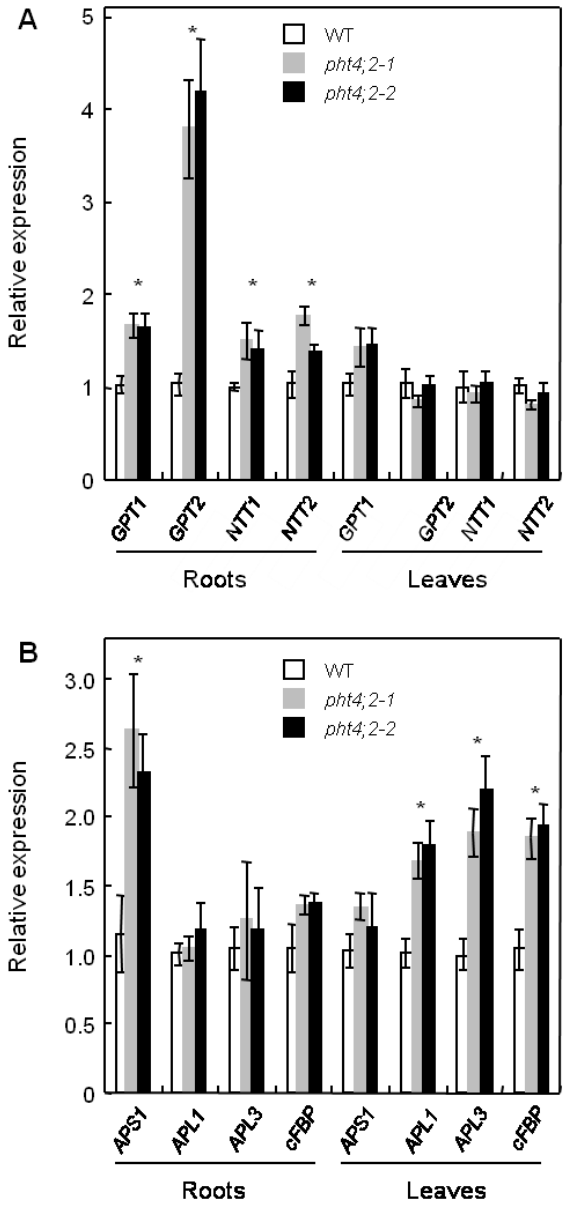

Figure 14. *PHT4;2* modifies the expression of multiple genes involved in plastid transport and carbon metabolism. Expression levels were determined by quantitative RT-PCR of total RNA from plants grown in hydroponics. A, Genes involved in plastid transport, including Glc6P/Pi exchange (*GPT1* and *GPT2*) and ATP/ADP exchange (*NTT*1 and *NTT2*). B, Genes involved in starch synthesis (*APS1*, *APL1* and *APL3*) and sucrose synthesis (*cFBP*). Values shown are mean ± SE for three independent analyses. * Significantly different from wild type ($P<0.05$, Student's t test).

Loss of PHT4;2 increases plant size and biomass

The *pht4;2* mutants have no obvious morphological or developmental phenotype when grown with a 14 h photoperiod. However, when plants were grown with a shorter photoperiod (8 h light), fully-expanded *pht4;2* rosettes were notably larger than those of wild type (Fig. 15A). Both mutant and wild-type plants had 43 ± 1 rosette leaves when flowering initiated, indicating that the increase in rosette size was not due to additional leaves but rather an increase in leaf size (Fig. 15B). Because individual leaves emerge and complete the expansion phase of organ growth at different chronological times, differences in rosette sizes were not detected until plants had grown for at least 5 wk but then increased to a maximum when flowering initiated at 8 to 9 wk (Fig. 15C).

The large-leaf phenotype was also observed when plants were grown hydroponically, and the magnitude of the size difference was typically greater than that seen with plants grown in soil. Rosette area of fully-expanded *pht4;2* mutants was 45 to 65% greater than wild type, and biomass was at least twice that of wild type (Table II). Roots at the time of harvest (8 wk) were tangled, so it was not possible to accurately assess growth of individual root systems. Therefore, we used the combined weight of root systems to derive an average fresh weight per plant. Results from four independent growth experiments consisting of 74 to 113 plants indicated no significant differences in root growth (0.86 ± 0.17, 0.88 ± 0.18 and 0.73 ± 0.10 g plant^{-1} for wild type, *pht4;2-1* and *pht4;2-2*, respectively). In addition, when plants were allowed to complete their life cycle, no differences between *pht4;2* mutants and wild type were detected in flowering time, flower size or seed size (data not shown).

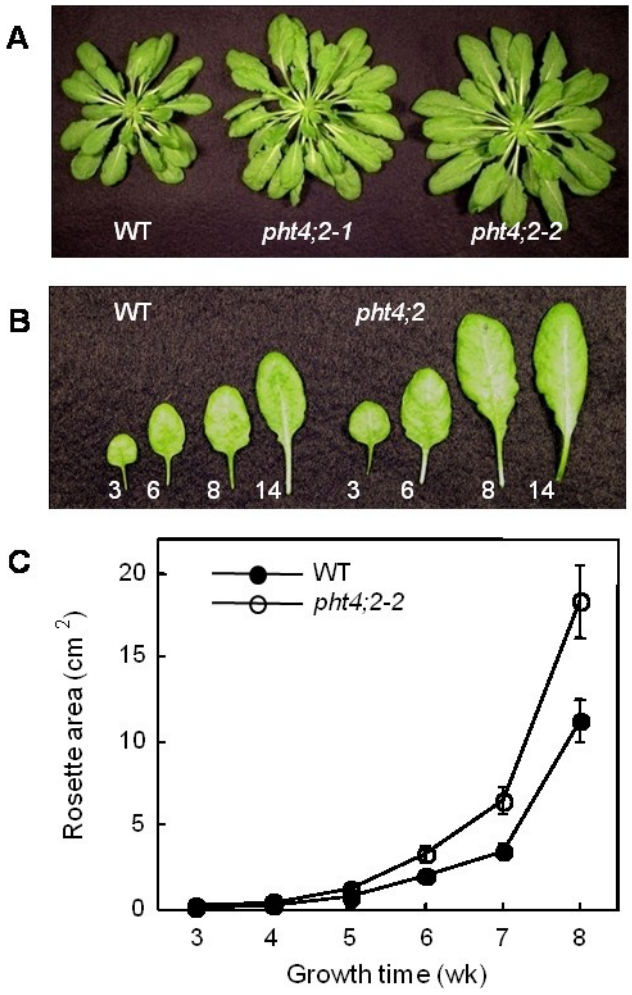

Figure 15. Increased size of *pht4;2* rosette leaves. A, Rosettes of representative 8-wk-old plants. B, Rosette leaf number 3, 6, 8 and 14 of representative wild-type (WT) and *pht4;2-2* plants. C, Increase in rosette area during vegetative growth. Values shown are mean ± SE, n=8.

It was possible that, in addition to increased area, leaf thickness also contributed to the greater biomass of *pht4;2* leaves. To estimate thickness of leaves throughout a rosette we took advantage of the relationship between leaf thickness and the product of specific leaf area (leaf area per unit dry mass) and leaf dry matter content (ratio of dry mass to fresh mass) (Vile et al., 2005). Leaf punches from the centers of ten fully expanded rosette leaves were collected from mutant and wild-type plants. Both specific leaf area, 0.51 ± 0.02 cm^2 mg^{-1}, and leaf dry matter content, 0.10 ± 0.01 mg mg^{-1} were identical for *pht4;2* and wild-type leaves. From these values and a leaf density of 1 g cm^{-3} (Vile et al., 2005), we calculated an average thickness of 196 ± 2 μm for both mutant and wild-type leaves, which is similar to values obtained from direct measurements of leaf sections and three-dimensional imaging of mature leaves (Wuyts et al., 2010). Consequently, the increased area of *pht4;2* leaves fully accounts for increased biomass.

Table II. Rosette area and biomass at the end of the vegetative growth stage. Plants were grown in hydroponics for 8 wk. Values are mean ± SE, n=10. * Significantly different from wild type ($P<0.05$, Student's *t* test).

Genotype	Area (cm^2)	FW (g)	DW (g)
Wild type	37.06 ± 2.82	0.78 ± 0.08	0.06 ± 0.01
pht4;2-1	53.76 ± 3.52	1.47 ± 0.13	0.12 ± 0.01
pht4;2-2	61.20 ± 3.87	1.78 ± 0.13	0.16 ± 0.01

In the course of our investigation of leaf size we noted that *PHT4;2* is located adjacent to *DET2* on chromosome 2 (loci At2g38060 and At2g38050, respectively) with 550 bp between the *PHT4;2* stop codon and the *DET2* translation start site. *DET2* encodes a steroid 5α-reductase that catalyzes a key step in BR biosynthesis (Noguchi et al., 1999). This close proximity raised the possibility that the large-leaf phenotype we attributed to disruption of *PHT4;2* was instead caused by over-expression of *DET2* via T-DNA activation (Weigel et al., 2000; Ren et al., 2004). However, this possibility is inconsistent with our finding that the large-leaf phenotype (assessed by rosette fresh weight) segregated as a recessive trait in F2 progeny of a cross between wild type and the homozygous mutant (14 wild type [1.69 ± 0.06 g]: 45 hemizygous mutant [1.56 ± 0.10 g]: 15 homozygous mutant [2.17 ± 0.12 g]; χ^2=3.48, p=0.17) (Fig. 16). Furthermore, quantitative RT-PCR indicated that *DET2* transcript level was unaffected by *pht4;2* mutation (data not shown).

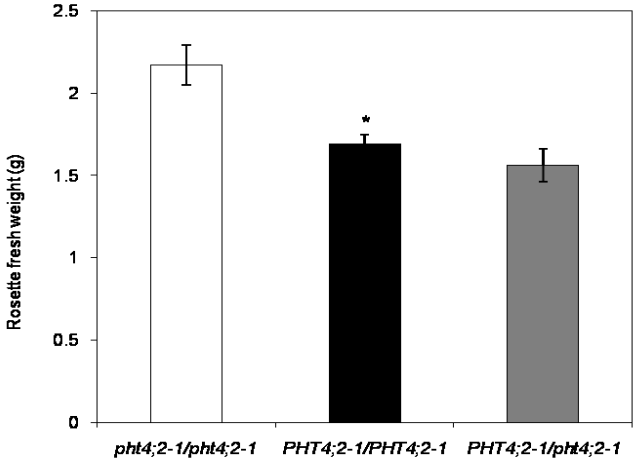

Figure 16. The *pht4;2* leaf biomass phenotype segregates as a recessive trait. A *pht4;2-1* X Wt F2 population was weighed and genotyped at the end of the vegetative stage.

Leaf cell size, number and ploidy

Leaf size is dependent on both the number and the size of cells in the organ. To determine whether enlargement of *pht4;2* leaves was associated with increased cell number, cell size or a combination of these parameters, we compared sizes of epidermal cells in the ninth rosette leaves of *pht4;2* and wild-type plants at different stages of leaf expansion. When plants were 7-wk-old, the leaf-size phenotype was apparent such that the area of the ninth rosette leaves of *pht4;2* plants was 25 to 30% greater than wild type. The average size of epidermal cells in these leaves, however, was not significantly different (Table III), indicating that *pht4;2* leaves have at least 25% more cells than wild

type. When this analysis was conducted with 5-wk-old plants, an age when leaf expansion was incomplete and leaf areas of *pht4;2* and wild-type plants were indistinguishable, epidermal cells of mutant leaves were 30% smaller than wild type (Table III), implying that mutant leaves contain more cells than wild-type leaves. Together, these results indicate that the large-leaf phenotype of *pht4;2* plants is the result of increased cell proliferation with subsequent expansion of individual cells to normal size at maturity.

Table III. Leaf cell sizes and numbers. The ninth rosette leaf was harvested from plants at growth times corresponding to incomplete and complete leaf expansion. Values are mean ± SE for three leaves. Cell areas are calculated from three regions within each leaf. * Significantly different from wild type (P<0.05, Student's t test).

	Leaf 9 area (cm^2)	Epidermal cell area (mm^2)	Epidermal cell number
Incomplete expansion (5 wk)			
Wild type	1.6 ± 0.1	3,770 ± 200	42,400 ± 2650
pht4;2-1	1.6 ± 0.1	2,820 ± 100*	56,800 ± 3,550*
pht4;2-2	1.7 ± 0.1	2,780 ± 370*	61,210 ± 3,600*
Complete expansion (7 wk)			
Wild type	2.2 ± 0.1	4,150 ± 660	53,060 ± 2,410
pht4;2-1	2.7 ± 0.2*	3,930 ± 300	68,790 ± 5,100*
pht4;2-2	2.7 ± 0.1*	3,750 ± 310	72,000 ± 2,670*

Repeated cycles of endoreduplication gives rise to somatic polyploidy, which is positively correlated with cell and leaf size (Melaragno et al., 1993; Vlieghe et al.,

2005). However, endoreduplication appears to be unaffected by loss of PHT4;2 because the distribution of ploidy levels in cells of mature *pht4;2* and wild-type leaves were nearly identical (Fig. 17). Endoreduplication occurs after cell division ceases and continues until leaf expansion is complete (Beemster et al., 2005). Consequently, the similar distribution of ploidy levels also suggests that additional cell proliferation in *pht4;2* leaves occurs predominantly, if not exclusively, at early stages in leaf development.

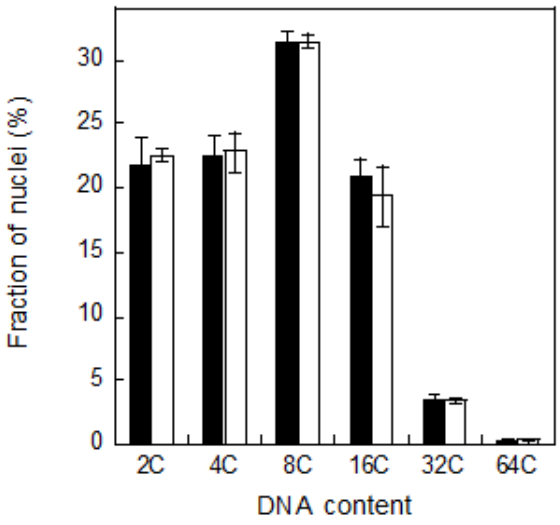

Figure 17. Distribution of ploidy in rosette leaves of WT and *pht4;2* plants. DNA content of nuclei isolated from wild-type (black) and *pht4;2-1* (white) rosette leaves were analyzed by flow cytometry. Values shown are mean ± SE for three independent analyses.

Photosynthetic activity

Leaf enlargement and altered carbon partitioning in *pht4;2* mutants suggested the possibility of a change in photosynthetic activity. The two mutant lines presented similar fluorescence characteristics to wild-type plants, as reflected in the F_0 and F_m values (Tsimilli-Michael and Strasser, 2008) (data not shown). Therefore, the maximum quantum yield for PSII photochemistry (F_v/F_m) was not significantly different in the wild-type, *pht4;2-1* and *pht4;2-2* plants, 0.812 ± 0.011, 0.809 ± 0.005 and 0.801 ± 0.003, respectively.

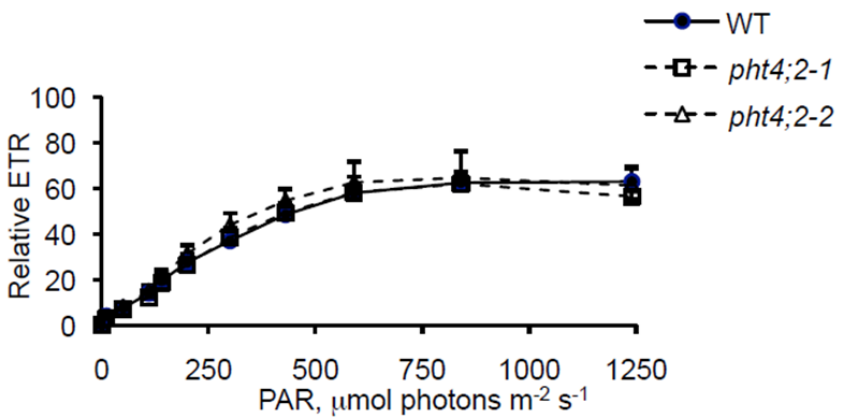

Figure 18. Relative Electron Transport Rate (ETR) of *pht4;2* plants. ETR was measured as a function of intensity of the photosynthetically active radiation (PAR). The ETR parameter was measured via the fluorescence parameter in light-adapted detached leaves. The data shown represent an average of three to four independent measurements ±SD (Figure by Cornelia Spetea and Jacob Kuruvilla).

To assess and compare the light saturation of photosynthetic performance in mutant and wild-type plants we recorded a light response curve of chlorophyll fluorescence and calculated the relative electron transport rate. As shown in Fig. 18, this analysis revealed that all plants display similar ETR values and reach saturation at approximately 500 μmol photons m^{-2} s^{-1}. Together, these data indicate that the lack of PHT4;2 does not modify photosynthetic electron transport in leaves. As expected from these data, total chlorophyll contents were not significantly different in wild-type, *pht4;2-1* and *pht4;2-2* leaves (1.14 ± 0.1, 1.15 ± 0.1 and 1.15 ± 0.1 mg g^{-1} FW, respectively). We concluded that the increased biomass of *pht4;2* rosettes is the result of a larger photosynthetic area and not from increased photosynthetic rate.

Discussion

Although ATP/ADP exchange fulfills the energy requirement of plastids with limited or no photosynthetic activity, the unbalanced phosphate moieties would lead to detrimental accumulation of Pi and negative charge within the stroma if not countered by Pi export. Earlier biochemical data suggested that an unknown transporter in cauliflower bud amyloplasts catalyzes Pi export in the absence of exogenous counter-exchange substrates (Neuhaus and Maass, 1996), but the effect of Na^+ and H^+ levels on this activity was not investigated. Our data presented here suggest that PHT4;2 mediates Na^+-dependent Pi transport in Arabidopsis root plastids and, given its spatial expression pattern, is likely to carry out the same function in other sink organs. Our analysis of

pht4;2 null mutants also revealed pleiotropic effects in starch accumulation throughout the plant and cell proliferation in leaves, which underscore the importance of plastidic Pi homeostasis to plant growth and physiology.

We evaluated Pi transport in root plastids isolated from *pht4;2* and wild-type plants and found that export and import activities were both reduced in mutant plastids, indicating that PHT4;2 is capable of catalyzing reversible Pi transport under our assay conditions (Fig. 12). Given that ATP consumption would generate considerable amounts of Pi within the stroma, it is possible that Pi import does not occur under physiological conditions. Moreover, because root plastids and chloroplasts are developmentally related and share many of the same biosynthetic and transport processes (Bräutigam and Weber, 2009; Daher et al., 2010), stromal pH and inner envelope membrane potential of root plastids are likely to be similar to those of dark-adapted chloroplasts (pH ~7; 20-100 mV, interior negative) (Demmig and Gimmler, 1983; Wu et al., 1991), and these conditions would favor Pi export.

Pi uniport, such as the activity described by Neuhaus and Mass (1996), is an attractive possible mechanism for PHT4;2, as this would rectify both the Pi concentration and charge imbalances derived from ATP/ADP exchange. Nevertheless, coupled transport, e.g., symport, as indicated from the effects of Na^+ and H^+ we observed with isolated plastids, is also possible provided that the associated charge imbalance is rectified by an independent activity. Indeed, the addition of Na^+, but not K^+, to plastids clearly stimulated the Pi import activity of PHT4;2. Pi import was not stimulated by external acidic conditions (pH 6.5) in the absence of Na^+ (Fig. 12A),

indicating that the presence of a H^+ gradient alone is insufficient to activate Pi transport. However, Na^+-dependent Pi import was largely inhibited when the imposed H^+ gradient was dissipated by a protonophore (FCCP, Fig. 12B), suggesting that other aspects of the H^+ gradient are important for Pi transport. For example, a change in stromal pH would affect the fraction of Pi ionic forms, $H_2PO_4^-$ and HPO_4^{2-}. Thus, if PHT4;2 preferentially transports monoanionic $H_2PO_4^-$, then its inward electrochemical gradient would be considerably less when the stroma and external solution have the same pH than when the stroma is more alkaline than the external solution. Alkalinization of the stroma may occur via Na^+/H^+ exchange, as this transport process has been reported to play an important role in homeostasis of cytosolic and stromal pH (Song et al., 2004).

Pi export mediated by PHT4;2 was also found to be Na^+ dependent (Fig. 12C). We propose that this export activity is the *in vivo* function of PHT4;2 in nonphotosynthetic plastids, as this would enable homeostasis with respect to Pi concentration. Although Pi export under conditions where Na^+ was present both during loading and export would suggest that transport can occur in the absence of a Na^+ gradient, a Na^+ gradient may in fact exist under these conditions if Na^+/H^+ exchangers use the imposed H^+ gradient to import Na^+ into the stroma. Additional studies using mutants with limited plastidic Na^+/H^+ exchange activities are needed to resolve this possibility. However, it is important to note that the lack of significant Pi export when the composition of the import and export solutions were the same (no pH or Na^+ gradient) strongly supports the idea that PHT4;2 requires a Na^+ gradient. Furthermore, this requirement may be common to PHT4 transporters because mutational analysis

identified a Ser that is critical for the Na^+-dependency of Pi transport by PHT4;1, and this amino acid is fully conserved in the PHT4 family (Ruiz Pavon et al., 2010).

pht4;2 mutants exhibited abnormal starch accumulation as well as increased leaf cell proliferation with a concomitant increase in biomass. These pleiotropic effects could initiate with altered homeostasis of Pi levels in the stroma of root plastids. Specifically, we expected a defect in Pi export to result in elevated stromal Pi levels. Confirmation of this effect through direct measurement in isolated plastids was compromised by ongoing metabolism during the isolation procedure. However, reduced starch accumulation in *pht4;2* roots was consistent with an increase in stromal Pi concentrations, as Pi is an inhibitor of starch biosynthesis (Preiss, 1982; Ballicora et al., 2004).

Starch levels were also reduced in *pht4;2* leaves. The lack of *PHT4;2* transcripts and protein in wild-type leaves suggests that the starch phenotype in mutant leaves is a secondary consequence of the metabolic defect in roots. For example, although the altered expression of other plastid transporter genes and *APS1* in roots, but not leaves, (Fig. 14A) suggests a local response to the defect in root plastids, altered expression of a subset of starch and Suc metabolism genes in leaves, but not roots, (Fig. 14B) implicates a defect in long-distance signalling of metabolic status. The strong induction of *GPT2* in *pht4;2* roots further substantiates the relationship between PHT4;2 and starch accumulation because *GPT2* is also induced in a number of starch-defective mutants (Kunz et al., 2010).

The partitioning of carbon between starch and Suc biosynthetic pathways is tightly regulated to coordinate carbon demands throughout the day and night. Thus, it

might be expected that reduced starch accumulation in *pht4;2* plants would be accompanied by an increase in Suc levels. However, no significant changes were detected in Suc levels in roots or leaves of *pht4;2* mutants. This finding does not preclude the possibility that the partitioning of carbon to other sugars, amino acids or lipids is altered, and that one or more of these metabolites are directly involved in stimulating cell proliferation in *pht4;2* leaves. Additional studies that include metabolite profiling of roots and leaves of *pht4;2* and wild-type plants are needed to resolve these possibilities.

An increase in the number of cells in *pht4;2* leaves fully accounted for the greater rosette area and biomass, as epidermal cell sizes and leaf thickness were equivalent to wild type when leaves were fully expanded. When leaves were examined prior to full expansion the increase in cell number was already evident, indicating that cell proliferation was augmented early in leaf development, which is in accord with the timing of the proliferative phase of leaf growth (Beemster et al., 2005). However, there was a corresponding reduction in cell size at this time point such that leaf sizes were equivalent to wild type. Thus, the leaf-size phenotype was apparent only after cells expanded to normal sizes. Although we detected no change in relative photosynthetic electron transport rate associated with *pht4;2* mutations, the greater total leaf area of the mutants resulting from increased cell proliferation would provide a proportional increase in the photosynthetic activity per plant.

The mechanisms controlling the size of leaves and other organs are poorly understood, largely because this trait is regulated through multiple pathways (Gonzalez

et al., 2009; Krizek, 2009). Moreover, Gonzalez et al., (2010) recently demonstrated that several of these pathways, including those associated with auxin, jasmonate, brassinosteroid and GA synthesis or signaling, as well as transcriptional regulation by GROWTH-REGULATING FACTOR5 (GRF5), which is not associated with changes in phytohormones, independently control cell proliferation and leaf size. Indeed, the phenotypes of lines evaluated in this study differ from each other and from *pht4;2,* primarily with respect to leaf positions. For example, overexpression of AVP1, a vacuolar pyrophosphate-dependent H^+ pump that is involved in auxin transport (Li et al., 2005), yields rosettes with a greater number of leaves, all of which are enlarged. Overexpression of JAW1, which is involved in the regulation of jasmonate biosynthesis (Palatnik et al., 2003; Schommer et al., 2008), leads to enlargement of only the first rosette leaves and these have a characteristic uneven shape. Leaf enlargement is also restricted to the first few rosette leaves in lines overexpressing GRF5 and BRI1, a brassinosteroid receptor (Wang et al., 2001; Horiguchi et al., 2005), whereas overexpression of GA20OX1, an enzyme involved in GA synthesis (Huang et al., 1998), yields enlarged young but not old leaves.

Cell cycle progression is responsive to carbon status (Riou-Khamlichi et al., 2000), and it is possible that the influence of *pht4;2* mutations on starch accumulation constitutes one of the multiple pathways that converge on control of cell proliferation and organ size. Starch-deficient mutants do not have abnormally large leaves (Ventriglia et al., 2008), suggesting that reduced starch accumulation is unlikely to be causal for the increase in cell proliferation underlying the *pht4;2* leaf-size phenotype. However, starch

accumulation in such mutants is affected throughout the entire plant so comparisons may be misleading if the leaf-size phenotype is related to carbon balance between source and sink organs. In addition, our results indicate that the mechanism responsible for increased cell proliferation is non-autonomous, suggesting that PHT4;2 plays a key role in coordinating metabolic signals throughout the entire plant.

Methods

Plant material and growth conditions

Arabidopsis thaliana T-DNA insertion lines SALK_019289 (*pht4;2-1*), and SALK_070992 (*pht4;2-2*) were obtained from ABRC. Insertion sites and zygosity were confirmed by PCR using combinations of *PHT4;2*-specific primers and primers that anneal to the T-DNA right and left borders. The sequence of amplicons that spanned insertion junctions was confirmed. Homozygous *pht4;2-1* and *pht4;2-2* plants were screened by DNA gel blot analysis using the *nptII* segment of the binary plasmid pROK2 as probe to identify individuals with insertions at a single locus.
Plants were grown in chambers at 21°C with 70% relative humidity and an 8 h photoperiod (150 μmol m^{-2} s^{-1}) in soil (SunGro Redi-earth, Bellevue, WA) or hydroponically as previously described (Noren et al., 2004; Guo et al., 2008a).

Analysis of *PHT4;2* promoter-GUS expression

A *PHT4;2* promoter-GUS transcriptional fusion (Guo et al., 2008a) was introduced into *Agrobacterium tumefaciens* strain GV3101 and used to transform

Arabidopsis (Clough and Bent, 1998). Transgenic seedlings were selected on half-strength Murashige and Skoog medium (Murashige and Skoog, 1962) containing 25 μg mL^{-1} kanamycin. At least 12 independent lines were examined for GUS activity by histochemical detection. Seedlings, flowers and siliques were fixed in 50 mM sodium phosphate pH 7.0, 4% (v/v) formaldehyde then infiltrated with 50 mM sodium phosphate pH 7.0, 0.1% (v/v) Triton X-100, 0.5 mM potassium ferrocyanide, 0.5 mM potassium ferricyanide, 10 mM EDTA, 0.05% (w/v) 5-bromo-4-chloro-3-indolyl glucuronide (X-gluc), and then incubated in the dark at 37˚C overnight. Green tissues were de-stained with 70% (v/v) ethanol prior to observation. Images were captured with a Nikon Coolpix 4300 camera mounted on an Olympus LMS 225R dissection microscope.

Quantitative RT-PCR analysis

Total RNA was isolated from roots or leaves using TRI reagent (Sigma Aldrich, St. Louis, MO), and traces of contaminating DNA were eliminated with TURBO DNA-free (Ambion, Austin, TX). Three biological replicates were used for each analysis. First-strand cDNA was synthesized from 1 μg total RNA using SuperScript first-strand cDNA synthesis kit (Invitrogen, Carlsbad, CA). Real-time PCR was conducted with Power SYBR Green Master Mix and the ABI Prism 7500 sequence detection system (Applied Biosystems, Foster City, CA). Expression levels were normalized to *EIF-4A2* (Guo et al., 2008a).

Root plastid isolation and Pi transport assays

Plastids were isolated from the entire root system of 6-wk-old plants as described (Emes and England, 1986). Briefly, roots (10-15 g) were washed in distilled water, chilled at 4ºC for 30 min then ground in four 5 s bursts in a blender with 40 mL of cold isolation buffer: 50 mM K-Tricine (pH 8.0), 0.3 M sorbitol, 1 mM EDTA, 2 mM $MgCl_2$ and 0.1 % (w/v) freshly added BSA. The homogenate was filtered through two layers of Miracloth then centrifuged at 1500 *g* for 3 min at 4ºC. The pellet was suspended in 0.5 mL isolation buffer then transferred to a tube containing 40 mL 10% (v/v) Percoll in isolation buffer. The mixture was centrifuged at 3000 *g* for 10 min at 4ºC. Intact plastids were pelleted while broken plastids and cell debris remained at the top of the Percoll solution. The intact plastids were suspended in 20 mL isolation buffer then pelleted again by centrifugation at 1500 *g* for 3 min. The pellet was finally suspended in 0.5 mL isolation buffer and maintained at 4ºC. Root plastids were typically 70-75% intact as estimated by phase contrast microscopy. The protein content of the plastid suspension was determined spectrophotometrically. For plastid enrichment, the activity of nitrite reductase (NiR) was assayed as previously described (Takahashi et al., 2001). For plastid purity, vacuolar contamination was determined by α-mannosidase (Stitt et al., 1989), and combined mitochondrial, cytosolic and peroxisomal contamination was determined by NADH-malate dehydrogenase (NADH-MDH) (Schneider and Keller, 2009).

Pi uptake by freshly isolated root plastids was assayed in 30 µL assay buffer at a final protein concentration of 1 mg mL^{-1} for 1 min at 22ºC. The assay buffer contained 50 mM Mg-HEPES adjusted to either pH 6.5 or 7.5 as indicated, 0.3 M sorbitol, 1 mM

$MgCl_2$ and 0 or 5 mM NaCl as indicated. The final concentration of [^{32}P]orthophosphate (60 mCi/mmol; 1 mCi = 37 MBq; Perkin Elmer, USA) was 50 µM. Transport inhibition studies were carried out with 150 µM mersalyl, 6 mM pyridoxal-5'-phosphate (PLP) or 50 µM FCCP, added 1 min before addition of Pi. Transport was terminated by the addition of 170 µL of cold assay buffer followed by centrifugation at 16000 *g* for 1 min. The pellet was washed with 200 µL cold assay buffer then suspended in 30 µL of 2 mM dodecyl maltoside and incubated for 5 min on ice. Accumulated Pi was measured by liquid scintillation spectrometry in 1.5 mL distilled water. Control experiments performed in the presence of 10 mM potassium phosphate buffer (pH 6.5 and 7.5) indicated 10-15% nonspecific binding, which was subtracted from the corresponding measured activity. Root plastids isolated from wild type and mutants were assayed in parallel for each experiment. Results are the average of 2-3 independent experiments performed in triplicates ± SD.

Pi export studies were conducted with the same buffers as for uptake. Plastids were first preloaded with Pi for 1 min in the indicated buffer then washed twice with the same buffer to remove excess Pi. Preloaded plastids were then incubated for 1 min in the indicated assay buffer at the same temperature. The assay was terminated by centrifugation, and the amounts of Pi remaining in the plastid pellet and exported to the assay buffer were determined by scintillation counting as described above. Results are the average of two independent experiments performed in triplicates ± SD.

SDS-PAGE and Western blotting

Root plastid proteins were separated by electrophoresis using 14 % (w/v) acrylamide SDS-gels. Following electroblotting to PVDF membranes (Millipore, Bedford, MA), the PHT4;2 protein was immunodetected using a specific antibody against the N-terminal peptide RYSSESDGKRRNA produced in rabbit by Innovagen (Lund, Sweden). The blots were further reacted with secondary donkey anti-rabbit antibody conjugated with horseradish peroxidase and chemiluminescent substrate kit (GE Healthcare, UK).

Extraction and measurement of Suc and starch

Leaf and root samples were harvested at the indicated times in the photoperiod then immediately frozen in liquid nitrogen. Suc was extracted with 80% (v/v) ethanol, 5% (v/v) formic acid at 80ºC for 20 min then the extraction was repeated with 80% ethanol. The supernatants were pooled, lyophilized, suspended in 10 mM Na-acetate (pH 5.5) then assayed for Suc. Pellets were dried and starch was gelatinized and hydrolyzed as described (Smith and Zeeman, 2006). Suc and starch concentrations were quantified using coupled assays in which the formation of NADH was monitored by absorbance at 340 nm using a Synergy HT microplate reader. All assays were performed in duplicate and values were determined from standard curves. At least four independent samples were collected for each time point and results are reported as mean ± SE**.**

Leaf and cell size analysis

The area of rosettes and individual rosette leaves was determined from digital images that included reference objects using the histogram function of Adobe Photoshop. To determine epidermal cell area, nail polish impressions of the abaxial epidermis were prepared from the ninth rosette leaf of at least three wild-type and *pht4;2* plants. Images were captured with constant magnification (400x) for three different locations in each leaf between 25% and 75% of the distance between the tip and the base of the blade, halfway between the mid-rib and leaf margin. Cells in each field of view were counted, and cell areas (mean ± SE) were determined from a total of at least 500 cells.

Ploidy analysis

Nuclei were isolated from fully expanded leaves of 8-wk-old plants as described previously (Galbraith et al., 1983). Briefly, leaves were finely chopped with a razor blade in 2 ml of ice-cold buffer containing 45 mM $MgCl_2$, 30 mM sodium citrate, 20 mM MOPS, pH 7 and 1 mg ml^{-1} Triton X-100. Tissue fragments were removed by filtration through 36 µm nylon mesh, and DNase-free RNase (10 µg ml^{-1} final) and propidium iodide (100 µg ml^{-1} final) were added. Nuclei were incubated for 30 min in the dark at room temperature before analyzing the distribution of DNA content using a FACScan flow cytometer. Results are from three independent plants of each genotype and at least 4000 nuclei for each analysis.

Photosynthetic activity in detached leaves

Chlorophyll fluorescence was measured using a pulse-amplitude fluorometer model PAM-210 (Walz, Effeltrich, Germany) in leaves detached from 16-h dark-adapted plants. The dark-adapted state fluorescence yield, F_0, was recorded by using a weak measuring light whereas the maximum fluorescence yield, F_m, was measured after application of a 1-sec pulse of saturating visible light (Schreiber et al., 1986). The maximum quantum yield of photosystem II photochemistry (F_v/F_m) was calculated using the equation $F_v/F_m = (F_m-F_0)/F_m$. The photosynthetic electron transport rate (ETR) was determined in detached leaves using PAM-210 by measuring the quantum yield of PSII photochemistry (Y') after every 20 sec of illumination with photosynthetically active radiation (PAR) of 0 to 1850 μmol photons m^{-2} s^{-1}, increased stepwise. The relative ETR was calculated by the equation ETR = 0.84 × 0.5 × PAR × Y (Genty et al., 1989). It was assumed that 84% of the incident light was absorbed (factor 0.84), and that an equal fraction of the absorbed quanta is distributed to photosystem II and I (factor 0.5). Results are the mean of 3 to 4 independent measurements ± SD.

CHAPTER IV

CHARACTERIZATION OF THE THYLAKOID PHOSPHATE TRANSPORTER PHT4;1 OF *ARABIDOPSIS THALIANA*

Introduction

The thylakoid membrane serves as a structural support for light-driven electron and proton transport, which are required for $NADP^+$ reduction and synthesis of ATP. Multiple protein complexes are found within or tightly associated with thylakoid membranes. These include photosystems (PS) I and II, the cytochrome b_6f complex and ATP synthase. Several thylakoid transmembrane proteins that do not appear to be directly associated with these complexes have also been identified (Andersson and Barber, 1994; Spetea et al., 2004; Thuswaldner et al., 2007). One of these proteins was recently confirmed to be an ATP/ADP transporter that supplies the thylakoid lumen with ATP required for energy-dependent reactions within this membrane-bound compartment (Thuswaldner et al., 2007).

Plants require light to carry out photosynthesis; however, exposure to high levels of light increases the production of reactive oxygen species and subsequent photo-oxidative damage. With prolonged exposure, photo-oxidative damage can cause death of the exposed tissue and eventually the death of the plant (Muller et al., 2001). Although light stress in plants is generally interpreted as excess light intensity, a more accurate definition is the absorption of light beyond what can be utilized during photosynthesis. Thus, light stress occurs when the ratio of photon flux density (PFD) to photosynthetic

capacity is high. Plants have developed different mechanisms for photo-protection and optimization of photosynthesis and growth under a wide range of light intensities, such as the movement of chloroplasts or whole leaves (Demmig-Adams and Adams, 1992; Muller et al., 2001), adjustment of leaf angle, increasing surface reflectance or production of other pigments that help decrease the amount of light absorbed by chlorophyll (Demmig-Adams and Adams, 1992).

The maintenance of Pi homeostasis within chloroplasts subcompartments is crucial to adequate chloroplast functionality. Several chloroplast inner envelope-localized transport proteins have been identified that facilitate the movement of Pi between the cytosol and chloroplast stroma (Flügge et al., 1989; Fischer et al., 1997; Eicks et al., 2002; Knappe et al., 2003). These proteins serve key roles in the control of photosynthesis and carbon partitioning. Recent data indicate that at least one Pi transporter, PHT4;1, is located in the thylakoid membrane (Ruiz Pavón et al., 2008) but little is known of the physiological significance of this activity or the role of Pi in the thylakoid lumen.

As part of a collaboration with Dr. Cornelia Spetea (University of Gothenburg, Sweden), we have isolated an Arabidopsis mutant that lacks a functional copy of the PHT4;1 thylakoid Pi transporter and used this mutant to study the influence of PHT4;1 on plant growth and photosynthetic activity. Rosette leaves of mature *pht4;1* plants are smaller than those of wild-type plants and exhibit altered transcriptional responses to light and other abiotic stresses as well as altered photosynthetic properties. These results underscore the importance of thylakoid Pi homeostasis for plant growth and health.

Results

Identification of a *pht4;1* Ds transposon insertion mutant

To gain a better understanding of the role of PHT4;1 in thylakoid functions and in overall plant metabolism, I isolated a mutant line, *pht4;1-1*, that lacks a functional *PHT4;1* allele. The insertion was confirmed by PCR and sequencing of the amplicons spanning the insertion junctions. The *pht4;1-1* line has a *Ds* transposon inserted 131 bp downstream of the translation start site, with no insertion or deletion of *PHT4;1* sequence at the insertion site. The structure of the mutant locus is shown in Fig.19A.

The *pht4;1-1* homozygous line was also screened by DNA gel blot for the presence of additional insertions (data not shown), and only homozygous plants that lacked ectopic insertions were used for subsequent studies. RT-PCR analysis of leaf RNA using primers that anneal downstream of the insertion site revealed no *PHT4;1* transcript in the homozygous plants suggesting that *pht4;1-1* mutants are null (Fig. 19B).

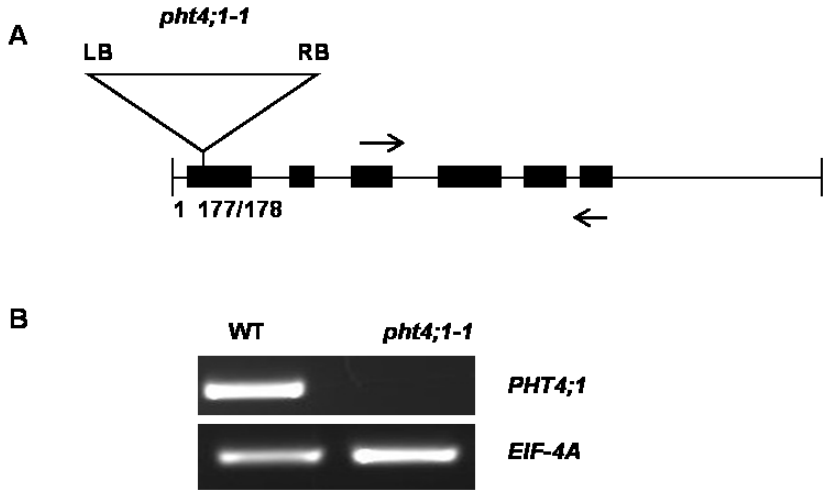

Figure 19. Molecular characterization of *pht4;1-1 Ds* transposon insertion mutants. A, Scheme indicating the positions of T-DNA insertions in *pht4;1-1*. Insertions were confirmed by PCR and DNA sequence. Arrows represent primers used for RT-PCR. B, RT-PCR analysis of total RNA isolated from leaves of wild-type and *pht4;1-1* plants.

Localization of PHT4;1 to thylakoid membranes

The localization of the endogenous PHT4;1 protein to thylakoids was confirmed by isolating thylakoid membranes from wild-type Arabidopsis and subjecting the proteins to immunoblot analysis. A single band of approximately 45 kDa was detected in wild-type preparations with a PHT4;1 specific antibody (Fig. 20). The 45 kDa band was not detected in thylakoid preparations from *pht4;1-1* mutants, further verifying that this mutation is null.

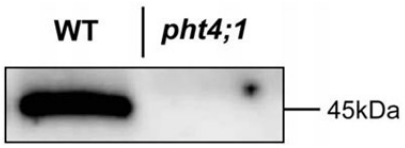

Figure 20. Thylakoids of *pht4;1* mutants lack detectable PHT4;1 protein. Immunoblot with anti-PHT4;1 antibody of thylakoids isolated from wild type (WT) plants and pht4;1 plants (10 µg Chl/lane) (Figure by Patrik M. Karlsson and Cornelia Spetea).

Plant size

The *pht4;1-1* mutants showed no obvious developmental phenotype when the plants were grown under a 14 h photoperiod. In this regard, *pht4;1-1* mutants are similar to *pht4;2* mutants, since both transporter mutants show no phenotype under long-day conditions. However when *pht4;1-1* plants were grown under a 8 h photoperiod, they showed a conditional phenotype. When grown under short day conditions, rosette leaves of *pht4;1-1* plants are smaller than leaves of wild-type plants (Fig. 21). No significant difference in the number of leaves per rosette was observed, which is indicative of reduced leaf size rather than a decreased rate of leaf emergence.

The smaller leaf size phenotype is observed both with plants grown on soil and hydroponically. Rosette areas of fully expanded *pht4;1-1* plants are about 80% of

wildtype, with a corresponding decrease in both rosette fresh weight and dry weight (Table IV).

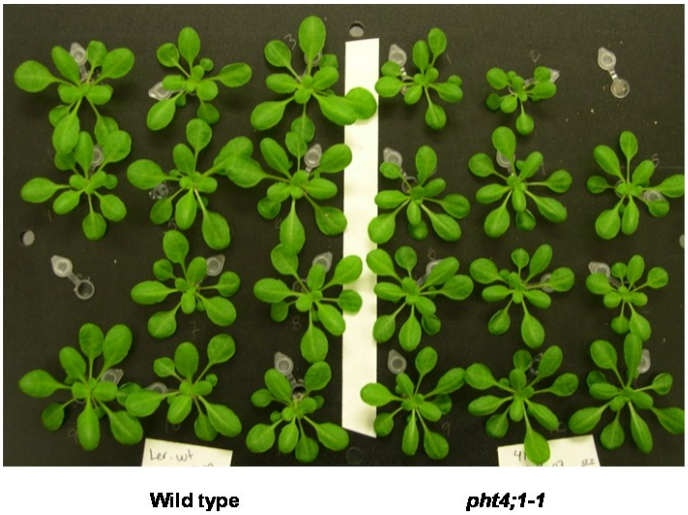

Figure 21. Decreased rosette size of *pht4;1-1* mutants. Rosettes of representative 5-week old wild type and *pht4;1-1* plants.

Table IV. Rosette diameter and biomass at the end of the vegetative growth stage (8 wk). Values are mean ± SE, n=10.

Genotype	Diameter (cm)	FW (mg)	DW(mg)
Wild type	4.76±0.13	135.8±8.3	12.4±9
pht4;1-1	3.95±0.16	107.1±9.1	9.9±1
p value	0.0012	0.015	0.038

Segregation analysis of *pht4;1-1* was carried out to determine linkage of *pht4;1-1* mutation with the smaller rosette phenotype. F2 progeny of a cross between *pht4;1-1* and wild-type were grown with an 8 h photoperiod. At the end of the vegetative growth phase (8 weeks), plants were genotyped and rosette fresh weights were determined (8 wild type [0.037 ± 0.026 g]: 8 hemizygous mutant [0.27 ± 0.027 g]: 8 homozygous mutant [0.28 ± 0.032 g]; χ^2=3.48, p=0.03). The results indicated that the *pht4;1-1* mutation co-segregates with the small-rosette phenotype and because the dry weights of hemizygous plants were equivalent to the homozygous plants, the growth phenotype is a haplo-insufficient trait (Fig. 22).

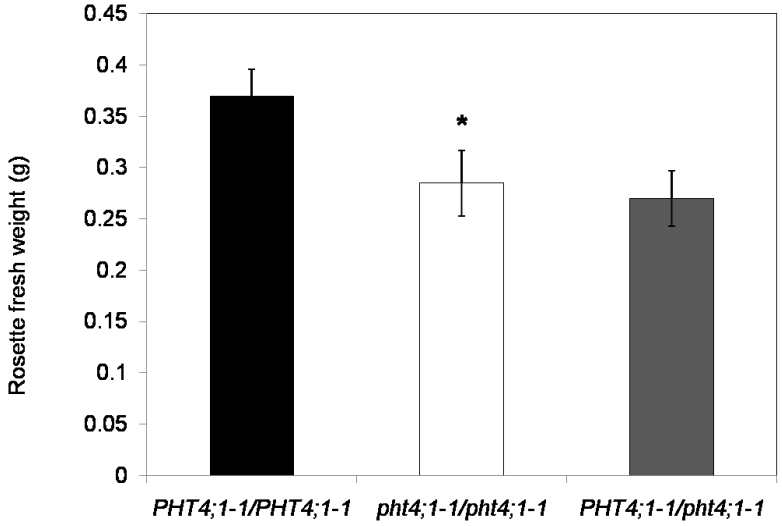

Figure 22. The *pht4;1-1* rosette size phenotype segregates as a haplo-insufficient trait. A *pht4;1-1* X Wt F2 population was weighed and genotyped at the end of the vegetative stage. N=8, $p < 0.03$

Complementation of the *pht4;1* size phenotype

To confirm that disruption of *PHT4;1* rather than an unrelated but linked mutation is responsible for the reduced leaf size phenotype of *pht4;1-1* plants, we tested whether a *PHT4;1* cDNA clone complements this phenotype. A *PHT4;1* cDNA was cloned downstream of the CaMV35S promoter and was transformed into wild-type and *pht4;1-1* backgrounds. Introduction of the wild-type copy of *PHT4;1* complemented the rosette growth defect of *pht4;1-1* plants, confirming that the absence of the functional

PHT4;1 protein was the cause for the reduced rosette growth phenotype. Over-expression of *PHT4;1* in wild-type plants did not affect rosette size (Fig. 23).

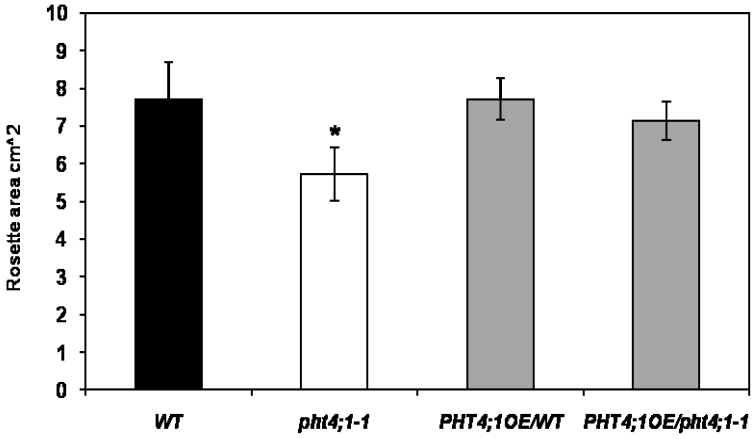

Figure 23. Rosette size complementation of a *PHT4;1* over-expression (OE) line. A CaMV35S-*PHT4;1* construct was introduced into wild type and *pht4;1-1* plants. Over-expressing lines showed a rosette size comparable to that of wild type, and bigger than rosettes of *pht4;1-1* plants, indicating that absence of PHT4;1 protein can cause decreased rosette size.

Effect of *pht4;1-1* mutation on expression of stress-response genes

Reduced leaf growth of *pht4;1-1* plants may be associated with an environmental stress response. That is, *pht4;1-1* plants may be more sensitive to abiotic stress than wild-type plants, and as a consequence, exhibit slower growth rate. To assess stress

responses of wild-type and *pht4;1-1* plants, detached leaves were exposed to high light, high salinity, oxidative and cold stress. Expression levels of the stress-induced genes *VDE* (violaxanthin de-epoxidase), *ZEP* (zeaxanthin epoxidase), *CBF3* (C-repeat binding protein 3), *sHSP* (class 1 small heat shock protein) and the chlorophyll-binding protein *ELIP2* (early light-induced protein 2) (North et al., 2005; Kleine et al., 2007; Miura et al., 2007; Rossel et al., 2007) were quantified by qRT-PCR.

The *pht4;1-1* leaves showed an increased expression of *VDE* under both salinity and cold stress (Fig. 24). There was no significant change in relative expression level of *ZEP* and *CBF3* between wild-type and *pht4;1-1*. Relative expression levels of *sHSP* was higher under both high light and oxidative stress in *pht4;1-1*. Finally, under high light treatment, *pht4;1-1* leaves showed a 50% decrease in relative expression levels of *ELIP2* when compared to wild-type leaves. These results confirm that *pht4;1-1* plants exhibit a wide range of altered stress responses, some of which may be contributing to the reduced leaf size phenotype.

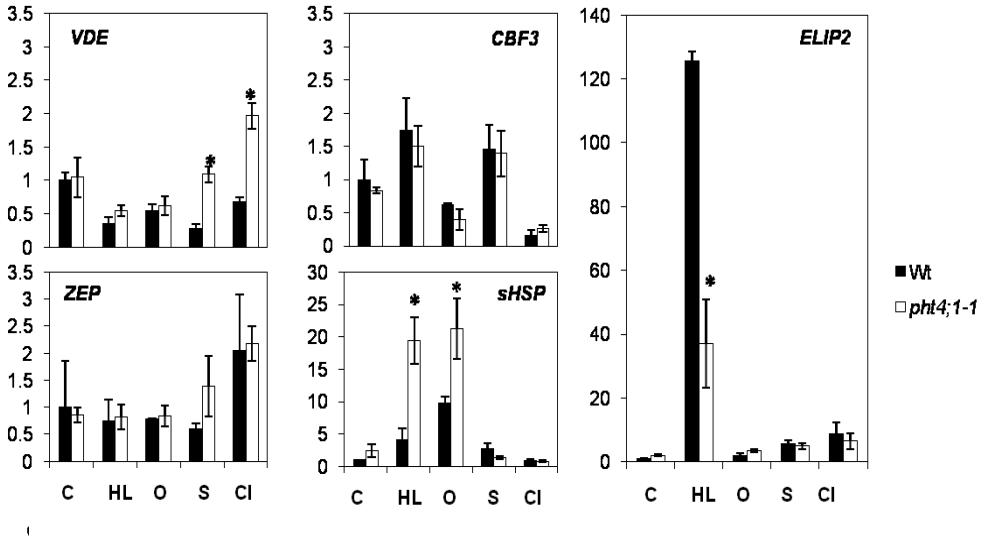

Figure 24. Relative expression levels of stress-induced genes in *pht4;1-1* leaves. Expression levels were normalized to *EIF-4A2* and are relative to the respective WT control. C, control; HL, high light; O, oxidative; S, salinity; Cl, cold.
*significant at $p<0.05$, Student's T-test.

Discussion

In nature, plants are exposed to varying light intensities, and thus may have evolved regulatory responses to protect the photosynthetic machinery from light stress. High light stress, like many other types of environmental stresses, results in the production of reactive oxygen species (Niyogi, 1999) that damage cellular components and even cause death. Chloroplasts and specifically, thylakoids, are important stress sensors in plants. In thylakoid membranes, the close proximity of O_2 liberated from water to the electron transport chain can generate reactive oxygen species that can

potentially oxidize pigments, proteins and lipids (Pessarakli, 1999). Hence, maintenance of homeostasis within the thylakoid compartments is crucial to plant response to abiotic stress. The PHT4;1 transporter localizes to the thylakoid membranes, and its expression is regulated by the circadian clock (Guo et al., 2008b), peaking in during the light. The present work indicates that PHT4;1 is necessary for appropriate responses to a number of abiotic stresses.

Reduction of photosynthetic efficiency can protect plants from photodamage. This mechanism helps deflect excessive light and dissipate it in the form of heat. Such a transition, known as non-photochemical quenching (NPQ), involves activation of the xanthophyll cycle In one of these biochemical reactions, the carotenoid violaxanthin (Vio) is transformed to zeaxanthin (Zea) by the enzyme violaxanthin de-epoxidase (VDE) (Demmig-Adams and Adams, 1992). However, the exact role of zeaxanthin in the quenching process is still unclear.

An increase in light dissipation and reduction of photosynthetic efficiency may have negative effects on plant development. An analysis of *pht4;1* plants under restrictive photoperiod conditions (8h photoperiod) showed that their leaves were smaller when compared to wild-type. Interestingly, this phenotype is reminiscent of the Arabidopsis ascorbate-deficient mutants, *vtc1* and *vtc2*, which also exhibit reduced leaf size and lower photosynthesis under short (10h) photoperiod conditions (Müller-Moulé et al., 2004). Reduced *ELIP2* transcript levels in *pht4;1-1* leaves that have been exposed to HL stress support this hypothesis, as *ELIP* transcript levels transiently increase shortly after HL exposure, and suppression of *ELIP1* and *ELIP2* can cause changes in

chlorophyll and zeaxanthin levels, increasing light sensitivity and reducing photosynthesis. The process by which ELIP accumulation causes these changes is not clear, although it is thought that it interacts with some components of the chloroplast biosynthesis pathway, thereby reducing the levels of some chlorophyll precursors (Tzvetkova-Chevolleau et al., 2007).

In Arabidopsis, expression of both *ZEP* and *VDE* is down-regulated by drought stress; however, an increase in *VDE* was observed in *pht4;1-1* mutants. VDE catalyzes the conversion of violaxanthin to zeaxanthin, which is the first committed precursor for abscisic acid (ABA) synthesis. ABA signaling triggers responses to various abiotic stresses like drought, salinity and cold, among others. The increased expression of *VDE* in *pht4;1-1* plants correlates with the increased sensitivity of *pht4;1-1* mutants to abiotic stress.

Taken together, these results indicate that disruption of the *PHT4;1* renders plants hypersensitive to multiple abiotic stresses, including photooxidative damage. Given the decreased growth of *pht4;1-1* plants, it is possible that these hypersensitivities lead to a reduction in net photosynthetic rate. Additional experiments are needed to determine the specific roles of PHT4;1 in photosynthesis. It will be particularly interesting to elucidate the relationships between PHT4;1, xanthophyll pigments and non-photosynthetic quench.

Methods

Plant material and growth conditions

An *Arabidopsis thaliana* (L.) Heynh *Ds* transposon insertion line (ABRC stock #CS171768, *pht4;1-1*) was obtained from the JIC Gene Trap collection. Insertion site and zygosity were confirmed by PCR using combinations of *PHT4;1*-specific primers and primers that anneal to the transposon Ds borders. The sequence of amplicons that spanned the insertion junctions was confirmed by DNA sequencing. Homozygous *pht4;1-1* plants were screened by DNA gel blot analysis using the GUS segment of the Ds transposon as a probe to identify individuals with insertions at a single locus. Plants were grown in chambers at 21°C with 70% relative humidity and an 8 h photoperiod (150 μmol m^{-2} s^{-1}) in soil (SunGro Redi-earth, Bellevue, WA) or hydroponically as previously described (Noren et al., 2004; Guo et al., 2008b).

RT-PCR analysis

Total RNA was isolated from wild-type and *pht4;1-1* leaves using TRI reagent (Sigma Aldrich, St. Louis, MO), and traces of DNA were eliminated with the TURBO DNA-free kit (Ambion, Austin, TX). First-strand cDNA was synthesized using SuperScript first-strand cDNA synthesis kit (Invitrogen, Carlsbad, CA). RT-PCR was conducted using primers that align downstream of the Ds transposon insertion. RT-PCR with primers specific to *EIF-4A2* was used an RNA input control.

Abiotic stress treatments

Wild-type (*Ler*) and *pht4;1-1* plants were grown in soil in individual pots for 7 weeks with an 8 hr photoperiod, 125 μmol m^{-2} s^{-1} light intensity. For each treatment, the 9^{th} or 10^{th} fully expanded rosette leaf was harvested from 3 individual plants 1 hr after onset of light so that the 3 hr treatments ended at the midpoint of the photoperiod. Unless indicated otherwise, stress treatments were carried out in ambient light (~12 μmol m^{-2} s^{-1}) at room temperature (22°C). Leaves were floated with abaxial side facing up.

For control conditions, leaves were floated in water at room temperature. For high light treatment, leaves were floated in 600 ml of water as a heat sink while subjected to 1000 μmol photons m^{-2} s^{-1} light intensity provided by a 150-W fiber optic system with dual gooseneck. Oxidative stress and salt treatments were carried out by floating the leaves in 20 mM hydrogen peroxide and 200 mM NaCl, respectively. Finally, the cold treatment consisted of floating the leaves in 4°C water. After 3 hr treatments, individual leaves were transferred to centrifuge tubes, snap-frozen in liquid nitrogen and stored at -80°C.

Total RNA was isolated from leaves using TRI reagent (Sigma Aldrich, St. Louis, MO), and traces of DNA were eliminated with TURBO DNA-free (Ambion, Austin, TX). First-strand cDNA was synthesized from 1 μg total RNA using SuperScript first-strand cDNA synthesis kit (Invitrogen, Carlsbad, CA). Real-time PCR was conducted with Power SYBR Green Master Mix and the ABI Prism 7500 sequence detection system (Applied Biosystems, Foster City, CA). Expression levels were normalized to *EIF-4A2* (Guo et al., 2008b).

SDS-PAGE and Western blotting

Arabidopsis thylakoids were isolated as described by Norén et al. (1999), and thylakoid proteins were separated by electrophoresis using 14 % (w/v) acrylamide SDS-gels. Following electroblotting to PVDF membranes (Millipore, Bedford, MA), the PHT4;1 protein was immunodetected using a peptide antibody against the 15 residues within the N terminus of the protein (73–88, CEGDKVSGNNDVVSDSP) produced in rabbits and purified by affinity chromatography by Innovagen (Lund, Sweden). The blots were further probed with secondary donkey anti-rabbit antibody conjugated to horseradish peroxidase and developed using a chemiluminescent substrate kit (GE Healthcare, UK). To verify the purity of the thylakoid preparations, antibodies against the thylakoid LHCII protein (Agrisera, Umeå, Sweden) were employed (data not shown).

Leaf size analysis

The area of rosettes was determined from digital images that included reference objects using the histogram function of Adobe Photoshop, as described in Chapter III.

CHAPTER V

CONCLUSIONS AND FUTURE DIRECTIONS

The PHT4 family of plant organellar Pi transporters was initially identified by sequence similarity to SLC17/Type I Pi transporters, a family of proteins that carry out transport of Pi, organic anions and chloride in animal cells. Functional studies confirmed that each of the six members of the PHT4 family in Arabidopsis catalyzes Pi transport with high specificity when expressed in yeast (Guo et al., 2008a). Subcellular localization studies with GFP fusions revealed that five of these proteins localize to plastids and one localizes to the Golgi apparatus. Phylogenetic analysis suggests that the PHT4 transporter family diverged prior to the monocot-dicot split about 140-150 Myr ago, as all six members have been preserved as distinct orthologs in Arabidopsis and rice. This level of conservation suggests unique physiological roles for each of the PHT4 members.

The current study has revealed differences in the spatial and temporal expression of the plastid-localized members of the Arabidopsis PHT4 Pi transporter family, which further supports the idea that the individual members of this family have specialized rather than redundant roles. Additionally, I presented evidence for the role of the PHT4;1 and PHT4;2 transporters in plant metabolism and development.

In nonphotosynthetic plastids, the strict requirement for import of ATP and precursor metabolites to fuel anabolic processes like synthesis of starch, fatty acids and amino acids (Neuhaus and Emes, 2000) would lead to an imbalance of stromal Pi if not

countered by unidirectional Pi export (Neuhaus and Maass, 1996). Based on expression patterns, I hypothesized that PHT4;2 contributes to this activity in roots and other non-photosynthetic tissues, and that PHT4;3 and PHT2;1 supplement PHT4;2 in distinct root plastid types (Fig. 2). Reduced Pi transport activities of plastids isolated from *pht4;2* roots supports this hypothesis (Fig. 12). Limited accumulation of starch in *pht4;2* roots (Fig. 13) further supports the *in vivo* role for PHT4;2 in Pi export because starch synthesis is allosterically inhibited by Pi accumulation (Preiss, 1982; Sivak and Walker, 1986; Ballicora et al., 2004). Although it could be expected that the reduction in starch levels would lead to a corresponding accumulation of sucrose (Suc), I found no significant differences in the accumulation of Suc in *pht4;2* roots or leaves. This does not preclude the possibility that carbon partitioning defects involving other sugars or amino acids and lipids exist.

The *pht4;2* mutants exhibit an unexpected growth phenotype in which fully-expanded leaves are larger than those of wild type when plants are grown with a short photoperiod. This leaf-size phenotype is a function of increased cell number with no change in cell size (Table II). Phytohormones such as auxin and cytokinin can affect organ formation and influence cell division and expansion. Therefore, several experiments were performed to determine whether changes in these hormones and their respective signaling pathways were responsible for the *pht4;2* leaf-size phenotype. First, the *pht4;2* mutants were crossed to the high-auxin mutant *yucca* (Zhao et al., 2001) and the low-auxin mutant *IAAL* (Romano et al., 1991), and the resulting double mutants *pht4;2/yucca* and *pht4;2/IAAL* were compared to wild-type and the individual parents.

The double mutants were indistinguishable from the *yucca* and *IAAL* parents, suggesting that the severe auxin phenotypes of *yucca* and *IAAL* mask the effects of the *pht4;2* mutation on leaf size. As an alternative approach, I crossed *pht4;2* to plants carrying the *DR5::GUS* auxin-responsive reporter and analyzed progeny for altered GUS expression patterns. I did not observe any effect of the *pht4;2* mutation on *DR5::GUS* expression. Similarly, transcript levels of the auxin-responsive genes *IAAL9*, *CKX4*, *CYP735A4* and *SAUR-AC1* were equivalent in wild-type and *pht4;2* plants. These results suggest that the *pht4;2* mutation has no effect on auxin levels or downstream components of auxin signaling.

I used strategies similar to those for auxin signaling to assess the effect of *pht4;2* mutations on cytokinin signaling. That is, *pht4;2* mutations had no effect on expression of the cytokinin-responsive *pARR5::GUS* reporter or endogenous cytokinin-responsive genes *CRE1*, *AHK2* and *AHK3*. Cytokinin-dependent leaf chlorophyll retention in dark-treated leaves (Riefler et al., 2006) was also equivalent for wild-type and *pht4;2* plants. Taken together, these results suggest that the increased leaf size of *pht4;2* is the result of a signaling pathway independent of auxin and cytokinin.

To broadly survey whether *pht4;2* mutations are associated with changes in the abundance of specific metabolites/signaling molecules we participated in a metabolite profiling workshop hosted by the Samuel Roberts Noble Foundation. As part of this workshop we prepared small-scale metabolite profiles of *pht4;2* and wild-type roots and leaves using GC-MS. The results revealed that *pht4;2* roots, but not leaves, have nearly 7-fold more trehalose (Tre) than wild-type. Unlike Suc, Tre is only present in trace

amounts (0.1 μM - 10 μM) in plant cells, so it may play a regulatory role rather than energy or structural roles (Gómez et al., 2006; Paul et al., 2008). Alterations in Tre synthesis genes are associated with developmental phenotypes in some plant species. Arabidopsis *tps1* mutants that lack a functional copy of the trehalose-6-phosphate synthase 1 (*TPS1*) gene exhibit arrest at the embryonic torpedo stage unless they are cold stratified for an extended period (1-3 weeks), and also have a slow development characterized by a reduced rate of cell division (Gómez et al., 2006), suggesting that TPS1 is essential for normal vegetative growth. However, *TPS* overexpression phenotypes seem to be dependent on the type of plant host. When the *TPS* homolog *OtsA* from *Rhizobium etli* is overexpressed in *P. vulgaris*, plants exhibit increased leaf biomass and higher seed yield than wild-type plants (Suárez et al., 2008). In contrast, Arabidopsis plants overexpressing *E. coli OtsA* exhibit increased T6P content and smaller rosette leaves than wild-type; whereas plants overexpressing *OtsB*, a trehalose phosphate phosphatase homolog accumulate less T6P and have larger leaves than wild-type plants (Schluepmann et al., 2003). Given these contradictory results, it is unclear whether the growth phenotypes are caused by T6P or Tre, but a role for Tre metabolism in plant growth is clear.

Because my metabolic profiling was conducted with few samples (two biological replicates), I wanted to assess the apparent correlation between *pht4;2* and Tre levels using an independent approach. I used qRT-PCR to determine the expression levels of the trehalose-6-phosphate synthesis genes *TPS1* and *TPS5*, as well as the trehalase *TRE1* gene. Trehalase catalyzes the conversion of Tre to Glc. The transcript levels of *TPS1*,

TPS5 and *TRE1* are all significantly greater in *pht4;2* roots than in wild type (Fig. 25), implicating a role for Tre signaling in the increased leaf size of *pht4;2* mutants.

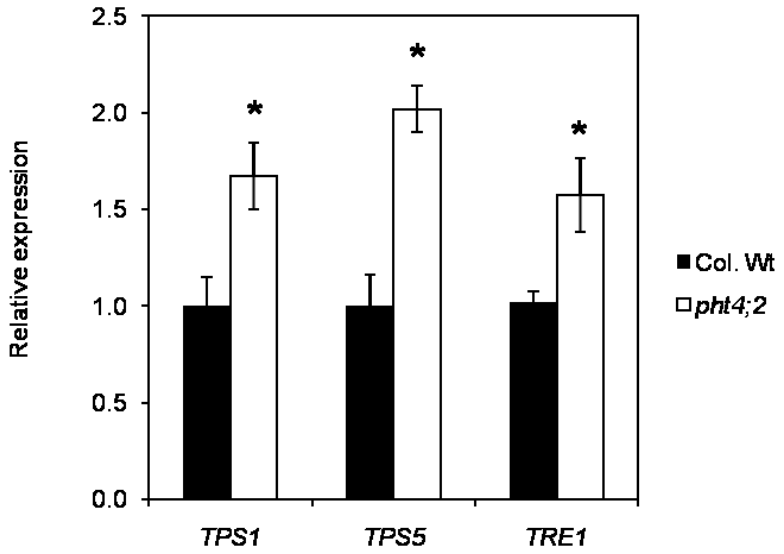

Figure 25. Relative expression levels of trehalose synthesis genes in *pht4;2*. A qRT-PCR analysis of mature *pht4;2* roots shows increased levels of the synthesis subunits of T6P synthase, *TPS1* and *TPS5* and of the trehalase 1 (*TRE1*) transcripts. Line represents expression levels in wild type leaves.

Because Tre levels and transcripts for Tre metabolism genes were elevated only in the roots of *pht4;2* plants, I hypothesize that Tre or Tre-6P represent a mobile signal between the root and shoot that influences cell proliferation in leaves. To first test the hypothesis that a root-derived mobile signal of any kind is responsible for the *pht4;2* leaf-size phenotype, I plan to conduct a grafting experiment. If the large-leaf phenotype of *pht4;2* mutants is caused by a signal originating from the root, wild-type shoots grafted on *pht4;2* root stock would exhibit enlarged leaves, much like the non-grafted *pht4;2* mutants. Conversely, a *pht4;2* shoot grafted on a wild-type root stock would show no increase in leaf size.

A transgenic approach will be required to test whether increased Tre or Tre-6P levels are causal for the *pht4;2* leaf-size phenotype. Specifically, Tre synthesis and Tre-6P phosphatase genes will be over-expressed under the control of a root-specific promoter in a wild-type background. Causality would be supported if one of these transgenic lines phenocopies the large-leaf phenotype of *pht4;2* mutants. The *PHT4;2* promoter directs relatively low expression. Therefore, to drive high, root-specific expression of Tre metabolism genes, I will use the *PYK10* myrosinase promoter. This promoter has been confirmed to mediate high levels of gene expression specifically in the root (Nitz et al., 2001). Primers designed to amplify a 1456-bp promoter fragment of *PYK10* (Werner et al., 2010) were used to carry out the cloning of the *PYK10* promoter. Confirmation of promoter activity and preparation of the required gene fusions are in process.

Although our knowledge of sugar signaling, cell cycle regulation and lateral organ size development is growing, it remains unclear how these different processes are coordinated. The morphological and molecular phenotypes of the *pht4;2* mutants suggest that these pathways are interconnected. Recently, Snf-related kinase 1 (SnRK1), a protein involved in sugar signal transduction, was found to respond to Pi-starvation (Fragoso et al., 2009). In addition, it has been proposed that SnRK1 may act as a link between sugar (Glc, Suc and Tre) signaling and cell cycle control in meristems (Francis and Halford, 2006). SnRK1 is a heterotrimer formed by a α-catalytic subunit and β- and γ- regulatory subunits, which in Arabidopsis are encoded by multiple genes. Some of the catalytic isoforms localize to chloroplasts (Fragoso et al., 2009), and hence are ideally positioned to mediate communication between plastidic Pi homeostasis, carbon metabolism and cell cycle in different plant organs. Additional experiments are needed to resolve whether PHT4;2 influences SnRK1 functions.

PHT4;1 is expressed predominantly in photosynthetic tissues and immunoblot results confirmed that PHT4;1 is localized in thylakoids (Fig. 20). Given this location, PHT4;1 may play a role in Pi recycling from the thylakoid lumen to the stroma. Transcript analysis showed that *PHT4;1* expression is controlled by the circadian clock. This constitutes the first instance that links circadian clock regulation of a Pi transporter. Characterization of *pht4;1-1* plants revealed a reduction in rosette size when plants are grown in short day conditions. The cause of this phenotype is not clear, but preliminary analyses indicate that the mutant is hyper-responsive to multiple types of abiotic stress. Specifically, altered expression levels of *ELIP2* and *VDE* (Fig. 24), which are involved

in chlorophyll and zeaxanthin synthesis, respectively, are indicative of an increased sensitivity to photooxidative damage. Mutants with altered abiotic stress-responses, such as the ascorbate-deficient mutants, *vtc1* and *vtc2*, have a reduced-size phenotype resulting from reduced photosynthesis as a response to hypersensitivity to oxidative stress (Müller-Moulé et al., 2004). It will be interesting to test whether the *pht4;1-1* mutants have altered photosynthetic capacity and whether the increased high-light sensitivity in *pht4;1-1* results in decreased photosynthesis.

In summary, the reduced leaf size phenotype of *pht4;1-1* mutants may be a result of hypersensitivity to photooxidative damage, which may lead to a decrease in net photosynthetic rate. Additional experiments are needed to determine the influence of PHT4;1 on the production of photosynthetic pigments as well as the pigments involved in non-photosynthetic quench (NPQ). Further analysis of PHT4;1 and each of the other PHT4 Pi transporter proteins is needed to provide additional insight into how Pi homeostasis in plastids of different tissues influences plant metabolism. Such knowledge may help us define the mechanisms whereby Pi regulation, carbon metabolism and cell proliferation are coordinated in different plant organs and lead to agricultural applications to maximize crop production on low-Pi soils or under abiotic stress.

LITERATURE CITED

Alonso JM, Stepanova AN, Leisse TJ, Kim CJ, Chen H, Shinn P, Stevenson DK, Zimmerman J, Barajas P, Cheuk R, Gadrinab C, Heller C, Jeske A, Koesema E, Meyers CC, Parker H, Prednis L, Ansari Y, Choy N, Deen H, Geralt M, Hazari N, Hom E, Karnes M, Mulholland C, Ndubaku R, Schmidt I, Guzman P, Aguilar-Henonin L, Schmid M, Weigel D, Carter DE, Marchand T, Risseeuw E, Brogden D, Zeko A, Crosby WL, Berry CC, Ecker JR (2003) Genome-wide insertional mutagenesis of *Arabidopsis thaliana*. Science **301:** 653-657

Amores MV, Hortelano P, García-Salguero L, Lupiáñez JA (1994) Metabolic adaptation of renal carbohydrate metabolism. V. In vivo response of rat renal-tubule gluconeogenesis to different diuretics. Mol Cell Biochem **137:** 117-125

Andersson B, Barber J (1994) Composition, organization, and dynamics of thylakoid membranes. *In* EE Bittar, J Barber, eds, Advances in molecular and cell biology, 10, pp 1-53. Elsevier. Amsterdam, The Netherlands.

Autran D, Jonak C, Belcram K, Beemster GTS, Kronenberg J, Grandjean O, Inze D and Traas J (2002) Cell numbers and leaf development in Arabidopsis: a functional analysis of the STRUWWELPETER gene. EMBO **21:** 6036-6049

Ballicora MA, Iglesias AA, Preiss J (2004) ADP-glucose pyrophosphorylase: a regulatory enzyme for plant starch synthesis. Photosynth Res **79:** 1-24

Barnes SA, Knight JS, Gray JC (1994) Alteration of the amount of the chloroplast phosphate translocator in transgenic tobacco affects the distribution of assimilate between starch and sugar. Plant Physiol **106:** 1123-1129

Bassham JA, Benson AA, Calvin M (1950) The path of carbon in photosynthesis. J Biol Chem **185:** 781-787

Beemster GT, De Veylder L, Vercruysse S, West G, Rombaut D, Van Hummelen P, Galichet A, Gruissem W, Inze D, Vuylsteke M (2005) Genome-wide analysis of gene expression profiles associated with cell cycle transitions in growing organs of Arabidopsis. Plant Physiol **138:** 734-743

Behnke HD (1973) Plastids in sieve elements and their companion cells. Planta **110:** 321-328

Behnke HD (1991) Distribution and evolution of forms and types of sieve-element plastids in the dicotyledons. Aliso **3:** 167-182

Bieleski RL (1973) Phosphate pools, phosphate transport, and phosphate availability. Annu Rev Plant Phys **24:** 225-252

Bogre L, Magyar Z, Lopez-Juez E (2008) New clues to organ size control in plants. Genome Biol **9:** 226

Booij-James IS, Swegle WM, Edelman M, Mattoo AK (2002) Phosphorylation of the D1 photosystem II reaction center protein is controlled by an endogenous circadian rhythm. Plant Physiol **130:** 2069-2075

Bräutigam A, Weber AP (2009) Proteomic analysis of the proplastid envelope membrane provides novel insights into small molecule and protein transport across proplastid membranes. Mol Plant **2:** 1247-1261

Chaw SM, Chang CC, Chen HL, Li WH (2004) Dating the monocot-dicot divergence and the origin of core eudicots using whole chloroplast genomes. J Mol Evol **58:** 424-441

Chloroplast isolation kit (2003) Technical bulletin. SIGMA, Saint Louis, Missouri

Clough SJ, Bent AF (1998) Floral dip: a simplified method for *Agrobacterium*-mediated transformation of *Arabidopsis thaliana*. Plant J **16:** 735-743

Daher Z, Recorbet G, Valot B, Robert F, Balliau T, Potin S, Schoefs B, Dumas-Gaudot E (2010) Proteomic analysis of *Medicago truncatula* root plastids. Proteomics **10:** 2123-2137

Daram P, Brunner S, Rausch C, Steiner C, Amrhein N, Bucher M (1999) *Pht2;1* encodes a low-affinity phosphate transporter from Arabidopsis. Plant Cell **11:** 2153-2166

De Veylder L, Beeckman T, Beemster GT, Krols L, Terras F, Landrieu I, van der Schueren E, Maes S, Naudts M, Inze D (2001) Functional analysis of cyclin-dependent kinase inhibitors of Arabidopsis. Plant Cell **13:** 1653-1668

Demmig-Adams B, Adams WW (1992) Photoprotection and other responses of plants to high light stress. Annu Rev Plant Physiol Plant Mol Biol **43:** 599-626

Demmig B, Gimmler H (1983) Properties of the isolated intact chloroplast at cytoplasmic K concentrations: I. light-induced cation uptake into intact chloroplasts is driven by an electrical potential difference. Plant Physiol **73:** 169-174

Disch S, Anastasiou E, Sharma VK, Laux T, Fletcher JC, Lenhard M (2006) The E3 ubiquitin ligase BIG BROTHER controls Arabidopsis organ size in a dosage-dependent manner. Curr Biol **16:** 272-279

Dodd AN, Salathia N, Hall A, Kevei E, Toth R, Nagy F, Hibberd JM, Millar AJ, Webb AA (2005) Plant circadian clocks increase photosynthesis, growth, survival, and competitive advantage. Science **309:** 630-633

Eicks M, Maurino V, Knappe S, Flügge UI, Fischer K (2002) The plastidic pentose phosphate translocator represents a link between the cytosolic and the plastidic pentose phosphate pathways in plants. Plant Physiol **128:** 512-522

Emanuelsson O, Brunak S, von Heijne G, Nielsen H (2007) Locating proteins in the cell using TargetP, SignalP and related tools. Nat Protoc **2:** 953-971

Emes MJ, England S (1986) Purification of plastids from higher-plant roots. Planta **168:** 161-166

Ferro M, Salvi D, Brugiere S, Miras S, Kowalski S, Louwagie M, Garin J, Joyard J, Rolland N (2003) Proteomics of the chloroplast envelope membranes from *Arabidopsis thaliana*. Mol Cell Proteomics **2:** 325-345

Ferro M, Salvi D, Riviere-Rolland H, Vermat T, Seigneurin-Berny D, Grunwald D, Garin J, Joyard J, Rolland N (2002) Integral membrane proteins of the

chloroplast envelope: identification and subcellular localization of new transporters. Proc Natl Acad Sci USA **99:** 11487-11492

Fischer K, Kammerer B, Gutensohn M, Arbinger B, Weber A, Hausler RE, Flugge UI (1997) A new class of plastidic phosphate translocators: a putative link between primary and secondary metabolism by the phosphoenolpyruvate/phosphate antiporter. Plant Cell **9:** 453-462

Fliege R, Flügge UI, Werdan K, Heldt HW (1978) Specific transport of inorganic phosphate, 3-phosphoglycerate and triosephosphates across the inner membrane of the envelope in spinach chloroplasts. Biochim Biophys Acta **502:** 232-247

Flügge U, Heldt HW (1991) Metabolite translocators of the chloroplast envelope. Annu Rev Plant Physiol Plant Mol Biol **42:** 129-144

Flügge UI (1992) Reaction mechanism and asymmetric orientation of the reconstituted chloroplast phosphate translocator. Biochim Biophys Acta **1110:** 112-118

Flügge UI (1999) Phosphate translocators in plastids. Annu Rev Plant Physiol Plant Mol Biol **50:** 27-45

Flügge UI (2003) Functional genomics of phosphate antiport systems in plastids. Physiol Plantarum **118:** 475-482

Flügge UI, Fischer K, Gross A, Sebald W, Lottspeich F, Eckerskorn C (1989) The triose phosphate-3-phosphoglycerate-phosphate translocator from spinach chloroplasts: nucleotide sequence of a full-length cDNA clone and import of the in vitro synthesized precursor protein into chloroplasts. EMBO J. **8:** 39-46

Fragoso S, Espíndola L, Páez-Valencia J, Gamboa A, Camacho Y, Martínez-Barajas E, Coello P (2009) SnRK1 Isoforms AKIN10 and AKIN11 are differentially regulated in Arabidopsis plants under phosphate starvation. Plant Physiol **149:** 1906-1916

Francis D, Halford N (2006) Nutrient sensing in plant meristems. Plant Mol Biol **60:** 981-993

Galbraith DW, Harkins KR, Maddox JM, Ayres NM, Sharma DP, Firoozabady E (1983) Rapid flow cytometric analysis of the cell cycle in intact plant tissues. Science **220:** 1049-1051

Genty B, Briantais JM, Baker NR (1989) The relationship between the quantum yield of photosynthetic electron transport and quenching of chlorophyll fluorescence. Biochim Biophys Acta **990:** 87-92

Gómez LD, Baud S, Gilday A, Li Y, Graham IA (2006) Delayed embryo development in the *ARABIDOPSIS TREHALOSE-6-PHOSPHATE SYNTHASE 1* mutant is associated with altered cell wall structure, decreased cell division and starch accumulation. Plant J **46:** 69-84

Gonzalez N, Beemster GT, Inze D (2009) David and Goliath: what can the tiny weed Arabidopsis teach us to improve biomass production in crops? Curr Opin Plant Biol **12:** 157-164

Gonzalez N, De Bodt S, Sulpice R, Jikumaru Y, Chae E, Dhondt S, Van Daele T, De Milde L, Weigel D, Kamiya Y, Stitt M, Beemster GT, Inze D (2010) Increased leaf size: different means to an end. Plant Physiol **153:** 1261-1279

Gross A, Brückner G, Heldt HW, Flügge UI (1990) Comparison of the kinetic properties, inhibition and labelling of the phosphate translocators from maize and spinach mesophyll chloroplasts. Planta **180:** 262-271

Guo B, Irigoyen S, Fowler TB, Versaw WK (2008b) Differential expression and phylogenetic analysis suggest specialization of plastid-localized members of the PHT4 phosphate transporter family for photosynthetic and heterotrophic tissues. Plant Signal Behav **3:** 784-790

Guo B, Jin Y, Wussler C, Blancaflor EB, Motes CM, Versaw WK (2008a) Functional analysis of the Arabidopsis PHT4 family of intracellular phosphate transporters. New Phytol **177:** 889-898

Häusler RE, Schlieben NH, Schultz B, Flügge U (1998) Compensation of the decreased triose phosphate/phosphate translocator activity by accelerated starch turnover and glucose transport in transgenic tobacco. Planta **204:** 366-376

Heineke D, Kruse A, Flügge U, Frommer WB, Riesmeier JW, Willmitzer L, Heldt HW (1994) Effect of antisense repression of the chloroplast triose-phosphate translocator on photosynthetic metabolism in transgenic potato plants. Planta **193:** 174-180

Hemerly A, Engler Jde A, Bergounioux C, Van Montagu M, Engler G, Inze D, Ferreira P (1995) Dominant negative mutants of the Cdc2 kinase uncouple cell division from iterative plant development. EMBO J **14:** 3925-3936

Horiguchi G, Ferjani A, Fujikura U, Tsukaya H (2006) Coordination of cell proliferation and cell expansion in the control of leaf size in *Arabidopsis thaliana*. J Plant Res **119:** 37-42

Horiguchi G, Kim GT, Tsukaya H (2005) The transcription factor AtGRF5 and the transcription coactivator AN3 regulate cell proliferation in leaf primordia of *Arabidopsis thaliana*. Plant J **43:** 68-78

Hruz T, Laule O, Szabo G, Wessendorp F, Bleuler S, Oertle L, Widmayer P, Gruissem W, Zimmermann P (2008) Genevestigator v3: a reference expression database for the meta-analysis of transcriptomes. Adv Bioinformatics **2008:** 420747

Huang S, Raman AS, Ream JE, Fujiwara H, Cerny RE, Brown SM (1998) Overexpression of 20-oxidase confers a gibberellin-overproduction phenotype in Arabidopsis. Plant Physiol **118:** 773-781

Jefferson RA, Kavanaugh TA, Bevan MW (1987) GUS fusions: β-glucuronidase as a sensitive and versitile gene fusion marker in higher plants. EMBO J **6:** 3901-3907

Kammerer B, Fischer K, Hilpert B, Schubert S, Gutensohn M, Weber A, Flügge U-I (1998) Molecular characterization of a carbon transporter in plastids from heterotrophic hissues: the glucose 6-phosphate/phosphate antiporter. Plant Cell **10:** 105-118

Kleine T, Kindgren P, Benedict C, Hendrickson L, Strand A (2007) Genome-wide gene expression analysis reveals a critical role for CRYPTOCHROME1 in the response of Arabidopsis to high irradiance. Plant Physiol **144:** 1391-1406

Knappe S, Flügge U-I, Fischer K (2003) Analysis of the plastidic phosphate translocator gene family in Arabidopsis and identification of new phosphate translocator-homologous transporters, classified by their putative substrate-binding site. Plant Physiol **131:** 1178-1190

Krizek BA (2009) Making bigger plants: key regulators of final organ size. Curr Opin Plant Biol **12:** 17-22

Kunz HH, Hausler RE, Fettke J, Herbst K, Niewiadomski P, Gierth M, Bell K, Steup M, Flugge UI, Schneider A (2010) The role of plastidial glucose-6-phosphate/phosphate translocators in vegetative tissues of *Arabidopsis thaliana* mutants impaired in starch biosynthesis. Plant Biol (Stuttg) **12 Suppl 1:** 115-128

Lee BH, Ko J-H, Lee S, Lee Y, Pak J-H, Kim JH (2009) The Arabidopsis GRF-INTERACTING FACTOR gene family performs an overlapping function in determining organ size as well as multiple developmental properties. Plant Physiol **151:** 655-668

Li J, Yang H, Peer WA, Richter G, Blakeslee J, Bandyopadhyay A, Titapiwantakun B, Undurraga S, Khodakovskaya M, Richards EL, Krizek B, Murphy AS, Gilroy S, Gaxiola R (2005) Arabidopsis H^+-PPase AVP1 regulates auxin-mediated organ development. Science **310:** 121-125

Li Y, Zheng L, Corke F, Smith C, Bevan MW (2008) Control of final seed and organ size by the DA1 gene family in *Arabidopsis thaliana*. Gene Dev **22:** 1331-1336

Lu H, McKnight TD (1999) Tissue-specific expression of the beta-subunit of tryptophan synthase in *Camptotheca acuminata*, an indole alkaloid-producing plant. Plant Physiol **120:** 43-52

Lundin B, Hansson M, Schoefs B, Vener AV, Spetea C (2007a) The Arabidopsis PsbO2 protein regulates dephosphorylation and turnover of the photosystem II reaction centre D1 protein. Plant J **49:** 528-539

Lundin B, Thuswaldner S, Shutova T, Eshaghi S, Samuelsson G, Barber J, Andersson B, Spetea C (2007b) Subsequent events to GTP binding by the plant PsbO protein: structural changes, GTP hydrolysis and dissociation from the photosystem II complex. Biochim Biophys Acta **1767:** 500-508

Malinova I, Setup M, Fettke J (2011) Starch-related cytosolic heteroglycans in roots from *Arabidospsis thaliana*. Plant Physiol doi:10.1016/j.jplph.2010.12.008

Massonnet C, Vile D, Fabre J, Hannah MA, Caldana C, Lisec J, Beemster GTS, Meyer RC, Messerli G, Gronlund JT, Perkovic J, Wigmore E, May S, Bevan MW, Meyer C, Rubio-Diaz S, Weigel D, Micol JL, Buchanan-Wollaston V, Fiorani F, Walsh S, Rinn B, Gruissem W, Hilson P, Hennig L, Willmitzer L, Granier C (2010) Probing the reproducibility of leaf growth and molecular phenotypes: a comparison of three Arabidopsis accessions cultivated in ten laboratories. Plant Physiol **152:** 2142-2157

Melaragno JE, Mehrotra B, Coleman AW (1993) Relationship between endopolyploidy and cell size in epidermal tissue of Arabidopsis. Plant Cell **5:** 1661-1668

Michael TP, McClung CR (2002) Phase-specific circadian clock regulatory elements in Arabidopsis. Plant Physiol **130:** 627-638

Mimura T (1999) Regulation of phosphate transport and homeostasis in plant cells. *In* WJ Kwang, ed, International review of cytology, 191, pp 149-200. Academic Press, New York

Miura K, Jin JB, Lee J, Yoo CY, Stirm V, Miura T, Ashworth EN, Bressan RA, Yun D-J, Hasegawa PM (2007) SIZ1-mediated sumoylation of ICE1 controls CBF3/DREB1A expression and freezing tolerance in Arabidopsis. Plant Cell Online **19:** 1403-1414

Mizukami Y, Fischer RL (2000) Plant organ size control: AINTEGUMENTA regulates growth and cell numbers during organogenesis. Proc Natl Acad Sci USA **97:** 942-947

Moretti S, Armougom F, Wallace IM, Higgins DG, Jongeneel CV, Notredame C (2007) The M-Coffee web server: a meta-method for computing multiple sequence alignments by combining alternative alignment methods. Nucleic Acids Res **35:** W645-648

Muchhal US, Pardo, JM, Raghothama, KG (1996) Phosphate transporters from the higher plant *Arabidopsis thaliana*. Proc Natl Acad Sci USA **93:** 10519-10523

Müller-Moulé P, Golan T, Niyogi KK (2004) Ascorbate-deficient mutants of arabidopsis grow in high light despite chronic photooxidative stress. Plant Physiol **134:** 1163-1172

Muller P, Li X-P, Niyogi KK (2001) Non-photochemical quenching. A response to excess light energy. Plant Physiol **125:** 1558-1566

Murashige T, Skoog F (1962) A revised medium for rapid growth and bioassays with tobacco tissue cultures. Physiol Plant **15:** 473-497

Neuhaus HE, Emes MJ (2000) Nonphotosynthetic metabolism in plastids. Annu Rev Plant Physiol Plant Mol Biol **51:** 111-140

Neuhaus HE, Maass U (1996) Unidirectional transport of orthophosphate across the envelope of isolated cauliflower-bud amyloplasts. Planta **198:** 542-548

Niewiadomski P, Knappe S, Geimer S, Fischer K, Schulz B, Unte US, Rosso MG, Ache P, Flügge UI, Schneider A (2005) The Arabidopsis plastidic glucose 6-phosphate/phosphate translocator GPT1 is essential for pollen maturation and embryo sac development. Plant Cell **17:** 760-775

Nitz I, Berkefeld H, Puzio PS, Grundler FMW (2001) Pyk10, a seedling and root specific gene and promoter from *Arabidopsis thaliana*. Plant Science **161:** 337-346

Niyogi KK (1999) Photoprotection revisited: genetic and molecular approaches. Annu Rev Plant Physiol Plant Mol Biol **50:** 333-359

Noguchi T, Fujioka S, Takatsuto S, Sakurai A, Yoshida S, Li J, Chory J (1999) Arabidopsis *det2* is defective in the conversion of (24R)-24-methylcholest-4-En-3-one to (24R)-24-methyl-5alpha-cholestan-3-one in brassinosteroid biosynthesis. Plant Physiol **120:** 833-840

Norén H, Svennsson P, Andersson B (2004) A convenient and versatile hydroponic cultivation system for *Arabidopsis thaliana*. Physiol Plant **121:** 343-348

Norén H, Svensson P, Andersson B (1999) Auxiliary photosynthetic functions of *Arabidopsis thaliana*—Studies in vitro and in vivo. Bioscience Rep **19:** 499-509

North HM, Frey A, Boutin J-P, Sotta B, Marion-Poll A (2005) Analysis of xanthophyll cycle gene expression during the adaptation of Arabidopsis to excess light and drought stress: changes in RNA steady-state levels do not contribute to short-term responses. Plant Science **169:** 115-124

Palatnik JF, Allen E, Wu X, Schommer C, Schwab R, Carrington JC, Weigel D (2003) Control of leaf morphogenesis by microRNAs. Nature **425:** 257-263

Paszkowski U, Kroken S, Roux C, Briggs SP (2002) Rice phosphate transporters include an evolutionarily divergent gene specifically activated in arbuscular mycorrhizal symbiosis. Proc Natl Acad Sci USA **99:** 13324-13329

Paterson AH, Bowers JE, Chapman BA (2004) Ancient polyploidization predating divergence of the cereals, and its consequences for comparative genomics. Proc Natl Acad Sci USA **101:** 9903-9908

Paul MJ, Primavesi LF, Jhurreea D, Zhang Y (2008) Trehalose metabolism and signaling. Annu Rev Plant Biol **59:** 417-441

Pessarakli M (1999) Handbook of plant and crop stress (2nd Edition). Marcel Dekker, New York

Preiss J (1982) Regulation of the biosynthesis and degradation of starch. Annu Rev Plant Biol **33:** 431-454

Pyke K (2009) Plastid biology. Cambridge University Press, Cambridge, UK

Raghothama KG (1999) Phosphate acquisition. Annu Rev Plant Phys Plant Mol Biol **50:** 665-693

Rath A, Glibowicka M, Nadeau VG, Chen G, Deber CM (2009) Detergent binding explains anomalous SDS-PAGE migration of membrane proteins. Proc Natl Acad Sci USA **106:** 1760-1765

Rausch C, Bucher M (2002) Molecular mechanisms of phosphate transport in plants. Planta **216:** 23-37

Rausch C, Zimmermann P, Amrhein N, Bucher M (2004) Expression analysis suggests novel roles for the plastidic phosphate transporter Pht2;1 in auto- and heterotrophic tissues in potato and Arabidopsis. Plant J **39:** 13-28

Reinhold T, Alawady A, Grimm B, Beran KC, Jahns P, Conrath U, Bauer J, Reiser J, Melzer M, Jeblick W, Neuhaus HE (2007) Limitation of nocturnal import of ATP into Arabidopsis chloroplasts leads to photooxidative damage. Plant J **50:** 293-304

Reiser J, Linka N, Lemke L, Jeblick W, Neuhaus HE (2004) Molecular physiological analysis of the two plastidic ATP/ADP transporters from Arabidopsis. Plant Physiol **136:** 3524-3536

Ren S, Johnston JS, Shippen DE, McKnight TD (2004) TELOMERASE ACTIVATOR1 induces telomerase activity and potentiates responses to auxin in Arabidopsis. Plant Cell **16:** 2910-2922

Riefler M, Novak O, Strnad M, Schmulling T (2006) Arabidopsis cytokinin receptor mutants reveal functions in shoot growth, leaf senescence, seed size, germination, root development, and cytokinin metabolism. Plant Cell **18:** 40-54

Riesmeier JW, Flügge UI, Schulz B, Heineke D, Heldt HW, Willmitzer L, Frommer WB (1993) Antisense repression of the chloroplast triose phosphate translocator affects carbon partitioning in transgenic potato plants. Proc Natl Acad Sci USA **90:** 6160-6164.

Riou-Khamlichi C, Menges M, Healy JMS, Murray JAH (2000) Sugar control of the plant cell cycle: differential regulation of Arabidopsis D-type cyclin gene expression. Mol Cell Biol **20:** 4513-4521

Romano CP, Hein MB, Klee HJ (1991) Inactivation of auxin in tobacco transformed with the indoleacetic acid-lysine synthetase gene of *Pseudomonas savastanoi*. Gene Dev **5:** 438-446

Rossel JB, Wilson PB, Hussain D, Woo NS, Gordon MJ, Mewett OP, Howell KA, Whelan J, Kazan K, Pogson BJ (2007) Systemic and intracellular responses to photooxidative stress in Arabidopsis. Plant Cell Online **19:** 4091-4110

Roth C, Menzel G, Petetot JM, Rochat-Hacker S, Poirier Y (2004) Characterization of a protein of the plastid inner envelope having homology to animal inorganic phosphate, chloride and organic-anion transporters. Planta **218:** 406-416

Ruiz Pavón L, Karlsson PM, Carlsson J, Samyn D, Persson B, Persson BL, Spetea C (2010) Functionally important amino acids in the Arabidopsis thylakoid phosphate transporter: homology modeling and site-directed mutagenesis. Biochemistry **49:** 6430-6439

Ruiz Pavón L, Lundh F, Lundin B, Mishra A, Persson BL, Spetea C (2008) Arabidopsis ANTR1 is a thylakoid Na^+-dependent phosphate transporter: functional characterization in *Escherichia coli*. J Biol Chem **283:** 13520-13527

Schluepmann H, Pellny T, van Dijken A, Smeekens S, Paul M (2003) Trehalose 6-phosphate is indispensable for carbohydrate utilization and growth in *Arabidopsis thaliana*. Proc Natl Acad Sci U S A **100:** 6849-6854

Schneider A, Häusler RE, Kolukisaoglu Ü, Kunze R, van der Graaff E, Schwacke R, Catoni E, Desimone M, Flügge UI (2002) An *Arabidopsis thaliana* knock-out mutant of the chloroplast triose phosphate/phosphate translocator is severely compromised only when starch synthesis, but not starch mobilisation is abolished. Plant J **32:** 685-699

Schneider T, Keller F (2009) Raffinose in chloroplasts is synthesized in the cytosol and transported across the chloroplast envelope. Plant Cell Physiol **50:** 2174-2182

Schommer C, Palatnik JF, Aggarwal P, Chetelat A, Cubas P, Farmer EE, Nath U, Weigel D (2008) Control of jasmonate biosynthesis and senescence by miR319 targets. PLoS Biol **6:** e230

Schreiber U, Schliwa U, Bilger W (1986) Continuous recording of photochemical and non-photochemical chlorophyll fluorescence quenching with a new type of modulation fluorometer. Photosynth Res **10:** 51-62

Schulz B, Frommer WB, Flügge UI, Hummel S, Fischer K, Willmitzer L (1993) Expression of the triose phosphate translocator gene from potato is light dependent and restricted to green tissues. Mol Gen Genet **238:** 357-361

Schulz A, Knoetzel J, Scheller HV, Mant A (2004) Uptake of a fluorescent dye as a swift and simple indicator of irganelle intactness: import-competent chloroplasts from soil-grown Arabidopsis. J Histochem Cytochem **52**: 701-704

Sharkey TD (1985) Photosynthesis in intact leaves of C3 plants: physics, physiology and rate limitations. Bot Rev **51:** 53-105

Sheu-Hwa C-S, Lewis DH, Walker DA (1975) Stimulation of photosynthetic starch formation by sequestration of cytoplasmic orthophosphate. New Phytol **74:** 383-392

Simillion C, Vandepoele K, Van Montagu MC, Zabeau M, Van de Peer Y (2002) The hidden duplication past of *Arabidopsis thaliana*. Proc Natl Acad Sci USA **99:** 13627-13632

Sivak MN, Walker DA (1986) Photosynthesis *in vivo* can be limited by phosphate supply. New Phytol **102:** 499-512

Smith AM, Zeeman SC (2006) Starch and soluble sugar extration and quantification mehods. Nat Protoc **1:** 1342-1345

Song CP, Guo Y, Qiu Q, Lambert G, Galbraith DW, Jagendorf A, Zhu JK (2004) A probable $Na^+(K^+)/H^+$ exchanger on the chloroplast envelope functions in pH homeostasis and chloroplast development in *Arabidopsis thaliana*. Proc Natl Acad Sci USA **101:** 10211-10216

Spetea C, Hundal T, Lundin B, Heddad M, Adamska I, Andersson B (2004) Multiple evidence for nucleotide metabolism in the chloroplast thylakoid lumen. Proc Natl Acad Sci USA **101:** 1409-1414

Steedman HF (1957) Polyester wax; a new ribboning embedding medium for histology. Nature **179:** 1345

Stitt M, Lunn J, Usadel B (2010) Arabidopsis and primary photosynthetic metabolism – more than the icing on the cake. Plant J **61:** 1067-1091

Stitt M, McLilley R, Gerhardt R, Heldt HW (1989) Metabolite levels in specific cells and subcellular compartments of plant leaves. Methods Enzymol **174:** 518-552

Suárez R, Wong A, Ramírez M, Barraza A, Orozco MdC, Cevallos MA, Lara M, Hernández G, Iturriaga G (2008) Improvement of drought tolerance and grain yield in common bean by overexpressing trehalose-6-phosphate synthase in rhizobia. Mol Plant Microbe Int **21:** 958-966

Takahashi M, Sasaki Y, Ida S, Morikawa H (2001) Nitrite reductase gene enrichment improves assimilation of NO(2) in Arabidopsis. Plant Physiol **126:** 731-741

Takizawa K, Kanazawa A, Kramer DM (2008) Depletion of stromal P_i induces high 'energy-dependent' antenna exciton quenching (q_E) by decreasing proton conductivity at CF_o-CF_1 ATP synthase. Plant Cell Environ **31:** 235-243

Tegeder M, Weber APM (2007) Metabolite transporters in the control of plant primary metabolism. *In* Annual Plant Reviews Vol. 22: control of primary metabolism in plants. Blackwell Publishing Ltd, pp 85-120

Thuswaldner S, Lagerstedt JO, Rojas-Stutz M, Bouhidel K, Der C, Leborgne-Castel N, Mishra A, Marty F, Schoefs B, Adamska I, Persson BL, Spetea C (2007) Identification, expression, and functional analyses of a thylakoid ATP/ADP carrier from Arabidopsis. J Biol Chem **282:** 8848-8859

Trentmann O, Jung B, Neuhaus HE, Haferkamp I (2008) Nonmitochondrial ATP/ADP transporters accept phosphate as third substrate. J Biol Chem **283:** 36486-36493

Tsimilli-Michael M, Strasser RJ (2008) Experimental resolution and theoretical complexity determine the amount of information extractable from the chlorophyll fluorescence transient OJIP. *In* JF Allen, E Gantt, JH Golbeck, B Osmond, eds, Photosynthesis. Energy from the sun. Springer, Dordrecth, The Netherlands, pp 697-702

Tzvetkova-Chevolleau T, Franck F, Alawady AE, Dall'Osto L, Carrière F, Bassi R, Grimm B, Nussaume L, Havaux M (2007) The light stress-induced protein ELIP2 is a regulator of chlorophyll synthesis in *Arabidopsis thaliana*. Plant J **50:** 795-809

Usami T, Mochizuki N, Kondo M, Nishimura M, Nagatani A (2004) Cryptochromes and phytochromes synergistically regulate Arabidopsis root greening under blue light. Plant Cell Physiol **45:** 1798-1808

Ventriglia T, Kuhn ML, Ruiz MT, Ribeiro-Pedro M, Valverde F, Ballicora MA, Preiss J, Romero JM (2008) Two Arabidopsis ADP-glucose pyrophosphorylase large subunits (APL1 and APL2) are catalytic. Plant Physiol **148:** 65-76

Versaw WK, Harrison MJ (2002) A chloroplast phosphate transporter, PHT2;1, tnfluences allocation of phosphate within the plant and phosphate-starvation responses. Plant Cell **14:** 1751-1766

Vile D, Garnier E, Shipley B, Laurent G, Navas M, Roumet C, Lavorel S, Diaz S, Hodgson JG, Lloret F, Midgley GF, Poorter H, Rutherford MC, Wilson PJ, Wright IJ (2005) Specific leaf area and dry matter content estimate thickness in laminar leaves. Ann Bot **96:** 1129-1136

Vitha S, Benes K, Phillips JP, Gartland KMA (1995) Histochemical GUS analysis. *In* KMA Gartland, MR Davey, eds, Agrobacterium protocols. Humana Press, Totowa, NJ, pp 185-193

Vlieghe K, Boudolf V, Beemster GT, Maes S, Magyar Z, Atanassova A, de Almeida Engler J, De Groodt R, Inze D, De Veylder L (2005) The DP-E2F-like gene DEL1 controls the endocycle in *Arabidopsis thaliana*. Curr Biol **15:** 59-63

Walker, DA, Cerovic, ZG, Robinson, SP (1987). Isolation of intact chloroplasts: general principles and criteria of integrity. Methods Enzymol **148**, p.155

Walker DA, Sivak MN (1986) Photosynthesis and phosphate: a cellular affair? Trends Biochem Sci **11:** 176-179

Walters RG, Ibrahim DG, Horton P, Kruger NJ (2004) A mutant of Arabidopsis lacking the triose-phosphate/phosphate translocator reveals metabolic regulation of starch breakdown in the light. Plant Physiol **135:** 891-906

Wang Z-Y, Kenigsbuch D, Sun L, Harel E, Ong MS, Tobin EM (1997) A Myb-related transcription factor is involved in the phytochrome regulation of an Arabidopsis *Lhcb* gene. Plant Cell **9:** 491-507

Wang ZY, Seto H, Fujioka S, Yoshida S, Chory J (2001) BRI1 is a critical component of a plasma-membrane receptor for plant steroids. Nature **410:** 380-383

Weigel D, Ahn JH, Blázquez MA, Borevitz JO, Christensen SK, Fankhauser C, Ferráandiz C, Kardailsky I, Malancharuvil EJ, Neff MM, Nguyen JT, Sato S, Wang Z-Y, Xia Y, Dixon RA, Harrison MJ, Lamb CJ, Yanofsky MF, Chory J (2000) Activation tagging in Arabidopsis. Plant Physiol **122:** 1003-1013

Werner T, Nehnevajova E, Köllmer I, Novák O, Strnad M, Krämer U, Schmülling T (2010) Root-specific reduction of cytokinin causes enhanced root growth, drought tolerance, and leaf mineral enrichment in Arabidopsis and tobacco. Plant Cell Online **22:** 3905-3920

White DW (2006) PEAPOD regulates lamina size and curvature in Arabidopsis. Proc Natl Acad Sci USA **103:** 13238-13243

Wu W, Peters J, Berkowitz GA (1991) Surface charge-mediated effects of Mg^{2+} on K^{+} flux across the chloroplast envelope are associated with regulation of stromal pH and photosynthesis. Plant Physiol **97:** 580-587

Wuyts N, Palauqui JC, Conejero G, Verdeil JL, Granier C, Massonnet C (2010) High-contrast three-dimensional imaging of the Arabidopsis leaf enables the analysis of cell dimensions in the epidermis and mesophyll. Plant Methods **6:** 17

Yuan Q, Ouyang S, Wang A, Zhu W, Maiti R, Lin H, Hamilton J, Haas B, Sultana R, Cheung F, Wortman J, Buell CR (2005) The institute for genomic research Osa1 rice genome annotation database. Plant Physiol **138:** 18-26

Zhao L, Versaw WK, Liu J, Harrison MJ (2003) A phosphate transporter from *Medicago truncatula* is expressed in the photosynthetic tissues of the plant and is located in the chloroplast envelope. New Phytol **157:** 291-302

Zhao Y, Christensen SK, Fankhauser C, Cashman JR, Cohen JD, Weigel D, Chory J (2001) A role for flavin monooxygenase-like enzymes in auxin biosynthesis. Science **291:** 306-309

APPENDIX A

Table IA. Primers used for the PCR genotyping of *pht4;2* and *pht4;1* lines.

Primer Name	Direction	Sequence
PHT4;2(2786→2765)	Reverse	5'-ATA TCC CGT CCC TAT TGT ACT T
PHT4;2(1855→1876)	Forward	5'-GTG ACT AAC AAC TGG GTG AGT T
PHT4;2 (278→304)	Forward	5'-GAT GAT GCC TGA GAG GAT TAA GGT AGT
PHT4;2 (806→828)	Reverse	5'-GTG ACC CAC ACG GCC ACA TTA T
PHT4;1(-486→465)	Forward	5'- ATC ATG ATC AAT ACT CTC TCG C
PHT4;1(565→544)	Reverse	5'- GAA AGA AGA CTG AAT CAG ACC A
EIF-4A2(882→911)	Forward	5'-GCA AGA GAA TCT TCT TAG GGG TAT CTA TGC
EIF-4A2 (1575→1549)	Reverse	5'-GGT GGG AGA AGC TGG AAT ATG TCA TAG

Table IIA. Primers used for RT-PCR.

Primer Name	Direction	Sequence
PHT4;2	Forward	5'-AGT AGT ATC GGA CTT CTT GAT
	Reverse	5'-AAA GTG TCC AAG GAG AGC GTT
PHT4;2 (1301→1327)	Forward	5'-CTT TAG CCA AGC TGG ATT TCT CCT CAA
PHT4;2 (1384→1360)	Reverse	5'-CAC AAT TCG AAA TAC CGT GCA GGA A
EIF-4A2(At1g54270)	Forward	5'-GCA AGA GAA TCT TCT TAG GGG TAT CTA TGC
EIF-4A2(At1g54270)	Reverse	5'-GGT GGG AGA AGC TGG AAT ATG TCA TAG
PHT4;1 (659→678)	Forward	5' CGA AGT GGG TTC CTG TGC AA
PHT4;1 (1276→1254)	Reverse	5' TGC ACA AAA CAG CCA TTG TAG GA

Table IIIA. Primers used for quantitative (qRT-PCR) transcript analyses of the PHT4 family.

Gene	Direction	Sequence
EIF-4A2	Forward	5′-CAA GGT GTC AAG GTT CAT GC
	Reverse	5′-CAA CGA CAA CAT GAA CAC CA
PHT4;1	Forward	5′-TCT TCT GGG GTT ACC TTC TTA CA CAGA
	Reverse	5′-TGA GAA TTG TAG CGA TTG ACC ACC AA
PHT4;2	Forward	5′-GAT GAT GCC TGA GAG GAT TAA GGT AGT
	Reverse	5′-TAA CAA CTC TGT CGG CGT TAC ATA GA
PHT4;3	Forward	5′-CAG AAT TTA TAA CGT CGG AGA GAG TCA AA
	Reverse	5′-AA AAT GAT TTG CTC CAT CCA CGA GAA AG
PHT4;4	Forward	5′-TGT GAA CAT GAG CAT TGC AAT TCT T
	Reverse	5′-CAA CAG TTG CAC TAC TCC AGT TAT ATT CT
PHT4;5	Forward	5′-TCC AGT CTT CCT TCT TTT GGG GTT ATG
	Reverse	5′-CGA AAG ACC ATG TAA AGA CAC CAA TCT
PHT4;6	Forward	5′-GAT TGG TTT CGA TAA CGA CAT CAG GAA
	Reverse	5′-ATT CCG GAC CTC TAA GCT CAA CTAA

Table IVA. Primers used for additional RT-PCR transcript analyses in *pht4;1* and *pht4;2*.

Gene	Direction	Sequence
SAUR-AC1	Forward	5'- TTT TTG AGG AGT TTC TTG GGT G
	Reverse	5'- CTG AGA TGT GAC TGT GAA GAA CA
CRE1	Forward	5'- AGA TCG ATT TTT GGC GTT CG
	Reverse	5'- CAG TCG GAT TTT CAG GAA GAG
AHK2	Forward	5'- TGG TGT AGC GTA TGC TTT GAA
	Reverse	5'- TGC ATC TCA TGG TTC CTT GA
AHK3	Forward	5'- TTC CAT GTG CTA GGG TTT GGT
	Reverse	5'- TTT CCC AGA CAG CAT ATC GA
IAAL9	Forward	5'- AGA AGG TTA ATG ATT CGC CG
	Reverse	5'- AAT GAA CCA GCT CCT TGC TT
CKX4	Forward	5'- TGT TCG TAC AAG ATG TTC CGT
	Reverse	5'- TGG AGA CAA TAG TCT TTT GGG
CYP735-A4	Forward	5'- TAA TGT GGA ACG GGA CAG AA
	Reverse	5'- ACC ATC TTG GCC ACA AAC TT

Table VA. Primers used for additional qRT-PCR transcript analyses in *pht4;1* and *pht4;2*.

Gene	Direction	Sequence
NTT1	Forward	5'-ACC CGT AGC AAG AAG AAG AAG GTG
	Reverse	5'-GCA ACC ACC AAA GTA GCA AGA TCC
NTT2	Forward	5'-TGT GTA GTG CGG TGC CCT TCA
	Reverse	5'-ATC GCA GTC TTG CCT TTA ACC TTG
GPT1	Forward	5'- TCG GAC CAC AGT TTG TCT GGT G
	Reverse	5'- TGG AGG AGA CAA TGA CGG AGA TA
GPT2	Forward	5'- TCT ATT GCC GTG GAA GGT CCT C
	Reverse	5'- ACT TTG TGC CAC TAC CCA CCA G
APS1	Forward	5'- AGG GCT GTG TTA TCA AGA ACT GC
	Reverse	5'- TAT GCA GGA ACG GAG TCC AAC C
APL1	Forward	5'- CGA ATC TTG CAC TCA CTG AGC ATC
	Reverse	5'- TGA TGG TGG CAG GTT TCT CCT TG
APL3	Forward	5'- AAA CCG AGA AGT GCC GGA TTG
	Reverse	5'- GTT GGA TGC TGC ATT CTC CCA AG
APL4	Forward	5'- CGT GTG CAC CAG TTA GTG AAA GC
	Reverse	5'- ACG CCC ACC TCG ATC AAT CTT TAC
cFBP	Forward	5'- ACC GGA ATT TCC CAG ACA AA
	Reverse	5'- TCA GCA GAT TTT GGA TCA GG
TPS1	Forward	5'- ATC ACC AAG ATC CTG ACC CAG AC
	Reverse	5' -CAA GCC CTT TGC TTA CTC CCT GAG
TPS5	Forward	5'-AGC TTA TGG AAC ACC TCG AAA GCG
	Reverse	5'-GAC CTT TGT TCA CAC CCT GTG G
	Reverse	5'-AGC CTT CCA TGT CTC AGA TTC CTC

Table VA continued

Gene	Direction	Sequence
TRE1	Forward	5’ -AGG GCA ATG GCT GGA TTA CTG G
	Reverse	5’-AGC CTT CCA TGT CTC AGA TTC CTC
VDE	Forward	5’- TTG CGC GTT CCT TAT TGT TCC ATC
	Reverse	5’- CGG TTT CAT CTG GAC GGT TAT TGC
ZEP	Forward	5’- GAA CGT ACT ATA AAG GGA GAA TGG
	Reverse	5’- CTG AGA CGA AGG GAT CAC AAT
CBF3	Forward	5’-GAT GAC GAC GTA TCG TTA TGG A
	Reverse	5’-TAC ACT CGT TTC TCA GTT TTA CAA AC
sHSP	Forward	5’-CCT GGA TTG AAG AAG GAG GAA
	Reverse	5’-TAG GCA CCG TAA CAG TCA ACA C
ELIP2	Forward	5’-CAC CAC AAA TGC CAC AGT CT
	Reverse	5’-TGC TAG TCT CCC GTT GAT CC

APPENDIX B

METHODS

Arabidopsis Chloroplast Isolation

Adapted from Chloroplast Isolation Kit –Technical Bulletin (SIGMA CP-ISO), Saint Louis, Missouri

Reagents:

1x Grinding Buffer (1000ml)
50mM HEPES-KOH pH 7.5
330mM D-Sorbitol
2mM EDTA
1mM $MgCl_2$
1mM $MnCl_2$
0.25% BSA (add before use)
100mM Sodium Ascorbate (add before use)

Chloroplast Resuspension Medium
300mM D-Sorbitol
0.1% BSA

25%BSA, filter sterilized

0.1 mg/ml Glutatione

80% Percoll, mix 4:1 Percoll:5xGB, 15µg/ml Glutathione
50% Percoll, mix 1:1 Percoll:2.5xGB, 15µg/ml Glutathione

Dissolve HEPES in 500ml of distilled H_2O, adjust pH to 7.5 using KOH, then add the rest of the components one at a time and wait for each to dissolve completely before adding the next. Bring to a volume of 990ml with more H_2O. BSA and Sodium Ascorbate should be added fresh before using.

Materials:
Clean razor blades
Waring blender
Scissors
Miracloth (Calbiochem)

Procedure
All buffers and equipment used should be pre-cooled. Keep Percoll gradients, water and buffers at 4ºC and the blender at -20ºC. The grinding buffer 1xGB with BSA needs to be at 4ºC or as a semi-frozen slush whenever possible.

Preparation of 50/80% Percoll gradient:
Each gradient can separate up to 4ml of chloroplast suspension
1. In a 13ml centrifuge tube, place 2.5ml of 80% Percoll and carefully layer 5ml of 50% Percoll on top.
Note: Percoll gradients can be stored at 4°C for up to two days if kept undisturbed.

Chloroplast Isolation
All steps should be performed at 2 to 4°C. For optimal yield of intact chloroplasts, leaves of two to three week old plants should be used. Plants should be kept in the dark before the preparation so it is recommended to cover them 12 to 14 hours before harvesting.

1. Fold two layers of Miracloth into a funnel shape, soak them in chilled 1xGB and place them into a suitable size funnel.
2. With clean scissors, harvest rosette leaves, and float them in chilled water. After all the plant material is harvested, blot excess water and register fresh weight.
3. Place leaves in a large weigh boat and add 2 ml of 1xGB per gram of fresh weight. Chop with a new, clean razor blade and transfer to blender.
4. Homogenize with two or three 2-second pulses (speed 5 in a seven speed Waring blender). Filter through 2 layers of Miracloth into a clean 250ml Nalgene centrifuge tube, squeeze gently to collect all of the liquid.
5. Put ground leaves back in blender and add another 2ml of 1xG. Repeat step 4.
6. Recover the total filtrate in 250ml centrifuge tubes. Centrifuge for 3min at 200xGB. A white (starch) pellet should form.
7. Transfer supernatant to clean, chilled 250ml tubes and centrifuge for 7 minutes at 1,000xg to sediment the chloroplasts as a green pellet.
8. Discard the supernatant and gently break the pellet by finger tapping. Resuspend the pellets in 2-4 ml 1xGB by gently swirling.
9. Using a wide-bore 1ml pipette tip, carefully apply the chloroplast suspension on top of the Percoll gradient.
10. Spin in a swing-out rotor (BECKMAN centrifuge, JS-13 rotor) for 15 min at 3,200xg. The broken chloroplasts will form an upper band and the intact chloroplasts will form a band at the interface between the 50% and 80% Percoll layers.
11. Collect the intact chloroplasts band with a wide-bore pipette tip; wash by resuspending in 3 volumes of 1xGB (no BSA) and centrifuge at 1,700xg for 1 minute.
12. Resuspend the chloroplast pellet in 0.5 ml of 1xGB without BSA. The chloroplast suspension should be kept in the dark, on ice, until further use.

<u>Estimation of chloroplast yield by chlorophyll concentration:</u>
The yield of isolated chloroplasts is usually expressed on a unit chlorophyll basis (mg of chlorophyll). For this procedure, chlorophyll is extracted from the chloroplasts suspension using an organic solvent like 80% acetone.

1. Add 10 µl of the chloroplast suspension to 1 ml of an 80% acetone solution and mix well.

2. Centrifuge for 2 minutes at 3,000 x g. Retain the supernatant.
3. Measure the absorbance of the supernatant at 652 nm. Use the 80% acetone solution as the reference blank.
4. Multiply the absorbance by the dilution factor (100) and divide by the extinction coefficient of 36 to obtain the mg of chlorophyll per ml of the chloroplast suspension.

$$\frac{\text{mg chlorophyll}}{\text{ml}} = \frac{A652 \times 100}{36}$$

To obtain the total chloroplast yield in µg chlorophyll per gram of fresh weight, multiply the mg chl/ml by the total ml of chloroplast suspension and divide by the number of grams of initial fresh weight. This chloroplast isolation protocol typically yields about 8 to 10µg chl/g of fresh weight.

Estimation of the percent of intact chloroplasts:

Reference: Walker et al. (1987) pp. 155

Method 1: Phase contrast microscopy

This method is based on the differences in refractive index between the intact chloroplasts and their aqueous medium. Walker et al. (1987) describes intact chloroplasts appear "pale yellow-green with a refractive halo" while broken chloroplasts appear dark green with no visible halo.

1. Place a drop of chloroplast suspension on a microscope slide, carefully place a cover slip on top and view under phase contrast.
2. Count the number of intact vs. broken chloroplasts on several fields and calculate the average of intactness.
3. Intactness percentages of at least 70% are recommended for photosynthesis or transport assays. This protocol usually yields chloroplasts with 80% to 90% intactness depending on the quality of plant tissue used.

Method 2: CFDA staining

Reference: Schulz et al. (2004)

Carboxyfuorescein diacetate succinimidyl ester (CFDA) is a molecule widely used for the staining on living cells. CFDA will diffuse freely into cells (or in this case, plastids) but will not produce fluorescence until its acetate groups are cleaved by the cell's esterases. Thus, broken chloroplasts are unable to cleave CFDA and will not produce this specific fluorescence. When examined under fluorescence microscopy under a fluorescein-specific filter, intact chloroplasts will look green, whereas broken

chloroplasts will not be visible. Using non specific wavelengths filter the chlorophyll in all the chloroplasts will be visible as red. When merging these two images into one, the broken chloroplasts still appear red whereas intact plastids look yellow because of the mixing of green (CFDA) and red (chlorophyll) fluorescence (Fig. 26).

1. Equilibrate an aliquot of chloroplast suspension with an equal volume of CFDA (final concentration 0.0025% w/v) and incubate 5 min in ice. Keep them away from light to avoid photobleaching and examine by fluorescence microscopy.

When counting the number of intact chloroplasts by this method, we found that it correlates with the numbers obtained by phase contrast.

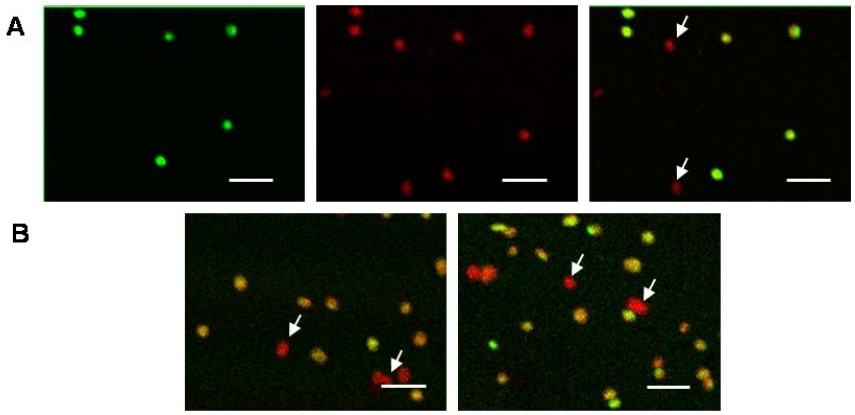

Figure 26. Evaluation of chloroplast intactness by CFDA staining. A, chloroplasts viewed immediately after isolation; Left, Fluorescein-specific wavelength; Center, chlorophyll autofluorescence; Right, Overlay. Intact chloroplasts appear yellow/green. B, overlay images of chloroplasts 60 min (left) and 120 min (right) after isolation. Bars: ~10µm. Arrows point to broken chloroplasts. Percent of intact chloroplasts varied from 78% to 84%.

DIC imaging of Arabidopsis tissues

Protocol based on notes received from Jim Mattsson, Simon Fraser University. See some of his images at http://www.sfu.ca/biology/faculty/mattsson/dic.html

1. Fix Arabidopsis leaves in 6:1 ethanol: glacial acetic acid. This can be done in 2ml microfuge tubes or 12-well plates. Cover samples with fixative solution and place open tubes in vacuum dessicator. Apply house vacuum for 15 min to remove trapped air bubbles and speed fixation. Close tubes and let sit 4-24 hrs at room temp.

2. Wash twice in 95% ethanol (leave 10 minutes or so before replacing).

3. Store in 70% ethanol at room temp. Fixed samples can be stored in 70% ethanol for several days or proceed to next step immediately.

4. Clear in 85% lactic acid (VWR cat no. MK267604). Add just enough lactic acid to cover tissue, let sit 2-24 hrs. Tissues will become nearly transparent.
   Note: lactic acid is corrosive. Clean up any spills quickly.

5. Mount in 30% glycerol, adaxial leaf surface up.
   Fixed leaves tend to fold on themselves when removed to the lactic acid. Using forceps take the leaf out of the acid and quickly transfer to a microscope on which a drop of 30% glycerol has been placed. Use the forceps or a fine paint brush to ensure the leaf is completely flat over the slide. If necessary, you can confirm that you have the adaxial side up before applying a coverslip by viewing under low magnification – you should see lots of trichomes.

6. Label the slide with date and sample info.
   If the slide is to be stored for more than 4-5 days, you can seal the cover slip with clear nail polish. Do not store prepared slides for more than two weeks, as the lactic acid-treated leaves tend to break down.

Alternative clearing with chloral hydrate:
Clear in 8:3:1 mix of chloral hydrate:glycerol:water (store cold).
Clearing works best on young tissue. If you use young leaves, you can mount the leaves directly in chloral hydrate solution and wait for a few minutes to overnight for clearing to occur. If it is tough, leave leaves in the solution in a vial for one to several days, then mount.

Determine number of leaf cells per fixed area:
Cells are visible under brightfield, but phase contrast yields much better images, and DIC may be better yet (Fig. 27). Cell counts should be done with Pallisade mesophyll cells since they have a nearly uniform shape. Alternatively, epidermal cells can also be used to determine cell density per fixed area, but their irregular shape and flat surface makes it harder to focus. Capture images at the distal, medial and proximal end of the leaf - all near the midline. Count cells per field of view (or other defined area).

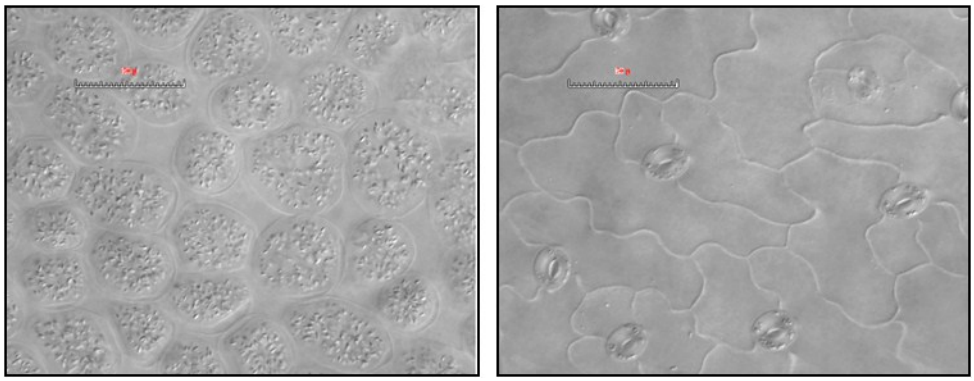

Figure 27. DIC images of WT leaves. Expanded leaves of 9 week old plants were fixed and bleached. DIC imaging on fixed leaves was carried out under a 40x objective. Left, mesophyll cells; Right, epidermal cells. Scale bars are 50µm.

Determine number of cells per leaf:

BEFORE FIXING, place the fresh leaf on paper next to printed defined areas (e.g., squares with 2, 4, 8, 12 mm sides). It may be necessary to place a transparency sheet on top to flatten the leaf. Use Photoshop to calculate the area of the leaf and squares. Save the image file with a meaningful name. Multiply the average cell per unit area (determined above) by the leaf area to determine the number of cells per leaf. This value is an estimate but it is suitable for comparisons between genotypes.

Total Starch and Soluble Sugar Assays

Reference:
Smith AM, Zeeman SC. (2006)

Reagents:

10 mM Na-acetate, pH 5.5:
Add 0.057 mL glacial acetic acid to 90 mL dH_20. Adjust pH to 5.5 with NaOH (~0.86 mL 1 M NaOH)
Adjust to 100 mL with dH_20

200 mM K-HEPES pH 7.5:
In 40 mL dH20, add 2.383 g HEPES (FW 238.3; Sigma, H3375). Adjust pH to 7.5 with KOH (~2.5 mL 2 M KOH). Adjust to 50 mL with dH_2O

0.2 M KOH
Add 2.81 g KOH (FW 56.11) to 200 ml dH_2O. Adjust to 250 mL with dH_2O

1.0 M acetic acid
5.75 mL glacial acetic acid diluted to 100 mL.

80% EtOH, 5% formic acid
Note: Formic acid (Sigma F0507), 95%, is volatile and highly corrosive. Open in fume hood and handle with care.

80% EtOH

Amyloglucosidase Stock (1.25 U/µl):
1.9 ml amyloglucosidase (Megazyme , E-AMGDF 3260 U/ml) +2.1 ml of 200 mM NaAc/ 30% glycerol, pH 4.6

100 mM ATP stock:
In 5.0 mL dH_20, dissolve 0.276g ATP disodium (FW 551.1).

50 mM NAD stock:
Weigh 0.332 g NAD (fw 663.43; VWR 80053-322). Bring to 10 mL with dH_2O.
Note: NAD and NADH are only good for 1 freeze-thaw cycle! Freeze in 600µL aliquots.

1M $MgCl_2$ stock:
Weigh 1.017 g $MgCl_2$ (fw 203.3; Sigma, M2670). Bring to 5.0 mL with dH_20

Hexokinase Stock (1000 U/mL):
In 1.0 mL 30% glycerol, add 9.17 mg hexokinase (VWR 101175-550, 1000U).

Glucose-6-P-dehydrogenase (G6PDH) Stock:
VWR 101174-382 (USB 16171) >5 kU/mL, or VWR 101169-590 (all) in 0.5 mL 30% glycerol (10 kU/mL).

Hexokinase/G6PDH Working Solution
(32 units/mL Hexokinase + 32 units/mL G6PDH): 160 ul hexokinase stock (1000 U/ml)m + 160 U G6PDH stock. Bring to 5 mL final vol. in 30% glycerol

Invertase Stock Solution (20 units/µL)
100 mg invertase (400 units/mg; Sigma I4504) in 2.0 mL of 30% glycerol

Invertase Working Solution (150 units/ml) or Sucrose Assay Reagent (Sigma, S1299):
15.0 µL of Invertase stock solution in 2.0 mL final vol of 10 mM Na-acetate (pH 5.5)
Note: Works best when made fresh.

Phosphoglucose Isomerase Working Solution (80 U/ml)
23.0 µL of PGI stock (3500 units/ml; Fisher NC9333115) in 1.0 mL final vol of 100 mM K-HEPES pH 7.5

Glucose Assay Reagent (MAKE FRESH!!):
Final solution is: 100 mM K-HEPES, 1.0 mM ATP, 2.0 mM NAD or NADP, 5.0 mM $MgCl_2$. Make enough for starch, sucrose, glucose, and fructose assays.
For 15 mL:
7.5 mL of 200 mM K-HEPES, pH 7.5
+ 150 µL of 100 mM ATP stock
+ 600 µL of 50 mM NAD stock
+ 75 µL of 1 M $MgCl_2$ stock
+ dH_2O to 15 mL total volume

Tissue Collection:

Harvest leaf material at the 8 to 12 leaf stage before bolting. Always take the same leaves because starch contents vary between individual leaves of a rosette, sometimes more than the equivalent leaves of two individuals. I usually use the 5^{th} and 6^{th} true leaves.

1. Collect two rosette leaves from each biological sample. Place in a pre-weighed 2 mL microfuge tube and determine fresh weight. Collect 4-5 biological replicates for each sampling point. For roots, harvest from hydroponically-grown plants and take the roots out carefully to avoid breaking off root tips. Blot roots on paper towel and chop with a razor. Randomly select portions for use in assays. Place in a pre-weighed 2 mL microfuge tube and determine fresh weight.

2. After weighing, freeze in liquid N_2. At this point, samples can be stored at -80°C for several months, or proceed immediately to *Soluble Sugar and Starch Preparation.*

Soluble Sugar and Starch Preparation:

1. Add 750 µL of 80% EtOH, 5% formic acid to samples, and grind briefly with a micro pestle. Incubate at 80ºC for 20 min. Cool down in an ice bath and spin samples for 5 min at max speed to pellet down tissues. Transfer EtOH solution to an empty, labelled 2 mL tube. (To heat, place tubes in eppendorf rack and clamp a second rack on top with rubber bands. This prevents the tubes from popping and samples being lost).
2. Add 750 µL 80% EtOH to tissues and incubate in clamped tube rack again for 20 min at 80ºC. Remove EtOH supernatant and add to the previous aliquot. For each sample, you should now have one tube containing bleached leaves with no EtOH solution left and one 2 mL tube containing approx 1.5 mL greenish EtOH solution. The latter contains the soluble sugars. Evaporate the EtOH solution in a Speedvac (3-4 hours) then resuspend the dried pellet in 300 µL of 10 mM Na-acetate (pH 5.5). Sonicate each sample for 30 seconds (10 seconds, place in ice, repeat two more times). Spin for 10 min. Use the supernatant for enzymatic assays.
3. To extract starch, dry the bleached leaves in Speedvac or 70ºC oven then add 0.25 mL 0.2 M KOH and grind with a micro pestle.
4. Add another 250 µL of 0.2 M KOH, washing the pestle while adding. Incubate at 95ºC for 1 hr in a clamped tube rack. This step makes the starch soluble.
5. Cool in an ice bath and bring to pH 5.0 by adding 100 µL of 1 M acetic acid. Check pH of one sample using test strips to verify. Centrifuge 10 min at max speed then transfer 50-100 µL (record volume!) to a new tube for digestion and analysis.
6. To each aliquot, add 5 µL amyloglucosidase (6.25 U). Incubate overnight at 30ºC. This step is the complete conversion of soluble starch to glucose.
7. Denature enzymes by incubating a 95ºC for 10 min. Cool in ice bath. Add 440 µl dH_2O and use for starch assay. (Note: further dilution may be necessary depending on your samples)

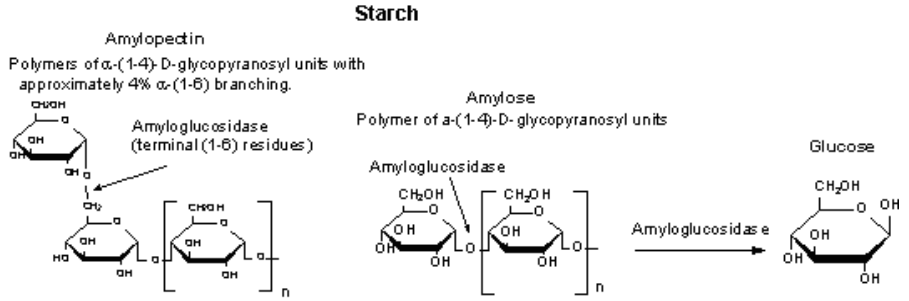

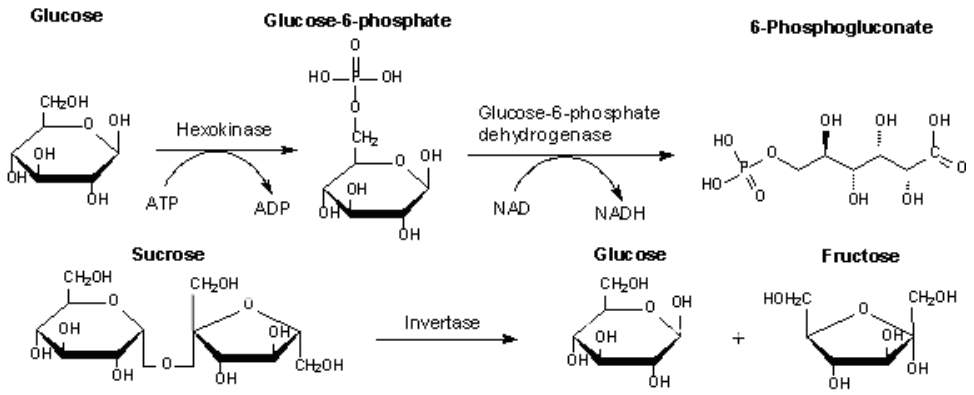

Assays: Perform all reactions in UV Star 96 well plates (flat bottom, ½ area; Bioone 675807) and read in plate reader.

Starch and Glucose Assay:

1. Add 150 µL of Glucose Assay Reagent to each well. Add 20 µL of sample to the corresponding well (2 replicates for each sample). Be sure to include the glucose standards (see below). Standards (0, 2, 10, 20, 50 and 100 nmol) are all 20 µL.
2. Measure the initial Abs 340 nm to determine the sample background.
3. Add 15 µL of Hexokinase/G6PDH Working Solution to each well, mix, and incubate for 20 minutes at room temp.
4. Measure the final Abs 340 nm.
5. Determine glucose content from standard curve (ΔAbs vs. Glc).

Sucrose Assay:

1. Add 15 µL of Invertase Working Solution to wells of a 96 well plate. Add 20 µL of sample to the corresponding well (2 replicates for each sample) mix, and incubate at room temp for 20 min. Make sure to include the glucose standards.
2. Add 150 µL of Glucose Assay Reagent to each well, mix, and measure the initial Abs 340 nm to determine the sample background.
3. Add 15 µL of Hexokinase/G6PDH Working Solution to each well, mix, and incubate for 15 minutes at room temp.
4. Measure the final Abs 340 nm.
5. Determine sucrose content from standard curve (ΔAbs vs. Glc). Note: must subtract free Glc content.

Fructose Assay:

1. Add 150 µL of Glucose Assay Reagent to each well. Add 20 µL of sample to the corresponding well (2 replicates for each sample). Be sure to include the glucose standards.
2. Read initial Abs 340 nm to determine the sample background.
3. Add 10 µL of Hexokinase/G6PDH Working Solution and 15 µL of PGI to each sample and incubate for 15 min at room temp.

4. Measure the final Abs 340 nm.
5. Determine fructose content from standard curve (ΔAbs vs. Glc). Note: must subtract free Glc content.

Glucose standards:
Prepare a 10 mM glucose stock in water. From this stock, prepare 2.5 mM and 0.5 mM dilutions. The table below shows how each standard is prepared – volumes are for a single sample.

nmol Glc	10 mM stock (µl)	2.5 mM stock (µl)	0.5 mM stock (µl)	Water (µl)	Final vol (µl)
0	0	0	0	20	20
2	0	0	4	16	20
10	0	4	0	16	20
20	0	8	0	12	20
50	5	0	0	15	20
100	10	0	0	10	20

Glucose Standard Curve:
1. Determine ΔAbs and Avg ΔAbs for each standard.
2. Plot Avg ΔAbs (y-axis) vs. glucose content in µmoles (x-axis). Calculate trend line equation (y=mx+b). Should have R^2 (> .97).
3. Example:

Glucose (µmol)	ΔAbs (340nm)	ΔAbs (340nm)	Avg ΔAbs (340 nm)
0	0	0.0	0.0
0.002	0.082	0.075	0.079
0.01	0.375	0.364	0.370
0.02	0.705	0.675	0.690
0.05	1.404	1.492	1.447
0.10	3.113	2.800	2.957

y=29.07x + 0.042 **R^2=0.999**

Calculations:
The linear equation from the glucose standard curve is used to calculate starch/sugar content in the plant tissue samples. Absorbance values for unknowns must fall within the range covered by the standards. To express results in □mol/FW, the initial FW and all dilution volumes must be accounted for. Starch will be reported in glucose equivalents.

Starch:
µmol Glc in well = (Avg ΔAbs – y int)/slope[y int and slope from Glc standard curve]
µmol Glc in starch aliquot = (µmol Glc in well/ 20 µL)*(450 µL water/enzymes + X µL starch aliquot)
µmol Glc in tissue = (µmol Glc in starch aliquot/ X µL starch aliquot) * 600µL KOH/acetic acid
µmol Glc equivents/g FW = µmol Glc in tissue/ g FW

Glucose:
µmol Glc in well = (Avg ΔAbs – y int)/slope
µmol Glc in tissue = (µmol Glc in well/ 20 µL) * 300 µL
µmol Glc/g FW = µmol Glc in tissue/ g FW

Sucrose:
µmol Suc in well = (Avg ΔAbs – y int)/slope
µmol Suc in tissue = (µmol Suc in well/ 20 µL) * 300 µL
µmol Suc/g FW = (µmol Suc in tissue/ g FW) – (µmol Glc/g FW)

Note: you must subtract the free Glc to determine Glc liberated by invertase

Fructose:
µmol Frc in well = (Avg ΔAbs – y int)/slope
µmol Frc in tissue = (µmol Frc in well/ 20 µL) * 300 µL
µmol Frc/g FW = (µmol Frc in tissue/ g FW) – (µmol Glc/g FW)

Note: you must subtract the free Glc to determine Frc converted by phosphoglucose isomerase

VITA

Name: Sonia Cristina Irigoyen Aranda

Address: 3258 TAMU, Department of Biology, BSBE 204
College Station, TX 77843-3258

Email Address: arandasci79@yahoo.com

Education: B.S., Biology, Universidad Autonoma de Nuevo Leon, 2002

M.S., Genetics, Universidad Autonoma de Nuevo Leon, 2005

Ph.D., Molecular and Environmental Plant Sciences,
Texas A&M University, 2011